On the Kinetics of Protein Misfolding and Aggregation

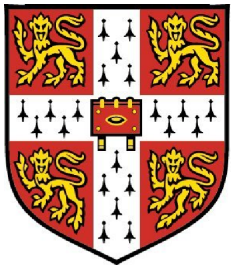

Alexander Kai Buell

Magdalene College

University of Cambridge, Department of Engineering

A dissertation submitted for the degree of

Doctor of Philosophy

This dissertation is the result of my own work at the University of Cambridge and includes nothing which is the outcome of work done in collaboration except where specifically indicated in the text. The length of this dissertation is ca. 58 000 words, including tables, figure legends, footnotes and references, and therefore does not exceed the word limit of 65 000 words. It includes 41 figures.

Cambridge, April 2011, Alexander Kai Buell

Acknowledgements

I would like to thank my PhD supervisor Professor Sir Mark Welland for taking me on as a student and for giving me the confidence and freedom to explore my own ideas and to pursue my scientific interests during the last three years.
I would like to express my deepest gratitude to Professor Christopher Dobson, my advisor and mentor during my PhD studies. It is a privilege and honour to contribute to his heroic efforts in understanding the molecular basis of protein misfolding and associated diseases. Thank you for providing this unique, thriving framework here in Cambridge for the study of this fascinating topic. Also thank you for the guidance and help and the inexhaustible patience with my manuscripts.
Without any doubt, the person I owe my most profound gratitude is Dr Tuomas Knowles. I would certainly not be where I am now without his tireless support and his unique creativity and energy that he brings into this research area, and that do not cease to inspire me. Most of the work described in this thesis was already contained to some degree in his early work and a great deal of what I now know about the physical aspects of protein aggregation or indeed scientific work, I have learned from him. Our collaborative work has led us to become friends and I sincerely hope that we will continue our collaborations for many years to come.
A big thank you also goes to Karen Valelli, for always being friendly and helpful, and knowing the importance of deadlines.
In addition, I would like to thank many other scientists that work in Cambridge and elsewhere in the world on this fascinating topic, and with whom I had the privilege to collaborate. In particular, I would like to thank Duncan White, Dr Anne Dhulesia, Dr Tom Oppenheim, Dr Christoph Meier, Dr Xavier Salvatella, Dr Gian Gaetano Tartaglia, Professor Michele Vendruscolo, Dr Myriam Ouberai, Dr Maria Mossuto, Tim Guilliams, Dr Simon Attwood, Professor Sarah Perrett, Dr Yi-Qian Wang, Li-Qiong Xu, Benedetta Bolognesi, Dr Sarah Shammas, Dr Nunilo Cremades, Dr Neil Birkett, Dr Christopher Waudby, Shuyu Wang, Dr. Laura Hennemann, Kai Braun, Peter Hung, Felix Roosen-Runge and many others.
I would also like to thank my parents, who always support and trust me in my decisions. This thesis is dedicated to them.

Abstract

Protein (mis)folding into highly ordered, fibrillar structures, amyloid fibrils, is a hallmark of several, mainly neurodegenerative, disorders. The mechanism of this supra-molecular self-assembly reaction, as well as its relationship to protein folding are not well understood. In particular, the molecular origin of the metastability of the soluble state of proteins with respect to the aggregated states has not been clearly established.
In this dissertation, it is demonstrated, that highly accurate kinetic experiments, using a novel biosensing method, can yield fundamental insight into the dynamics of proteins in the region of the free energy landscape corresponding to protein aggregation.
First, a section on Method development describes the extension and elaboration of the previously established kinetic assay relying on quartz crystal microbalance measurements for the study of amyloid fibril elongation (Chapter 3). This methodology is then applied in order to study in great detail the origin of the various contributions to the free energy barriers separating the soluble state of a protein from its aggregated state. In particular, the relative importance of residual structure, hydrophobicity (Chapter 4) and electrostatic interactions (Chapter 5) for the total free energy of activation are discussed.
In the last part of this thesis (Chapter 6), it is demonstrated that this biosensing method can also be used to study the binding of small molecules to amyloid fibrils, a very useful feature in the framework of the quest for potential inhibitors of amyloid formation. In addition, it is shown that Thioflavin T, to-date the most frequently employed fluorescent label molecule for bulk solution kinetic studies, can in the presence of potential amyloid inhibitor candidates be highly unreliable as a means to quantify the effect of the inhibitor on amyloid formation kinetics.
In summary, the work in this thesis contributes to both the fundamental and the applied aspects of the field of protein aggregation.

Contents

List of Figures

List of abbreviations

Aβ - amyloid β
AFM - atomic force microscopy
CD - circular dichroism
CR - Congo red
DH - Debye-Hückel
DI - de-ionized
DLS - dynamic light scattering
PB - phosphate buffer
PBS - phosphate buffer saline
PI3K - phosphatidylinositol-3-kinase
QCM - quartz crystal microbalance
SAM - self-assembled monolayer
SPR - surface plasmon resonance
ThT - Thioflavin T
TST - transition state theory
TTR - transthyretin
UV - ultra-violet

Chapter 1

Introduction

1.1 Protein folding and misfolding

Proteins are the primary functional molecules of life. They fulfil a large variety of tasks, from acting as enzymes, hormones and chemically selective channels through membranes to scaffold materials and building blocks of muscles. The principle that enabled evolution to use this class of molecules for such a variety of functions is simple: proteins are bio-polymers built from a limited amount of chemically very distinct building blocks, the amino acids. The linear sequence of amino acids determines all the properties of the protein; however, in order to be able to perform its function in the organism, the majority of the proteins has to fold into a highly specific 3-dimensional structure. The question how the newly assembled amino acid chain attains its final structure, "the folding problem", is one of the big problems in chemical biology [1]. Figure 1.1 shows a scheme (from [2]) that illustrates that a protein, after having been synthesized by the ribosome, has a large number of possible conformations it can take.

In fact, the number of theoretically possible conformations is astronomical, as has first been pointed out by Levinthal [3]. In his famous "back of an envelope" calculation, he showed the impossibility of a protein folding mechanism where the polypeptide samples the entire conformational space, as this would lead to folding timescales comparable to the age of the universe, whereas experimentally determined folding rate constants are often of the order of $1s^{-1}$ and can be more than thousand fold higher [4]. As an alternative for the random search of conformational space, the so called "folding funnel" [5; 6] was proposed (Figure 1.2).

In this picture, a protein moves on a free energy surface, a multidimensional mathematical construct where the total Gibb's free energy of the protein (including the solvating water molecules) is a function of all conformational degrees of freedom. The shape of this energy landscape here resembles a funnel, such that the large ensemble of unfolded initial states corresponds to the mouth and the folded final state to the spout. The energetic downhill nature of folding is here explained by assuming that all native-like intra molecular contacts are on average more favourable than non-native ones, leading to an ever decreasing free energy during the folding. However, this picture does not imply the complete absence of any free energy barrier

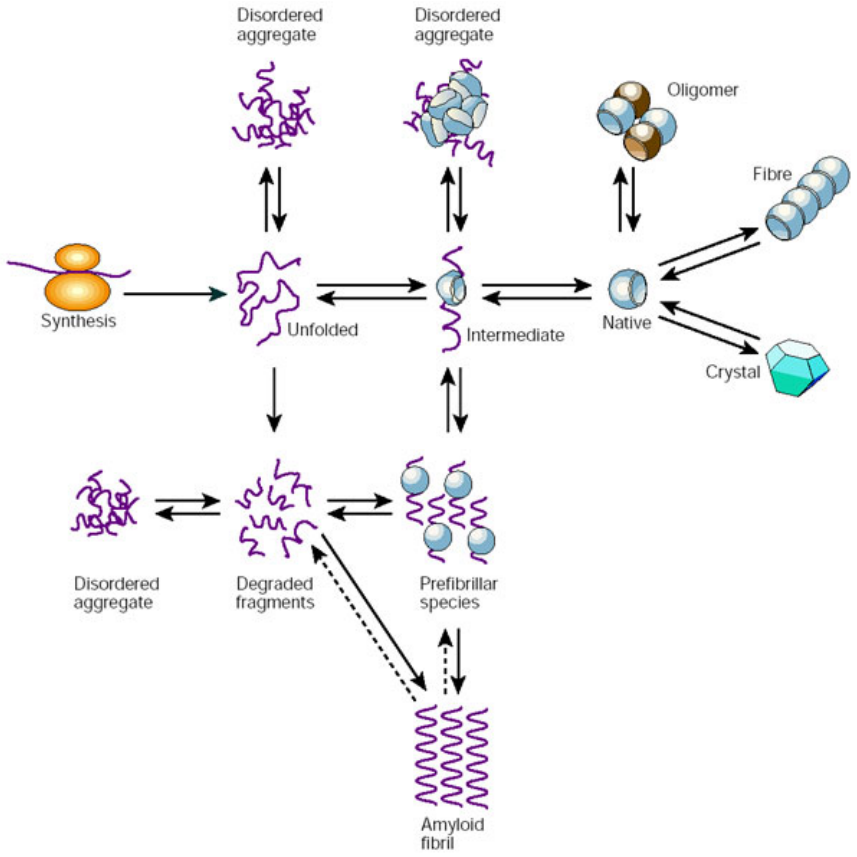

Figure 1.1: This scheme, taken from [2], illustrates the folding process of a newly synthesized polypeptide chain, showing that there can be intermediates on the way from the unfolded to the folded protein, especially for large complex proteins. Many potential side tracks exist, some of them dead ends, like the formation of insoluble fibrillar structures, amyloid fibrils, a process referred to as "misfolding".

for folding. The loss of conformational freedom leads to a decrease in chain entropy that, together with the decrease in energy, can produce a free energy barrier. The cooperativity of folding increases the funnel-like character of this landscape: the formation of native contacts makes the folding polypeptide more compact, therefore further reducing the conformational space that needs to be sampled. Potential kinetic trapping of the folding protein in intermediate minima, in analogy to a similar process in spin glasses [8] called "frustration" is minimized in this view of folding by evolutionary pressure to select amino acid sequences that show minimal frustration. On a more quantitative level, the crucial issue of the relative importance of the various fundamental forces that govern the kinetics and thermodynamics of the folding of a polypeptide chain into a functional protein structure is still a topic of great current interest and debate [9]. Thus, for example, the single most important factors in the determination of folding rates and stabilities have been reported to be as varied as protein size [10; 11], side chain interactions [12], and hydrogen-bonded

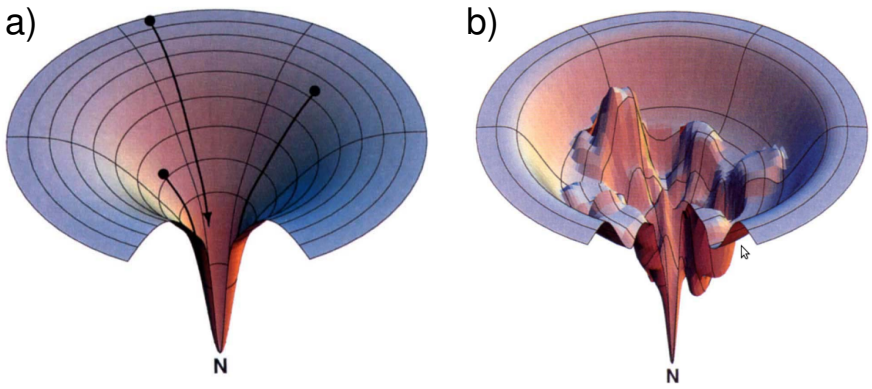

Figure 1.2: From [7]. a) Idealized "folding funnel" energy landscape. As the chain forms increasing numbers of intra-chain contacts, and lowers its internal free energy, its conformational freedom is also reduced. b) Rugged energy landscape with kinetic traps, energy barriers and some narrow through-way paths to the native state. Folding can be multi-state.

backbone-interactions [1]. This variability is in part a result of the fact that the absolute free energy differences between different states (e.g. folded and unfolded) on the free energy surface of a polypeptide are typically very small, whereas the component enthalpic and entropic contributions are usually much larger and compensate each other [9].

Going back to Figure 1.1, it can be seen that amongst the many potential sidetracks on the way from an unfolded to a folded protein, there is one that leads to the formation of ordered fibrillar structures, called amyloid fibrils [13]. Due to the well defined structural properties of the end product, this process was dubbed "misfolding". Amyloid has first been discovered in the connection with diseases, as early as several centuries ago [14]. Initially the material was thought to consist of carbohydrates, due to the possibility to stain it with iodine (hence the name) [14]. Only much later, the fibrillar nature of the protein aggregates was recognized [15]. Interestingly, it was known as early as 1944 that insulin, upon heating and acidification reversibly self-assembles into fibrillar structures [16]. However, the connection that the structure adopted by the protein within the fibrils was very similar to the structure of the proteins within disease associated aggregates was made much later. Today, several dozens of diseases, most of them neurodegenerative disorders (e.g. Alzheimer's disease, Parkinson's disease, Huntington's disease, the prion diseases), but also diseases affecting other organs (e.g. type 2-diabetes, systemic amyloidosis) can be linked to amyloid [17] in that fibrillar proteinacious deposits are hallmarks of these disorders. Table 1.1 gives an (incomplete) overview over various human disorders associated with amyloid.

Amyloid fibrils are highly ordered, linear structures that can be viewed as (pseudo) one-dimensional crystals and that consist of thousands of individual protein molecules, leading to a high aspect ratio of the fibrils, with diameters ranging up to 10 nm and

amyloidogenic peptide or protein	**associated disease**	**associated function**
Aβ and τ	Alzheimer's disease	n/a
Prion protein (PrP)	Spongiform encephalophaties	n/a
α-synuclein	Parkinson's disease	n/a
Huntingtin	Huntington's disease	n/a
Lysozyme	Lysozyme systemic amyloidosis	n/a
Pro-islet amyloid polypeptide	Diabetes type 2	n/a
β2-microglobulin	Hemodialysis-related amyloidosis	n/a
Transthyretin	Senile systemic amyloidosis	n/a
Ig light chains	Primary systemic amyloidosis	n/a
Serum amyloid A	Secondary systemic amyloidosis	n/a
Fibrinogen	Fibrinogen α-chain amyloidosis	n/a
Calcitonin	Medullary carcinoma of the thyroid	n/a
Curlin	n/a	in curli of E. Coli
Yeast Ure 2p	n/a	nitrogen metabolism regulator
Yeast Sup35	n/a	translation termination factor
Fungal Het-S	n/a	regulator of vegetative cell fusion
Pmel 17	n/a	Melanin biosynthesis

Table 1.1: List of disease related (from [17]) and functional (from [18]) occurrences of amyloid in nature. In total, more than 30 amyloid diseases have been reported to date. The number of identified functional occurrences of amyloid is much smaller, but steadily growing.

maximum lengths of more than thousand times this value. In the last decade and pioneered through work carried out in Cambridge, it is becoming increasingly evident that the amyloid phenomenon is not restricted to disease, but that a large variety of proteins can be made to form amyloid fibrils *in vitro* under appropriate conditions (see e.g. [19]). Amyloid fibrils are stabilized through intermolecular hydrogen bonds and contain mainly β-sheet as secondary structure element [20]. To obtain atomic resolution structural data of amyloid fibrils has proven to be a major chal-

lenge. Electron and atomic force microscopy allow the determination of the overall topology (length, width, twist) [21; 22] and mechanical properties [20] of mature fibrils. X-ray fibre diffraction yields characteristic distances within the proto-filaments, such as the characteristic reflections at 4.7 $\mathring{A}$ and 10 $\mathring{A}$ that stem from the inter-strand and inter-sheet distances respectively [13; 23]. When the fibrils are aligned, the X-ray pattern shows two sets of perpendicular crescent shaped reflections; the origin of this scattering pattern is the arrangement of the protein subunits within the fibrils, the tertiary and quaternary structure, that has been dubbed "cross β" structure [24]. The β-strands are here orthogonal to the long fibril axis (see Figure 1.3).
A slightly higher level of detail can be achieved with the limited proteolysis [25] and hydrogen exchange [26; 27] methodologies. These techniques provide insight into the parts of the polypeptide sequence that are more or less structured and therefore accessible in the fibrillar fold. Yet higher resolution can be achieved with experimental approaches that have experienced a dramatic improvement in the last years, namely cryo electron microscopy [28; 29] and solid state NMR spectroscopy [30]. The large size of amyloid fibrils (MDa) renders classical solution state NMR experiments infeasible. The highest resolution to date (atomic resolution) was achieved by performing X-ray crystallography of micro-crystals formed from short peptide sequences [31] that are part of the amyloidogenic sequence of larger polypeptides and proteins. These short peptides can form both fibrils and microcrystals, and the structure of the monomeric unit within the crystal is thought to be very similar to the structure of the fibril. Figure 1.3 gives an illustration of the architecture of an Aβ (1-42) amyloid fibril.

The generic nature of the interactions stabilizing amyloid fibrils together with findings on the relative stabilities of amyloid and folded proteins led to the hypothesis that in fact any polypeptide sequence can form these structures that might even represent the global free energy minimum of the polypeptide [2; 34]. The initial hypothesis of the entirely aberrant nature of amyloid fibrils had to be reconsidered after the discovery of functional amyloid. Nature seems to make use of the remarkable mechanical properties [20] and self assembly of amyloid in a range of different circumstances, ranging from a scaffold for melanin bio-synthesis [35] over fungal coatings [36] to non-genetic inheritance [37]. The bottom of Table 1.1 gives several examples for proteins that are believed to form amyloid in a functional context.
Figure 1.1, illustrates that many of the possible conformations of the polypeptide chain are interconnected through open (mis-)folding pathways. This picture suggests that the fundamental driving forces that govern the formation of amyloid fibrils are the same as those governing protein folding: the formation and breakage of hydrogen bonds [31] and of hydrophobic [38] and electrostatic interactions [39]. The remarkable structural similarity of amyloid fibrils formed from a variety of polypeptides with unrelated primary structures [40] suggests that the thermodynamics and kinetics of their formation could be more straightforward to understand than the equivalent quantities in protein folding, a process leading to a large number and variety of different final structures [41]. Such a study is attempted in this thesis, mainly relying on highly accurate measurements of the kinetics of amyloid fibril

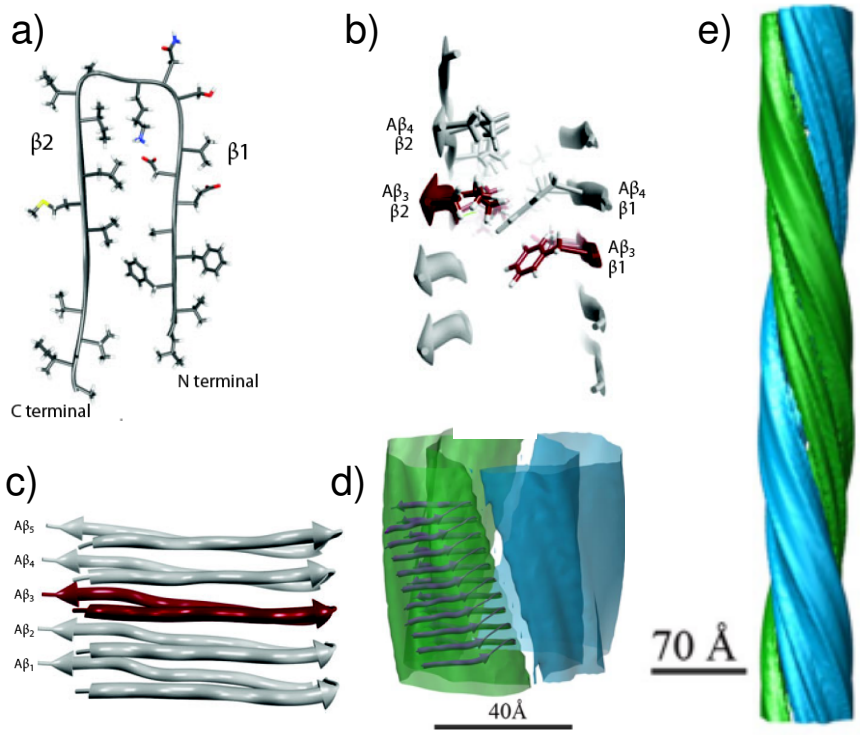

Figure 1.3: The cross-β structure of an Aβ amyloid fibril (a-c from [32] and [33] and d-e from [29]). a) A single Aβ (1-42) monomer in the fiber conformation is shown down the fiber axis. The N-terminal β-strand and the C-terminal β-strand are labeled β 1 and β 2, respectively. b) A view of Aβ (1-42) fiber structure from the side, perpendicular to the fiber axis. A single Aβ (1-42) monomer is shown in red, with the neighbouring monomer in grey. This illustrates how the side chains from one unit in this structure (Aβ 3, strand β 2) form an interface with the neighbouring molecule (Aβ 4, strand β 1). c) Full structure of Aβ (1-42) viewed perpendicular to the fibre axis. A single monomer is displayed in red, with the others in grey, together forming a piece of an Aβ proto-filament. d) It is indicated how the proto-filaments wrap around each other to form the mature fibril. e) The global topology of a mature Aβ (1-42) amyloid fibril.

elongation. This approach, that aims to elucidate the molecular mechanisms of this self-assembly reaction not only has implications for the quest to fight the disorders associated with it, but due to the intricate links between folding and misfolding can contribute to the solution of the above stated "folding problem". Before attacking this problem, in the following two sections a historical perspective on the development of the notion of "reaction kinetics" will be given, followed by a more specific focus on the development of the measurement of protein aggregation kinetics.

1.2 History of chemical kinetics

As outlined in the previous section, kinetic measurements of a macromolecular self-assembly reaction, amyloid fibril elongation, are the central theme of this thesis. It therefore seems in place to give a brief historical overview how the notion of reaction kinetics and dynamics arose. The first part of the following section closely follows the discussion in [42].

The qualitative notion of duration of a chemical reaction or the rapidity with which it proceeds certainly is very old. It was necessary for man to be able to predict the duration of processes such as fermentation, combustion or metal oxidation, in order to exploit them optimally. However, records of systematic measurements start comparatively late. In the second half of the 18th century, the German chemist Carl Friedrich Wenzel qualitatively described the dependence of the rate of dissolution of metals in acid on the concentration of acid [43]. Even though this study was not the only one in these early days of the discipline, no serious quantitative attempts were made to study reaction rates. However, this changed in 1850, when the German physicist Ludwig Ferdinand Wilhelmy studied the rate of inversion of sucrose [44]. Wilhelmy for the first time set up a differential equation for this reaction that he had found to be proportional to both the sugar and added acid. He then integrated this equation and showed that the mathematical solution was consistent with his experimental results. In 1864, Guldberg (mathematician) and Waage (chemist) in Norway published their law of mass action, where they arrived at an expression for the equilibrium concentrations of chemical species by equating the rate equations of forward and backward reaction [45]. However, they had deduced these rate equations, incorrectly, from the stoichiometric equations, arriving at the correct final expression. At about the same time, another collaboration between a mathematician and a chemist proved fruitful for chemical kinetics, this time in Oxford. George Vernon Harcourt performed important kinetic experiments (e.g. between hydrogen peroxide and hydrogen iodide). However, he needed the help of his colleague and mathematician William Esson to analyse the data correctly. Together, they described what we would today call first and second order reactions and consecutive reactions [46].

However, the greatest contributions to chemical kinetics in the 19th century were made by the Dutch chemist Jacobus Henricus van't Hoff. In 1884 he published a book [47], where he summarized the research that had been published to this date and completed it with data that had been acquired in his Amsterdam laboratory in the three previous years. Despite the sparse available data, van't Hoff managed to extract many new fundamental principles and to obtain deep insight into chemical kinetics. Among many other things, he introduced the symbol "$\rightleftarrows$" to express the notion of a dynamical equilibrium, he studied the influence of the surface of the reaction vessel on the kinetics of gas phase reactions, he properly defined the order of a reaction and he introduced logarithmic plots of kinetic data to determine the order of a given reaction. However, probably his most important contribution is the expression for the so-called "van't Hoff isochore":

$$\frac{d\mathrm{lnK}}{dT} = \frac{\Delta q}{RT^2} \tag{1.1}$$

where K is the equilibrium constant and the heat of reaction q is written today as ΔH^0. Even though this equation is concerned with chemical equilibrium, van't Hoff extended it by using the relationship between the forward and backward rate constants and the equilibrium constant $K = \frac{k_1}{k_{-1}}$:

$$\frac{d\mathrm{lnk_1}}{dT} - \frac{d\mathrm{lnk_{-1}}}{dT} = \frac{q}{RT^2} \tag{1.2}$$

He regarded the heat of reaction as the sum of two terms $q = E_1 - E_{-1}$, so that

$$\frac{d\mathrm{lnk_1}}{dT} - \frac{d\mathrm{lnk_{-1}}}{dT} = \frac{E_1}{RT^2} - \frac{E_{-1}}{RT^2} \tag{1.3}$$

Identifying the first and second terms on either side of the equation, van't Hoff obtained the following general relationship for the influence of the temperature on a rate constant (integrated with respect to temperature):

$$\mathrm{lnk} = -\frac{E}{RT} + const. \tag{1.4}$$

which is equivalent to writing $k = Ae^{-E/RT}$. van't Hoff already realized that the energy E is not necessarily temperature independent. Even though this equation is normally attributed to Svante Arrhenius, a Swedish chemist and close collaborator of van't Hoff, his contribution was the interpretation of a variety of experimental results using this equation [48]. In addition, he proposed a physical interpretation of this equation in terms of an equilibrium between reactant and active molecules, that undergo reaction readily. Despite the fact that Arrhenius acknowledges van't Hoff's priority in his article, this equation is now generally known as the "Arrhenius-equation".

Conceptually, it was easy to apply this equation to simple gas-phase reactions, where the collision frequency could be calculated in a straightforward manner using kinetic theory of gases, even though the exact physical origin of the (activation) energy term remained unclear.

However, before such an approach could be used to improve the descriptions of reactions in the condensed phase, the stochastic (Brownian) dynamics of particles or molecules immersed in liquid had to be understood. This task was completed independently by Albert Einstein [49] and Marian von Smoluchowski [50]. For the simple case of two reactive spheres A and B of concentrations [A] and [B], diffusion coefficients D_A and D_B and radii R_A and R_B, the diffusion limited reaction rate is given by [51]:

$$r = 4\pi(D_A + D_B)(R_A + R_B)[A][B] \tag{1.5}$$

an equation that was, for example, used much later to predict the maximum theoretical rate for enzymatic reactions [52]. In order for the next conceptual leap in reaction kinetics to be possible, quantum mechanics had to be developed, as a

means to calculate the energy surface and therefore the energy of activation in the Arrhenius equation from first principles. The first such attempt was made in Berlin by Michael Polanyi and his postdoc Henry Eyring in 1931 for the simple reaction [53]:

$$H + H_2 \rightarrow H_2 + H \tag{1.6}$$

where they themselves dubbed their approach semi-empirical, using experimental data and quantum chemical calculation to describe the energy landscape. However, it should take three more years, until what we now know as transition state theory (TST), was born. In 1934 Eyring, by that time back in the US, published a paper where he used the combination of quantum mechanics and statistical mechanics to compute absolute reaction rates [54]. Quantum mechanics again serves the construction of the energy landscape and therefore the energy difference between the lowest energy state of the reactants and the highest energy state on the pathway towards products, and therefore the (pseudo)equilibrium concentration of "activated complex". Statistical mechanics then allows to calculate the frequency of decay of this activated complex into products. The final expression for the reaction rate constant as computed with TST is

$$k = \frac{k_B T}{h} \frac{Q_{TS}}{Q_R} e^{-\frac{E_a}{k_B T}} \tag{1.7}$$

where Q_{TS} and Q_R are the partition functions of the transition state ("activated complex" in Eyring's words) and of the reactants respectively, E_a is the activation energy, k_B is the Boltzmann constant and h is Planck's constant. The pre-factor $\frac{k_B T}{h}$ has dimensions of a frequency and gives the rate of decomposition of the TS. It is derived from the fact that in the TS one vibrational mode changes from being bound to dissociative. Up to this day, TST and its applications and variations is a very active field of research within the physical chemical community.
At about the same time as the birth of TST, and rather independently of it, a Scandinavian school, under the guidance of Niels Bohr, worked on the problem of the origin of the "activation" of the reactants. In the years between 1915 to 1928, the so-called "radiation hypothesis" was fiercely debated, mainly advocated by Jean Perrin [55].[1] Among the researchers not convinced by this hypothesis was a young Chemist, Jens Anton Christiansen, who came to work with Niels Bohr in Copenhagen after his PhD thesis. There, he met Hendrik Anthony Kramers, a Dutch Physicist who had done his PhD with Bohr. Their approach to tackling chemical reaction dynamics and kinetics was inspired by Einstein's and Smoluchowski's work on diffusion mentioned earlier; instead of the activation of the reactants by (black body) radiation, they favoured the collisional mechanism. The collaboration between Christiansen and Kramers ultimately proved very fruitful, as it culminated in 1940 in the publication by Kramers of a paper entitled "Brownian motion in a field of force and the diffusion model of chemical reactions" [56]. In this work, Kramers

[1] With great regret, but for the sake of brevity, a discussion of the work of Lindemann and Hinshelwood, and subsequently of Rice-Ramsperger-Kassel-Marcus (RRKM) on the theory of collision induced unimolecular reactions in the gas phase, obviously of great importance, will be omitted here.

examines the problem of escape of a particle from a metastable state by diffusional barrier crossing. The necessary energy for the barrier crossing, the "activation energy" is provided by the thermal energy of a bath of solvent molecules, that, at the same time also exerts friction on the particle with friction constant $\xi = \frac{k_B T}{D}$. The rate of barrier crossing (for moderate to strong friction) can be expressed as [56]:

$$r = \left[\left(\sqrt{\frac{\xi^2}{4} + \omega_b^2} \right) - \frac{\xi}{2} \right] \frac{\omega_0}{2\pi\omega_b} e^{-\frac{E_b}{k_B T}} \tag{1.8}$$

where ω_0 and ω_b are the frequencies characterizing the curvature of the energy as a function of the one dimensional reaction coordinate at the bottom of the well and at the barrier top, respectively. This expression reduces to $r = \frac{\omega_0 \omega_b}{2\pi\xi} e^{-\frac{E_b}{k_B T}}$ in the limit of high friction ($r \to 0$ for $\xi \to \infty$). For low friction, equation 1.8 reduces to $r = \frac{\omega_0}{2\pi} e^{-\frac{E_b}{k_B T}}$, a result analogous to transition state theory with only one degree of freedom. Despite its high relevance for chemical problems, Kramer's theory remained largely unnoticed in the chemical community until the late 1970s [57].
The second half of the twentieth century did not yield any major conceptual advances in the field of chemical kinetics. However, more and more advanced experimental methods led to the possibility to carry out kinetic experiments with an ever better temporal resolution, and therefore to directly measure what had hitherto been rather theoretical concepts. This development culminated in the work of Ahmed Zewail (Nobel Laureate 1999), who, by means of femtosecond pump-probe laser spectroscopy, was able to obtain a direct spectroscopical signature of a transition state structure of a gas phase reaction [58]. For experimental studies of macromolecular (protein) dynamics in condensed phases, the last decades proved equally spectacular, leading from the first systematic studies of refolding kinetics [59; 60] in the late 1960s, to the very fastest single molecule folding kinetic studies possible today [61].

1.3 Protein aggregation kinetics

The aggregation of proteins into ordered fibrillar structures is by no means restricted to amyloid fibril formation. Both in a functional, as well as in a disease context, this phenomenon is prominently involved in several cases. Examples for the former class are the polymerization of actin (the study of which was pioneered by Oozawa [62]) and flagellin (from the flagella of bacteria), the most prominent example for the latter class is the polymerization of sickle cell hemoglobin, that was studied in detail by William Eaton [63]. These early studies of aggregation kinetics were performed using techniques such as turbidity measurements, sedimentation assays, calorimetry, measurements of the changes in linear birefringence or viscosity and one-dimensional NMR. The systematic study of amyloid fibril formation kinetics *in vitro* in order to obtain deeper insight into the disease mechanisms started when it was discovered that Thioflavin T, a fluorescent dye that had been used since the late 1950s to stain amyloid in tissue sections [64], could also be used as a convenient means to study

amyloid formation in vitro [65; 66; 67]. It is interesting to note that systematic *in vitro* studies of amyloid formation kinetics started much later than comparable studies for other fibrillar proteins (see above), despite the fibrillar nature being discovered at around the same time.
In addition to the dye label assay, specific for amyloid, the experimental techniques that had been established for the study of other fibrillar forms of proteins, and that are mentioned above, were subsequently also applied for amyloid studies. Those are for example turbidity [68], time-dependent sedimentation [69], light scattering [70; 71] and various spectroscopic techniques. Very important fundamental insight into amyloid formation kinetics was and is still today being gained from these experiments, and will be discussed in later chapters. However, most of these experimental techniques have severe drawbacks, such as very complex analysis (light scattering), sensitivity to non-fibrillar aggregation (light scattering, turbidity, centrifugation) and reliance on a label molecule the labeling mechanism of which is poorly understood (ThT-fluorescence). Several of these assays, together with their associated drawbacks will be discussed in more detail and contrasted to the biosensing methods developed here later in this thesis. Despite its late start, the field of *in vitro* amyloid kinetics soon reached a level that by far exceeds any of the research programs dedicated to other fibrillar proteins. This development is obviously due to the high medical relevance of amyloid formation, the phenomenon being linked to multiple diseases, as shown in Table 1.1. This high interest inevitably led, around the turn of the millennium, to the development of new ways to measure amyloid formation kinetics, mainly based on the monitoring of amyloid elongation on surfaces. There had been studies as early as the late 1990s, where the incorporation of radio-labelled amyloidogenic peptide into surface-bound amyloid deposits had been monitored, mainly in order to simulate the behaviour of brain plaques [72]. Two parallel routes of surface-bound measurements were developed, single molecule (or better "single fibril") elongation experiments and ensemble experiments. The single molecule experiments consisted of total internal reflection fluorescence microscopy (TIRF) [73] and atomic force microscopy (AFM) [74]. The first surface-based ensemble measurements relied on surface-plasmon resonance (SPR, discussed in detail in the Methods chapter) [75]. Finally, in 2007, the first reports on the use of quartz crystal microbalances for the study of amyloid fibril elongation kinetics were published [76; 77]. This thesis contains the description of the further development and of multiple applications of this new technique. It will be demonstrated here, that this novel route to measuring amyloid kinetics, due to its highly quantitative nature, is capable of providing valuable new insight into this extensively studied complex of problems.

Chapter 2

Experimental Section

2.1 Proteins

The proteins used for the formation of amyloid fibrils and the kinetic experiments of fibril elongation were either expressed according to standard protocols (human α-synuclein [78], bovine PI3K-SH3 [19]) or purchased from commercial suppliers (bovine insulin and its B-chain, hen egg white and human lysozymes, bovine β-lactoglobulin, bovine and human α-lactalbumins, from Sigma Aldrich (Dorset, UK) and Aβ (1-42) from Bachem (Basel, Switzerland). The Ure2p yeast prion protein was a kind gift from Dr Yiqian Wang, Beijing, human β2-microglobulin from Professor Vittorio Bellotti, Pavia, and human glucagon from Novonordisk, Denmark. Aβ (25-35) was synthesized via solid phase peptide synthesis by Dr Myriam Ouberai and purified by reverse phase HPLC, similarly to the protocol for the synthesis of Aβ (1-40) described in [79]. After purification, the eluted Aβ (25-35) was frozen in liquid nitrogen and lyophilized. During the lyophilisation, the peptide solution melted partly and had to be refrozen; this partial melting explains the presence of small seed fibrils in the peptide, as observed during the experiments described in Chapter 4. Peptides and proteins were usually stored in dry form at -20°C. Exceptions are Ure2p (concentrated stock solutions in 50 mM Tris buffer pH 8.4, with 200 mM NaCl added stored frozen at -20°C) and the B-chain of bovine insulin (peptide as received was dissolved in water and snap frozen).

All received or purchased peptides and proteins, except for Aβ (1-42), were used as received. The Aβ (1-42) peptide from Bachem had to be specifically treated, as described in detail in [80]. 1 mg of the peptide was dissolved in 1 ml trifluoroacetic acid (TFA), and sonicated with a probe sonicator for 30 s. Then the peptide solution was snap frozen in liquid nitrogen and lyophilized over night. The pellet was redissolved in 1 ml hexafluoroisopropanol (HFIP); this process sometimes took several minutes during which the solution was stored on ice. The solution was then divided into aliquots of 50 μl and the HFIP evaporated in a speed-vac for several hours. The dry aliquots were then stored at -20°C. This treatment was shown to break up pre-existing aggregates contained in the commercially available peptide, that strongly accelerate fibril formation (see discussion in the section on Method development). The quantity of pre-existing aggregates seems to depend on the particular batch of

peptide. It could in all cases be minimized by the chemical treatment described above. Figure 3.1 demonstrates that the frequency shift induced by contact with the TFA/HFIP treated Aβ peptide is minimal, indicating that no large aggregates are present (see subsection on biosensing for details).

2.2 Buffers and solutions

Many of the experiments described in this thesis were carried out in 0.01 M HCl. This solution was prepared by adding 2 ml of 1M HCl (Sigma Aldrich, Dorset, Uk) into a glas bottle and filling the bottle with de-ionised water to the 200 ml mark. The experiments with human lysozyme were carried out in HCl pH 1.2; here the pH was adjusted with the help of a pH electrode. For the experiments in Chapter 5, concentrated stock solutions (100 mM or 1 M) of the different salts were prepared in 0.01 M HCl, that were diluted with 0.01 M HCl and the protein stock solution for the measurements. Phosphate buffer saline (PBS) was prepared by disolving PBS tablets (Sigma Aldrich, Dorset, UK). This PBS buffer contains 10 mM phosphate buffer pH 7.4, 137 mM NaCl and 2.7 mM KCl. The 100 mM phosphate buffer (PB) for the Aβ (1-42) experiments was prepared by diluting a 500 mM PB stock solution 1:5 with DI water. The stock solution had been prepared by weighing out the appropriate amount of Na_2HPO_4 and NaH_2PO_4. Usually, solutions were not filtered or degassed.

In most cases, concentrated protein stock solutions of 1 mg/ml or higher were prepared, that were subsequently diluted to the appropriate concentrations for the QCM or other experiments. In most cases, the concentrated protein stock solutions were prepared in the same buffer in which the measurements were carried out. However, in the case of human lysozyme, stock solutions in water were used. The concentrations of protein solutions were measured and controlled either by weighing out the dry protein (large volumes and concentrations) or by measuring the absorption at 280 nm and using published absorption coefficients. In the case of human lysozyme protein stock solutions in water were prepared, the concentrations measured and the solutions aliquoted, lyophilized and the aliquots stored at -20℃. In the case of the Aβ (1-42) peptide, after each round of TFA/HFIP treatments, one aliquot was sent for exact concentration determination by ninhydrin amino acid analysis (Department of Biochemistry).

For the ThT experiments of insulin fibril elongation (Chapter 5), the DLS experiments of insulin fibril elongation (Method development and Chapter 5) and for the ITC experiments (Future work chapter) of insulin fibril elongation, both the seed fibril suspensions and the solutions of monomeric protein were filtered through a 220 nm syringe filter (Millipore), to avoid the introduction of dust particles that can disturb the measurements through light scattering (DLS and ThT) or enthalpic effects (ITC).

2.3 Seed fibril formation

The transformation of the soluble monomeric proteins into insoluble amyloid fibrils also followed the published protocols in most cases: PI3K-SH3 [19], α-synuclein [81], bovine insulin [76], insulin B-chain [82], hen egg white [83] and human lysozyme [84], bovine β-lactoglobulin [85], α-lactalbumin [86] and yeast Ure2p Sc/Sp [87]. In other cases, where the protein under study formed amyloid particularly readily under acidic conditions (e.g. human glucagon and human β2-microglobulin), it was usually dissolved in 0.01 M HCl. In most cases the final pH was not adjusted to compensate for the buffering effect of the protein. Therefore, if different protein concentrations were used, the ionic strength, rather than the solution pH was controlled, as the influence of this variable was studied in detail in Chapter 5.

In most cases, the protein solutions were stirred magnetically, considerably accelerating the fibrillization reaction. In particular for α-synuclein, some mechanical action like shaking or stirring was indispensable - quiescent samples never became fibrillar, as judged by AFM imaging. In general, stirring appeared to be more efficient in inducing fibrillization compared to shaking. For the Aβ (1-42) a particular procedure was applied. The observation that the commercially available peptide contained pre-formed aggregates was exploited by producing aliquots in NaOH that were subsequently diluted into 100 mM phosphate buffer at pH 7.4 (see Aβ (1-42) surface attachment protocol at the beginning of the next chapter for details). Aβ (1-42) and α-synuclein fibrils were in most cases freshly prepared for each experiment, as the fibrils were not stable for prolonged times. The Ure2p Sc and Aβ (25-35) fibrils could be stored at 4℃ for several weeks. All other fibril samples (under acidic conditions) were stored at room temperature.

2.4 Reduction and passivation of disulphide links in human lysozyme

In order to probe the influence of the disulphide links on the stability and amyloidogenicity of a protein (see Chapter 4), the 4 disulfide links in human lysozyme were cleaved by reduction and passivated. The protein was incubated for 2 h with an 80-fold excess of tris(2-carboxyethyl)phosphine (TCEP) in 50 mM Tris, pH 8.5 and 6 M GndHCl for 2 h, while shaking. An 80-fold excess (with respect to protein) of iodoacetamide (IAA) was added and the solution was again stirred for 2 h. Finally, the solution was dialysed for 24 h against 10 mM formic acid, and the resulting protein solution was lyophilized for several days. Mass spectrometric analysis confirmed the quantitative cleavage of the four disulphide bonds and subsequent passivation of the thiols (Figure 2.1). This protocol was provided by Dr Anne Dhulesia.

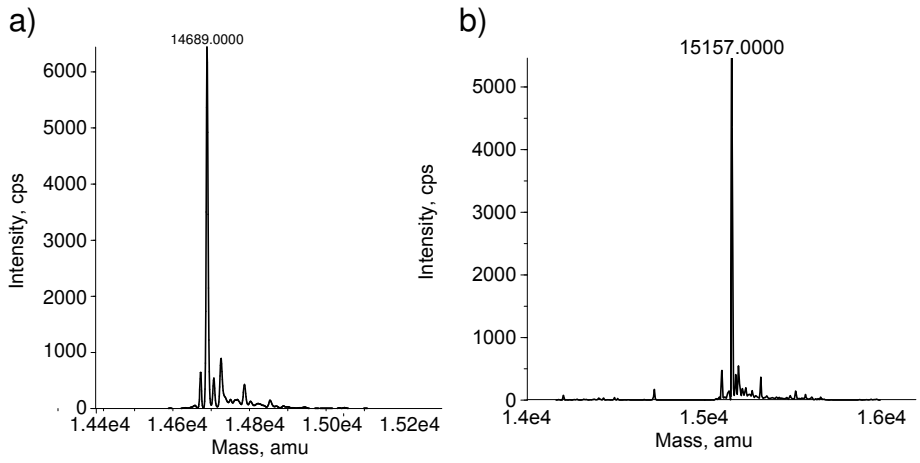

Figure 2.1: Mass spectra of WT human lysozyme. a) Native form b) reduced and alkylated form.

2.5 Calculation of entropies of transfer of peptides and proteins as a measure of their hydrophobicity

The basis of the calculation of the average free energies of transfer of the core residues of amyloid fibrils (for Figures 4.8 and 4.10) are the partition coefficients between water and octanol of N-acetyl-aminoacid-amides, as reported by Fauchere and Pliska [88] and the free energy values that Eisenberg and McLachlan have calculated from these coefficients [89]. The original measurements had been carried out at neutral pH. In the case where the kinetic measurements of amyloid growth were carried out at acidic pH, error bars were therefore added in the hydrophobicity dimension, that are proportional to the number of acidic amino acids in the respective core region of the protein. An estimate of the magnitude of such errors was performed by comparing the partitioning coefficients measured by Kim and Szoka [90] for several amino acids (within tripeptides) at different pH values. In addition, for the reduced form of human lysozyme, the free energy of transfer of glutamine, rather than that of cysteine was used for the 8 modified cysteine residues, as the introduced modification, that prevents the disulphide bonds from reforming, resembles a glutamine residue.

In order to compute the average free energies of transfer for folded proteins, the interior of proteins and the exterior of proteins of mesophilic bacteria (see top of Figure 4.8 b), the average amino acid composition of these respective parts was taken from [91], averaging between intracellular and extracellular proteins.

2.6 Spectroscopic techniques to study protein unfolding and aggregation

2.6.1 CD spectroscopy

The circular dichroism experiments described in Chapter 4 were carried out using a Jasco J-810 spectropolarimeter equipped with a Peltier holder. Spectra were recorded using cells of 0.1 and 1 cm path length for the far- and near-UV, respectively, with a protein concentration of ca. 20 μM, at 35°C.

2.6.2 Thioflavin T fluorescence

As discussed in the introduction, Thioflavin T is the most commonly used label molecule in kinetic assays of amyloid fibril formation and growth. When ThT molecules bind to amyloid fibrils, the excitation spectrum undergoes a characteristic red-shift that allows to excite the fluorescence around 440 nm and to measure the emitted fluorescence at 480 nm [67]. When ThT is used in kinetic assays, usually the fundamental assumption is made that its fluorescence reports accurately on the quantity of amyloid fibrils present in a given sample. In Chapter 6 of this thesis, a case will be discussed where this assumption is severely invalidated, strongly underlining the necessity for label-free alternatives to probe amyloid fibril formation kinetics. Here, the discussion will be restricted to two observations that have implications for the following chapters. In Figure 2.2, it is demonstrated that, all other conditions being equal, the ionic strength and the temperature influence the fluorescence efficiency of ThT bound to amyloid.

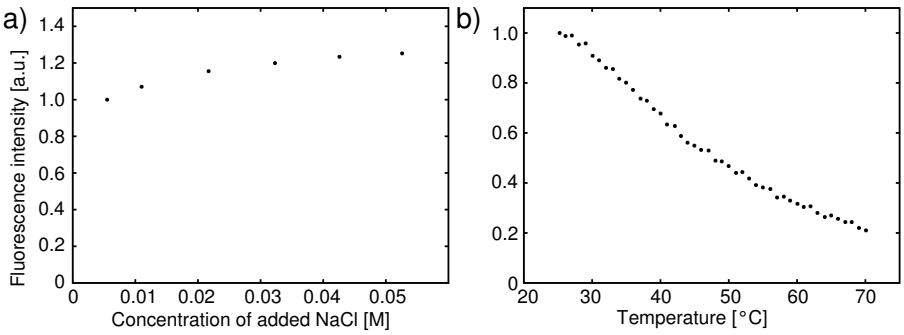

Figure 2.2: a) The dependence of the fluorescence of ThT bound to insulin amyloid fibrils on the concentration of NaCl was probed. It can be seen, that even small concentrations of this salt can enhance the fluorescence by 20% (details in the main text) b) a similar experiment was performed to probe the temperature dependence of the fluorescence efficiency of ThT bound to amyloid fibrils, in this case formed from the protein hen lysozyme. The drastic decrease in fluorescence over the temperature range studied stresses the need for appropriate normalization of the fluorescence data when the temperature dependence of amyloid formation is studied.

Figure 2.2 a) shows an experiment, where increasing quantities of NaCl were added to aliquots of an insulin fibril suspension (0.06 mg/ml in 0.01 M HCl). It can be seen that the fluorescence level varies by more than 20%. It is important to note that this variation cannot be explained through a change in the equilibrium between free soluble protein and fibrils, as the equilibrium is already very much shifted towards the fibrillar state [34] in the absence of added salt, with much less than 20% free monomer that would be required to explain the increase in fluorescence with a shift in equilibrium. In addition, the change in fluorescence is immediate upon addition of salt (time resolution of experiment < 1 min) and a shift of the equilibrium would take longer to complete, as estimated from measurements of absolute elongation rates (see Chapters 4 and 5). In Figure 2.2 b), a similar experiment is shown, but here, the change in fluorescence with temperature is probed for hen lysozyme amyloid fibrils ($\sim$ 5 mg/ml fibrils, 100 μM ThT). The fluorescence of a given aliquot decreases to 20% of its initial value in the temperature range from 25-70°C. Taken together, these findings indicate that care has to be taken in the analysis of fluorescence data from experiments probing the influence of these factors and appropriate normalizations have to be carried out. Interestingly, ThT does not show the same strong temperature dependence of its fluorescence efficiency for all proteins (see discussion of Aβ (25-35) experiments).
Below, the exact protocols for the elongation assays that are quoted in later chapters are given. All kinetic experiments with ThT were performed using an Optima platereader, with bottom optics. 96 well plates with low protein binding were used. The measured fluorescence per data point was the average of 50 excitation flashes. Excitation wavelength was 440 nm, emission was recorded at 485 nm. Maximum amplitude shaking was employed after each cycle, and no additional shaking was used.

Temperature dependence of human Aβ (25-35) amyloid elongation:
After initial experiments had shown that seeding the peptide sample did not noticeably accelerate the fibrillation kinetics, AFM imaging of the supposedly monomeric synthesized peptide revealed that very short seeds were already present (see Figure 4.4). The seeds probably formed during the freeze drying process, where the mixture of acetonitrile and water (from the elution of the reversed phase column) melted partly, and had to be refrozen. During the melting, presumably very high peptide concentrations were sampled, leading to the formation of aggregates. Therefore, subsequent runs were performed without seeding. This raises the question, whether the assay can still be considered as a pure elongation assay or if primary nucleation contributes significantly to the kinetic profile. However, as can be seen from the fluorescence traces in Figure 4.4, no acceleration of the reaction is observed, and the overall profile corresponds very well to that of a seeded reaction (see e.g. [92]). In addition, the fact that the fluorescence increased by more than an order of magnitude during the time course of the reaction indicates that the initial proportion of seeds must be of the order of 10 % or less. Therefore, aliquots of 0.1 mg Aβ (25-35) in 180 μl of water were prepared, and 5 μl of a 2 mM ThT stock solution in water were added. The aliquots were snap frozen in liquid nitrogen and stored

at -20℃. Such an aliquot, when melted and monitored in the platereader, did not show any increase in fluorescence over several hours. Therefore, 20 μl of PBS were added, which led to the traces shown in Figure 4.4. At this stage, an additional crucial point has to be mentioned, emphasizing the care that has to be taken in using ThT for kinetic studies. If the PBS was added before the addition of ThT, the fluorescence traces had a completely different character. The total fluorescence increase was only of the order of 50% and this increase was completed after 30-60 min. It was crucial to add the PBS last, in order to get the curves of Figure 4.4. These experiments were carried out in the temperature range from 28 to 40℃; in this case the temperature dependence of the final fluorescence level was not pronounced; therefore no normalization was carried out. As can be seen from Figure 4.4, a clear difference in elongation kinetics could not be resolved in the temperature range studied. It is therefore concluded that the enthalpy of activation $\Delta H^{\ddagger}$ must be of the same order as for the proteins with the smallest measured values by QCM (see Chapter 4), i.e. of the order of 25 kJ/mol, or smaller.

Temperature dependence of human glucagon amyloid elongation:
Separate aliquots for monomer and fibrils were prepared. 50 μl of 5 mg/ml sonicated (1 min) seed fibrils were diluted with 1500 μl 0.01 M HCl. 50 μl of 1 M NaCl in HCl were added, and the fibril suspension divided into 10 aliquots that were snap frozen in liquid nitrogen and stored at -20℃. 1.8 mg glucagon was dissolved in 300 μl of HCl 0.01 M and 50 μl of a 2 mM ThT stock solution in water was added. The solution was divided into 10 aliquots, snap frozen and stored at -20℃ as well. For the measurement, the aliquots containing the fibrils were pre-heated to the temperature that was to be studied and the small volume of concentrated monomer solution was added. This strategy allowed to minimize initial non-linearities of the data, due to the opposing effects of fibril elongation, leading to an increase in fluorescence and the decrease of fluorescence due to the temperature increase. Glucagon showed a strong dependence of the endpoint fluorescence on the temperature, therefore the fluorescence traces had to be normalized on the same final level of fluorescence. The initial slope was then taken as being proportional to the elongation rate.

Ionic strength dependence of bovine insulin amyloid elongation:
Seeded ThT fluorescence experiments with bovine insulin were performed at 40℃. The aliquots contained 0.01 mg/ml seed fibrils (sonicated for 10 min as described in more detail in the section on Method development, 0.5 mg/ml protein monomer, and 0.2 mg/ml ThT in 0.01 M HCl. The fluorescence curves were scaled to the same maximal fluorescence value, in order to account for different final levels (see raw data in Figure 2.2). Then the initial linear part of the curves were fitted with a linear function and the slopes were taken to be proportional to the elongation rates.

2.7 Biosensing measurements of fibril elongation

One of the objectives of this thesis is to demonstrate that surface-based measurements of amyloid elongation kinetics are a powerful means of getting fundamental insight into the regions of free energy landscapes of proteins corresponding to ordered aggregation. These measurements, where an ensemble of surface-bound seed fibrils is brought into contact with a solution of soluble protein are in contrast to the more traditional solution state assays, such as light scattering and Thioflavin T fluorescence, that are discussed elsewhere in this chapter and in the introduction. The large majority of kinetic experiments described in this thesis have been performed by using quartz crystal microbalances (QCM). However, another surface-based technique has been examined in less detail for its suitability of being used for kinetic elongation assays: surface plasmon resonance (SPR).

2.7.1 Surface plasmon resonance (SPR) measurements

Surface plasmon resonance has been used for almost 30 years now to study biomolecular interactions [93; 94]. SPR is routinely used to study in a qualitative way the interactions between different macromolecules, one of which is attached to the surface ("ligand") and the other ("analyte") is flushed over the surface and potentially captured by the ligand. It can also be used for more quantitative studies of the association and dissociation rates of the two interacting partners, as well as for measurements of the binding equilibria, that are closely connected to the on- and off-rates.
The physical basis of SPR is illustrated in Figure 2.3.

When a light beam falls onto a glass surface with a sufficiently large angle, it will be totally reflected. However, if the glass is covered with a gold layer, a certain angle θ_r exists, under which the reflected light is less intense than the incident beam. This is due to the absorption of some of the electromagnetic energy by the electron gas of the gold layer. If a certain resonance condition is fulfilled (energy and momentum conservation) between the incident photons and oscillations of the electron gas along the surface, so called plasmons, then the incident beam excites these plasmons. Due to the fact that the electromagnetic field oscillations can penetrate a certain distance ($\sim$ 300 nm) into the liquid that covers the gold surface (as exponentially decreasing evanescent waves), the refractive index in the liquid layer close to the surface influences the resonance condition of the surface plasmons. When molecules such as proteins attach to the surface, this leads to a change in refractive index and therefore to a shift in the resonance condition. The incident angle of least reflected intensity will be slightly shifted and it is this shift that is measured. The relationship between the quantity of absorbed material and the induced shift in angle can be empirically calibrated. The angle shift is quoted in so called response units (R.U.), and one response unit corresponds to a shift in resonant angle of $\sim 10^{-4\circ}$ [95].
In the framework of the studies described in this thesis, SPR was used to monitor the elongation of surface-bound insulin seed fibrils. Here, the seeds play the role

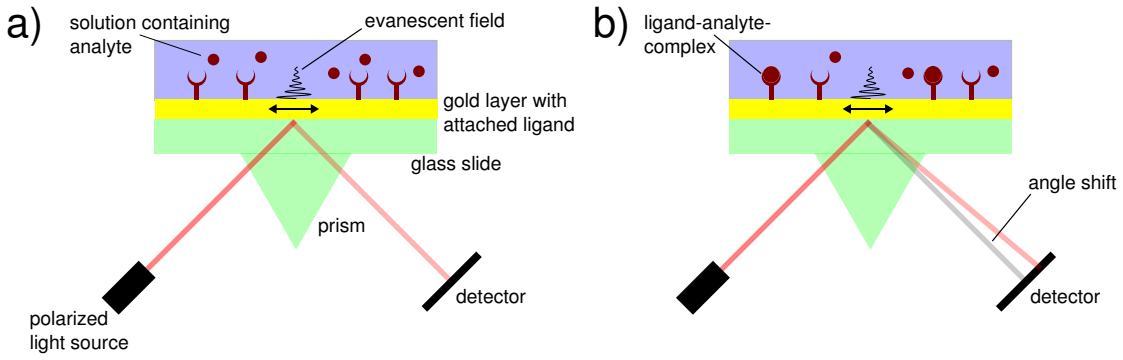

Figure 2.3: a) Illustration of the geometry of an SPR set-up. The incident beam is totally reflected at the boundary between glass and a thin gold layer, and the reflected beam is weakened in intensity compared to the incident beam, at a certain angle θ_r. The gold layer is covered with the ligand and the analyte solution is brought into contact with the surface. b) If the analyte interacts with the ligand, the refractive index of the layer closest to the surface increases and this change in refractive index leads to a shift in the resonance condition of the incident beam with the surface plasmons. This shift in angle of least reflected intensity is measured.

of the ligand and the soluble protein that of the analyte. The addition of soluble protein onto the seeds induces the required shift in resonant angle. SPR has been used in a number of studies to study protein aggregation [75; 96; 97; 98]. In all of these studies, the protein (aggregates and soluble) was brought into contact with the SPR surface via the flow system. In the present study, however, the sensor surface was incubated with the seed fibrils *ex situ*, similar to the QCM experiments, in order to avoid contamination of the flow system with protein aggregates, and also in order to be able to control more accurately the fibril attachment process. Below, the detailed protocol is given for these experiments.

Protocol for an SPR measurement of insulin amyloid fibril elongation: The surface attachment of the insulin seeds was performed in analogy to the preparation of QCM sensors (see section on cysteine attachment in the following chapter). The gold substrates used were 10x12 mm gold substrates from Ssens, Netherlands, and they were glued into the original cassette from Biacore with double sided tape. The sensor was inserted into a Biacore 3000 (GE Healthcare) and equilibrated in 0.01 M HCl (filtered and degassed) until a stable baseline was established. The elongation of the seed fibrils on the SPR sensor was monitored at 40°C, the maximum temperature achievable with this system. The seeds were repeatedly incubated with insulin monomer solution under varying conditions and the rate of net shift in "response units" during an incubation (see Figure 5.1) was taken to be proportional to the elongation rate, and fitted with a linear function, similar to the QCM measurements (see below).

2.7.2 Quartz crystal microbalance (QCM) measurements

Quartz crystal microbalances have been used to measure thicknesses and masses of thin films for more than 50 years now. Sauerbrey in 1959 [99] first realized that the frequency of a quartz oscillator vibrating in shear-mode linearly decreased for small added masses, according to:

$$\Delta f \approx \frac{f_0}{\rho_0 h_0 A} \Delta m \tag{2.1}$$

where Δf is the frequency change induced by the added mass, f_0, ρ_0 and h_0 are the resonant frequency, density and thickness of the quartz disk, respectively, A is the active area of the disk and Δm is the small added mass. However, this simple relationship is only valid for thin films on a quartz resonator that is otherwise in contact with vacuum or air. In the 1980s, it was empirically realized that the damping induced by contact of the quartz with liquid did not prevent the use of a QCM in liquid. The theoretical framework for operation of QCM in liquid was then established by Kanazawa [100]. He showed that the viscous drag that the liquid exerts on the QCM leads to an additional frequency shift, compared to operation in vacuum or air, that depends on the density and viscosity of the liquid:

$$\Delta f = -f_0^{\frac{3}{2}} \sqrt{\frac{\rho_l \eta_l}{\pi \rho_0 \mu_0}} \tag{2.2}$$

where ρ_l and η_l are density and viscosity of the liquid, and μ_0 is the shear modulus of the quartz. The shear waves decay exponentially into the liquid, with decay constant $\delta = \sqrt{\frac{\eta_l}{\pi \rho_l f}}$ [100]. δ is of the order of 250 nm in water. This development opened up the possibility to use a QCM for biosensing. Further conceptual advance in respect to biosensing applications was made when it was understood, how the viscoelastic properties of layers of material attached to the surface of the QCM influence the oscillatory behaviour of the quartz disk. Voinova et al. solved the problem for two viscoelastic layers on top of the QCM surface that is in contact with a Newtonian fluid [101]. The continuum mechanical approach presented in this work is more readily accessible to non-specialists than the alternative description in terms of Butterworth-van-Dyke (BvD) equivalent circuits (see e.g. [102]), as no analogy between a physical parameter of the oscillator and a lumped element of the equivalent circuit has to be drawn. One of the most important consequences of the viscoelastic properties of biological materials in the context of QCM biosensing is the so-called "missing mass" effect [103]; the finite rigidity of the attached biological material (e.g. proteins or lipids) can lead to an underestimation of the attached mass from the induced frequency shift, when it is interpreted according to the Sauerbrey equation (2.1). The non-validity of the Sauerbrey-equation can often already be inferred from the observation that the normalized higher harmonics show a different frequency shift; in the framework of Sauerbrey's simple theory, no difference is expected. It is therefore in principle possible to characterize in detail the viscoelasticity of a surface-bound layer through an analysis of the differential mass sensitivity of the frequency overtones. All of these theoretical descriptions

are, however, only valid for smooth homogeneous layers of added material. The most recent conceptual advance in the development of liquid QCM is the attempt to understand the influence of surface and add-layer roughness on the frequency shift and energy dissipation of the QCM. Experimental [104] and theoretical [105] studies show that solvent trapped within the groves formed by a rough add-layer can lead to an additional frequency shift, leading, in turn to an overestimation of the attached mass. Figure 2.4 illustrates the principle of QCM operation in liquid, in a mode of operation where the crystal is periodically excited to vibrate and the frequency of vibration, as well as the damping and associated decay constant is measured (QCM-D).

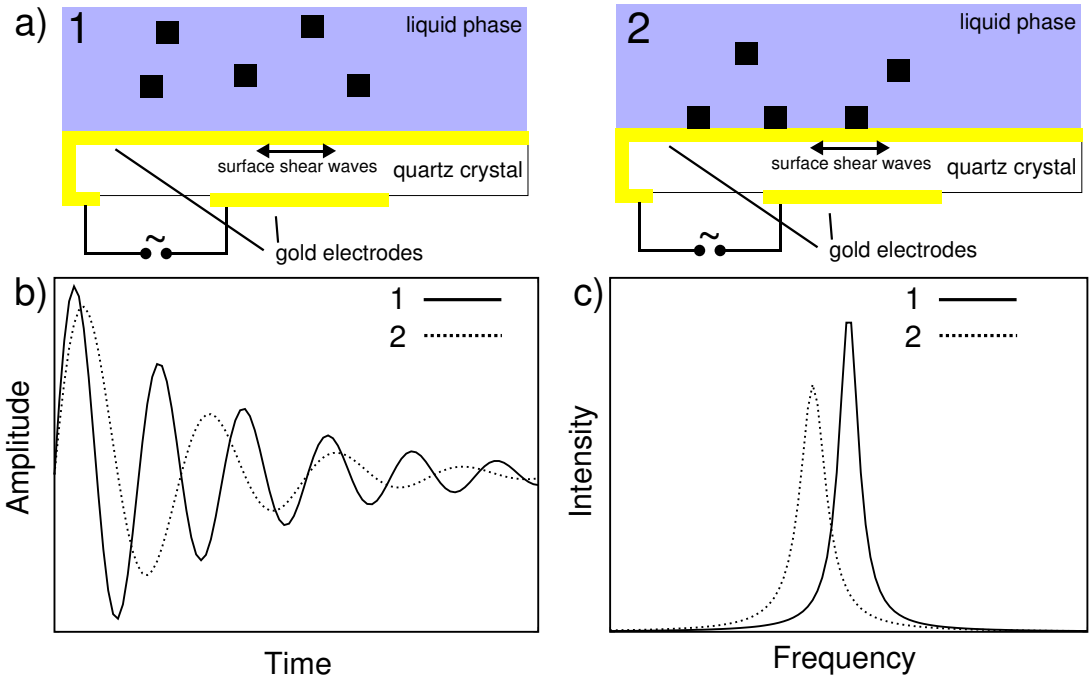

Figure 2.4: a) The gold-coated quartz crystal is immersed in liquid, and excited to vibrate in shear mode (1). An analyte is brought into contact with the surface and the attachment of this analyte to the surface is monitored in real time (2). b) The time domain signal is shown, a damped harmonic oscillation. Attachment of viscoelastic material to the surface leads to a more strongly damped, lower frequency vibration of the crystal, compared to the situation before the attachment. c) The frequency domain signal. The dissipation manifests itself in a broadening of the peak, and the frequency is shifted.

The use of QCM to study protein aggregation and amyloid formation is quite recent, and was pioneered in Cambridge [76]. However, several other groups are using QCM as well to study various stages in the pathway from soluble protein to ordered aggregates, [77; 106; 107], as well as the chemical and mechanical properties of these aggregates [108; 109].

General protocol and indications for QCM measurements: The initial experiments were carried out with a QCM D300 (Q-Sense, Västra Frölunda, Sweden), where only one sensor could be monitored at one time and the liquid was introduced into the cell via a gravity flow system. However, the majority of the experiments was carried out with the more recent model E4 (also Q-Sense), where 4 sensors could be monitored simultaneously and the liquid was introduced via a peristaltic pump where the flow rate can be more easily controlled. In all cases, gold coated QSX 301 sensors were used (Q-Sense), due to the ease of functionalization of the gold. The surface functionalization and amyloid seed fibril attachment is described in detail below in the section on Method development. After introducing the sensor into the microbalance, the system was left to equilibrate for a minimum of 12 h (D300) or 3 h (E4) to allow for a stable baseline to be established (drift smaller 1 Hz/h). If the sensor had already been incubated in buffer before inserting it into the microbalance, the establishment of the baseline was faster. The protein solutions were introduced from Eppendorf tubes, usually 300 μl at a flow rate of 150 μl/min. The volume used was much larger than the volume of the QCM flow cell (40 μl); this was necessary in order to ensure that the sample had completely replaced all of the previous solution from the flow system. The rates of frequency shift induced by the elongation of the surface-bound fibrils varied by several orders of magnitude, ranging from a few Hz per hour to several dozens of Hz per minute, depending on the protein under study and the conditions employed. Measurements were carried out in the absence of flow, therefore for the very lowest concentrations and the fastest growing protein fibrils, depletion effects could be observed. As discussed below, the quantitative depletion of the cell can be used to calibrate the frequency response.
For data analysis, the fundamental frequency was never used; it is well-known [110] that due to the lack of energy confinement to the centre of the sensor in the case of the fundamental frequency, boundary effects, such as the way the sensor is mounted, as well as external perturbations such as pressure and temperature changes affect the fundamental frequency more than the higher overtones. Usually, the harmonics with N = 3,5,7 were used for analysis; this is justified below. The frequency response of the different overtones was usually not identical, and fibrils made from different proteins showed different degrees of divergence of their frequency response. This observation, in combination with the possibility to monitor the energy dissipation of the oscillations with this set-up (the dissipation $D = \frac{1}{\pi f \tau}$ is defined in terms of the time decay constant τ of the quartz oscillations; the QCM-D technology is based on pulsed excitation of the quartz resonator, rather than continuous excitation) might allow in principle to extract material properties of the surface-bound fibril layer. However, as can be seen from many AFM images in this thesis, the surface-bound fibrils do not form a smooth homogeneous layer, but rather a dense network leading to an increase in roughness compared to the uncoated sensor. In addition, the elongation of the seed fibrils is likely to lead to a different degree of coupling between the sensor surface and the liquid, compared to the coupling between the passivated sensor surface and the liquid, due to the different hydrophobicity of protein and passivation layer. Taken together, the effects stemming from the viscoelasticity of the protein fibrils and the changing roughness and surface chemistry will lead to a

proportionality coefficient between attached fibril mass and induced frequency shift that is very difficult, if not impossible to calculate from first principles. Therefore, it was decided early on in the work that led to this thesis, that an empirical approach where the mass sensitivity coefficient is calibrated, will be adopted. This approach is described in the chapter on method development. However, much of the work described in this thesis (Chapters 5 and 6) relies on the measurement of relative changes in rate, rather than absolute rate measurements; in these cases the divergence of the harmonics did not have much impact, as the relative change in rate was in most cases virtually independent of the particular overtone under consideration. A given sensor can only be used for a series of measurements up to a certain total frequency shift; this total frequency shift ranged from $\sim$ 50 Hz to $\sim$ 200 Hz, depending on the protein and the seed fibril length and surface density. The higher the fibril surface density, the more total frequency shift could be induced without an observable decrease in mass sensitivity. This range was empirically determined by reproducibility tests; at the end of a series of elongation experiments under changing conditions, the seed fibrils were again incubated with monomer under the same condition as in an initial experiment, and the reproducibility was assessed. Outside this usable range, the divergence between different harmonics increases strongly. The physical origin of this limited usability of a single sensor is likely to be crowding of the elongated seed fibrils that prevents them from elongating further. Additionally, the finite rigidity of the fibrils together with the fact that only the seed fibrils were covalently attached to the surface, and not the freshly elongated parts, it is possible that the entire fibril does not follow the vibration of the crystal any more when the total fibril length exceeds a certain threshold.

At the end of a QCM experiment, the flow cell and tubing system was cleaned with 1 N NaOH solution for several minutes and then extensively flushed with DI water. In the cases where QCM fibril elongation experiments were carried out with low concentrations of soluble protein (of the order of 10 μM), it sometimes took several injections of soluble protein to obtain a reproducible rate of frequency shift. This observation indicates that some of the protein was absorbed in the freshly cleaned flow system, such that the concentration of soluble protein inside the cell and in contact with the QCM sensor was not well controlled. Once the flow system is saturated with a coating of protein, the experiment regains its usual high reproducibility.

2.8 Cleaning and reuse of QCM sensors

The gold coated QCM chips to which amyloid fibrils were attached in this study were cleaned and reused. To remove the protein fibrils, the crystals were immersed in 7 M sodium hydroxide solution at 80°C for 2 h. The self-assembled monolayers (SAM) of either PEG thiol or cystamine on the gold surface were removed electrochemically [111]. A voltage of -2 V was applied to the gold surface of the crystal for ca. 1 min against a gold counter electrode in 100 mM phosphate buffer. The chips were then rinsed with distilled water and dried with nitrogen for reuse. Alter-

natively, after the removal of the proteinacious material by the NaOH treatment, the sensors were UV/O_3 cleaned by exposing them for 10-20 min to the intense UV light (172 nm) in an Excimer photon source sample cleaner. The reactive oxygen species that form will etch off any organic contaminations. The cleaning results from the use of this method yielded larger contact angles (estimated) compared to the electrochemical cleaning.

2.9 Dynamic light scattering

2.9.1 Size measurements

The basis of dynamic light scattering is the measurement of the auto-correlation function of the light scattered by particles or molecules in solution and collected by a light-sensitive detector [112]. The idea is that the fluctuations of the detected light reflect the erratic thermal motion of the scattering centers. The autocorrelation function of a property A (e.g. the light intensity at the photodetector) is defined as [112]:

$$\langle A(0)A(\tau)\rangle = \lim_{T\to\infty}\frac{1}{T}\int_0^T dtA(t)A(t+\tau) \tag{2.3}$$

For many random physical processes, the auto-correlation function decays exponentially, due to the short term memory of such (Markoff) stochastic processes. If the fluctuation of the quantity A is defined as $\delta A(t) = A(t) - \langle A\rangle$, where $\langle A\rangle$ is the mean of the quantity A, the correlation function of the fluctuation then simply decays according to:

$$\langle \delta A(0)\delta A(\tau)\rangle = \langle \delta A^2\rangle e^{-\frac{\tau}{\tau_r}} \tag{2.4}$$

as $\delta A(0)$ has zero mean. τ_r is called the correlation time of the system. In a homodyne light scattering experiment, the scattered light is only correlated with itself. In a heterodyne experiment, on the other hand, the scattered light is superimposed to a small portion of the initial light beam that had been separated via a beam splitter. The set-up used in the experiments described in this thesis were all homodyne scattering experiments. It can be shown that for a spherical particle performing Brownian motion, the homodyne correlation function can be written as [112]:

$$F(q,t) = \langle N\rangle^2 + \langle N\rangle^2 e^{-2q^2Dt} \tag{2.5}$$

where N is the number of scattering centres in the scattering volume, and $\mathbf{q}$ is a vector defined in terms of the wavevector of incident and scattered light according to $\mathbf{q} = \mathbf{k_i} - \mathbf{k_s}$; q is constant and known for a given scattering geometry. Therefore, a fit of the correlation function to an exponential function allows the determination of the diffusion coefficient of the spherical particle. This diffusion coefficient can then be related to the size of the particle via the Einstein relation:

$$D = \frac{k_B T}{\xi} \tag{2.6}$$

where the friction coefficient ξ is given by the Stokes equation for a sphere with sticky boundary conditions $\xi = 6\pi\eta R$, with R the radius of the sphere.

2.9.2 ζ-potential measurements

If a particle or molecule in solution is subjected to an external force, its motion will be a superposition of the motion induced by the force and its intrinsic Brownian motion. In the case of a charged particle in an electric field E, the terminal velocity v of the particle induced by the field is $v = \mu E$, where the mobility μ is given by $\mu = \frac{Q}{\xi}$, with Q the charge of the particle. However, if the solution contains an electrolyte, this simple relationship does no longer hold. As was shown by Helmholtz and Debye and Hückel [113], some counter ions will attach to the particle and form the so called Helmholtz-plane. In addition, a cloud of counter-ions will form around the charged particle and the potential drops exponentially around the charged particle, according to:

$$V(r) = \frac{Q_{eff}}{4\pi\epsilon_0\epsilon_r r} e^{-\kappa r} \tag{2.7}$$

where κ is the inverse of the screening length and depends on the ionic strength of the solution (see the appendix to Chapter 5 for a derivation). If the particle is subjected to an external field, it will start to migrate and only the tightly attached ions will be able to follow this movement. There will be a slip plane between ions that follow the movement and those that don't and the potential difference between this slip plane and the bulk of the solution is called the ζ-(zeta-) potential. For a given composition of the suspension medium, the ζ-potential is a measure of the surface charge of the particle. In the presence of a double layer of counterions, the mobility of the charged particle under the influence of an external electric field is reduced. It was shown by Henry [114], that the mobility can then be written:

$$\mu = \frac{2\epsilon\zeta}{3\eta} f(\kappa R) \tag{2.8}$$

where the cgs units of Henry's original paper have been converted to SI units, and where ζ is the ζ-potential, and f(κR) is called Henry's function. This function varies between 1.0 to 1.5 for variations of the product κR of the inverse Debye screening length (a measure for the thickness of the double layer) and the particle radius from 0 to ∞. The former situation corresponds to Hückel's approximation, the latter to Smoluchowski's approximation. Smoluchowski's approximation is valid for most cases, where charged particles are immersed in aqueous electrolytes. However, in the case of short amyloid fibrils or even monomer in low conductivity media, such as is the case in the measurements carried out for this thesis, the product κR is of the order of one, in a region where neither of the approximations is strictly valid. In addition, the above discussion based on a simple picture of the electrical double

layer is only strictly valid for moderate surface charges (< 25 mV). However, for the qualitative comparison between the charge state of fibrils and soluble protein attempted in Chapter 5, the similarity in the systems will lead to a reasonable comparability.

2.9.3 General protocols for size and ζ-potential measurements of proteins

The use of dynamic light scattering to follow the elongation of seed fibrils is described in detail at the end of the next chapter. Here the description is limited to the measurement of sizes of soluble protein. DLS measurements were carried out, using a Malvern zetasizer nano (Malvern, Worcestershire, UK). Usually, 300 μl of sample were filled into a small volume disposable plastic cuvette (Fisher scientific). The standard settings of the zetasizer were used for the automatic data analysis. In most cases (except for very monodisperse samples), the maximum of the number distribution by size was taken as the size of the particles. In cases where the scattering was very much dominated by a single population of particle sizes, the Z-average (cumulant mean) value of the size was used. DLS size measurements were often used for qualitative checks of the aggregation state of protein solutions, that were the starting point for aggregation assays.
Dye interaction experiments of Chapter 6: Concentrated stock solutions of CR (2 mM) and ThT (1 mM) in water were prepared and these stock solutions were diluted with 100 mM PB to the appropriate concentrations of 50 μM (CR) and 30 μM (ThT). The dye solutions were not filtered, as some of the dye was absorbed in the filter, and therefore the concentrations would be changed upon filtering, but in order to minimize interference with the measurement by dust particles, the PB was filtered before the dilution. Then the size distribution of the dilute dye solutions was measured. The ThT solution was weakly scattering and could not readily be distinguished from pure buffer. A 1:1 mixture of these solutions was then prepared, i.e., a solution containing 25 μM CR and 15 μM ThT, and the size distribution was again measured. The concentration of the ThT solution was chosen lower than that for the CR solution, because a ThT solution at 50 mM already showed the presence of aggregates. Therefore, to facilitate the detection of the formation of ThT-CR clusters, a 30 μM solution of ThT was used.

The ζ-potential of sonicated fibrils and soluble protein (bovine insulin) was measured using clear disposable zeta cells (Malvern, UK). The acidic solution conditions necessary to induce insulin fibrillation made the use of the dip cell with Pd electrodes (Malvern) impossible, as electrode blackening occurred immediately and a black precipitate was formed at the electrodes. However, the gold coated electrodes of the disposable cells were less prone to induce the formation of this precipitate. In addition, it was attempted to load a small volume of the sample with a gel loading tip to the bottom of the cell, that had previously been filled with buffer. This method, if carefully performed will minimize the contact between the protein solution and the electrodes. However, as an additional complication, that could not be avoided, gas bubbles formed at the electrodes, probably due to outgasing and

electrolysis occurring in the acidic solution due to the application of high voltages. The bubbles had to be periodically removed after a few measurements, as long term reproducibility was impaired by the gas bubbles at the electrodes. In general the measurements of the ζ-potential of sonicated amyloid insulin fibrils (100-200 nm) were characterized by a good reproducibility, and the size distribution was not altered by the application of the voltage, as confirmed by size measurements before and after the ζ-potential measurements. The ζ-potential of soluble protein was more difficult to measure, and the reproducibility was less good. In addition, small aggregates formed during the application of the voltage; therefore the results have to be interpreted more carefully. All these difficulties have been reported before and discussed and analyzed in detail in [115]. However, the qualitative conclusion drawn in Chapter 5, that soluble protein and fibrils have similar charge densities is unlikely to be affected by these considerations, as the fibrils were found to have systematically higher ζ-potential ($> +35$ mV); this finding allows to draw the conclusion that amyloidogenic proteins do not have to be globally neutral in order to incorporate into amyloid fibrils, contrarily to recent reports [116].

2.10 Atomic force microscopy (AFM)

All AFM images shown in this thesis were acquired with tapping mode in air using a Molecular Imaging PicoPlus (Tempe, AZ) atomic force microscope. The cantilevers employed were NSC36 SiN cantilevers (MikroMasch, San Jose, CA), with a resonant frequency of ~ 150 kHz.
In most cases where AFM images of the fibril-coated gold surfaces of QCM sensors were taken, the surfaces had been imaged after the end of the experiment. However, it is also possible to dry the sensor surface directly after seed fibril attachment for imaging. If the sensor is afterwards immersed back into buffer, the seeding efficiency is not appreciably decreased. Therefore, intermediate drying (not exceeding several hours) does not seem to induce irreversible structural changes in the amyloid seed fibrils.

2.11 Mass spectrometry

All mass spectrometric experiments the results of which are presented in this thesis were carried out by Asha Boodhun at the mass spectrometry facilities of the Department of Chemistry.
In order to determine the degree of chemical modification of the activated amyloid fibrils, they were dissociated either via abrupt changes in pH (2.0 to ca. 12.0 in the case of PI3K-SH3 and 7.4 to ca. 0.5 in the case of α-synuclein) or via suspension in DMSO (α-synuclein) and then examined by mass spectrometry. The protein samples were purified from buffer salts and excess reagents with Ziptip C18 (Millipore, MA) and eluted in 50% acetonitrile and 0.1% formic acid. 2 μL samples were electrosprayed from a gold-coated borosilicate capillary (Proxeon, Odense, Denmark). Mass spectra were recorded on a QSTAR Pulsar instrument (Applied Biosystems,

Foster City, CA) with a capillary voltage of 1200 V and declustering potentials of 45 V and 15 V. De-convoluted protein spectra were generated using Bioanalyst software (Applied Biosystems).

2.12 Preparation of gold surfaces with different roughnesses

Template-stripped gold (RMS roughness ca. 0.5 nm) was produced as described previously [117]. Rough gold surfaces (RMS roughness ca. 1.5 nm) were prepared by evaporating on to a freshly cleaved mica surface an adhesion layer of 2 nm of chromium followed by 100 nm of gold using a BOC Edwards Auto 306 evaporator (Crawley, UK). The biosensors used had a variable roughness between 0.8 nm and 2 nm, the largest roughness being observed for sensors after cleaning (see below).

2.13 Differential scanning calorimetry (DSC)

The calorimetric experiments shown in Figure 4.9 were performed with a VP-DSC calorimeter (Microcal, Amersham, UK). Solutions of the native and reduced forms of human lysozyme (in independent experiments) were introduced into the sample cell. The protein concentrations were 33 μM, the solution pH 1.2 and the total chloride concentration 200 mM (adjusted with NaCl). The reference cell was filled with a solution of the same composition, but lacking the protein. Then the temperature was scanned from 25 to 70℃. The raw data was treated with the Origin software provided with the instrument. Both the signal of the reference cell and the baseline were subtracted from the signal, yielding the traces as shown in Figure 4.9.

2.14 Isothermal titration calorimetry (ITC)

The basic principle of ITC is that a cell containing the sample and a reference cell are kept at constant temperature by controlled heating. When a reaction takes place in the sample cell that consumes or releases heat, the heating rate has to be changed in order to keep the temperature of the sample equal to the temperature of the reference cell. The time integral over the differential heating rate gives the total heat released or consumed by the reacting species. ITC has experienced an impressive boost in development and application in recent years [118], however, the present discussion will be limited to its application for the study of amyloid fibril elongation. Several studies have been published, where the authors have studied the enthalpy release associated with the elongation of amyloid fibrils [116; 119; 120]. In these experiments, a small amount of soluble protein is titrated into the sample cell that contains seed fibrils, and the heat released by the incorporation of the soluble protein into the seed fibrils is monitored. Alternatively, the sample cell is filled with soluble protein and a small quantity of seed fibrils is titrated into the sample cell, leading to the conversion of the soluble protein in the cell to insoluble fibrils.

Initial experiments along these lines were performed for this thesis; the results are mentioned and discussed in the chapter on future work. Below, the experimental protocol is given.

Protocol for ITC measurement of the enthalpy release from insulin amyloid fibril elongation: A solution of 0.5 mg/ml insulin monomer and a suspension of 0.5 mg/ml sonicated (10 min at 100 W, 3s pulses, 3s off) insulin amyloid fibrils (both in 0.01 M HCl) were dialysed overnight at 4℃ against a large volume of HCl 0.01 M, in order to ensure that the pH values were identical in both solutions, and that any residual salts (from the protein) were sufficiently diluted such that their heat of dilution upon titration would not interfere with the calorimetry experiment. The sample cell of the isothermal titration calorimeter (VP-ITC, Microcal, Amersham, UK) was filled with 1.5 ml of the soluble insulin solution and the injection needle was loaded with the fibril suspension. After the establishment of a stable baseline, 100 μl of the fibril suspension were injected, and the fibrillization reaction monitored. After the signal had recovered to the baseline, a second injection of 100 μl was performed in order to check whether all the monomer in the sample cell had been consumed. These experiments were carried out at 50 and at 55℃; the results are shown in the Future work chapter.

Chapter 3

Method development

3.1 Fibril surface attachment

This section is mainly based on the paper "Surface attachment of protein fibrils via covalent modification strategies", Buell et al., J. Phys. Chem. B 2010, [121]. Contributions of co-authors will be indicated appropriately.

In order for the biosensing methods described earlier to be able to develop their full potential, it is necessary to ensure an irreversible linkage of the amyloid seed fibrils, the elongation of which is studied, to the surface of the sensor. If this requirement is not fulfilled, one of the key advantages of this experimental approach is not realized, namely the fact that a constant number of seed fibrils is monitored during the time course of an experiment, enabling a particularly straightforward analysis of the change in aggregation kinetics upon a change in conditions.
These considerations highlight the need for an approach where the attachment of amyloid fibrils to surfaces, in particular gold surfaces due to their widespread use in biosensing, can be carefully controlled. In most cases where attachment of a macromolecule to gold is required, the general approach is to use a linker molecule containing a thiol group and to exploit the high propensity of the latter to form a covalent gold-sulphur bond [122]. Subsequently, the attachment of amyloid fibrils or other protein structures to the layer of linker molecules can be achieved either via an amide coupling reaction [96; 97] or through antibody-antigen interactions [107]. Both methods have been applied to amyloid fibrils under solution conditions (e.g. pH and temperature) where the particular fibrils under investigation are stable. In most cases where QCM experiments with Aβ (1-42) were performed for the work described in this thesis, a variant of this surface attachment method was applied, that is illustrated in Figure 3.1. In this method, it was made use of the fact that in the commercially available peptide (in this case TFA salt from Bachem, Basel, Switzerland), pre-formed aggregates seem to be present that can act as seeds. When the peptide is dissolved in buffer (100 mM PB or PBS), fibrils can be seen (by AFM imaging) a few minutes later. This behaviour is very useful for the preparation of seed fibrils, but the peptide that is to be used for the actual fibril elongation measurements has to be pre-treated (see the precise protocol in the section on proteins

at the beginning of this chapter) especially to break down the pre-existing aggregates. Also, due to the rapid formation of the fibrils from the untreated peptide, the QCM sensors have to be incubated with the Aβ solution *ex situ*, rather than brought into contact with the solution through the flow system of the QCM device. Initial attempts of *in situ* fibril deposition experiments, were characterized by a lack of reproducibility and control over the quantity of fibrils deposited; this was presumably due to a varying degree of absorption of the fibrillar peptide inside the tubing. From these experiments, it was concluded that all the fibril depositions on QCM and SPR sensors had to be carried out *ex situ*.

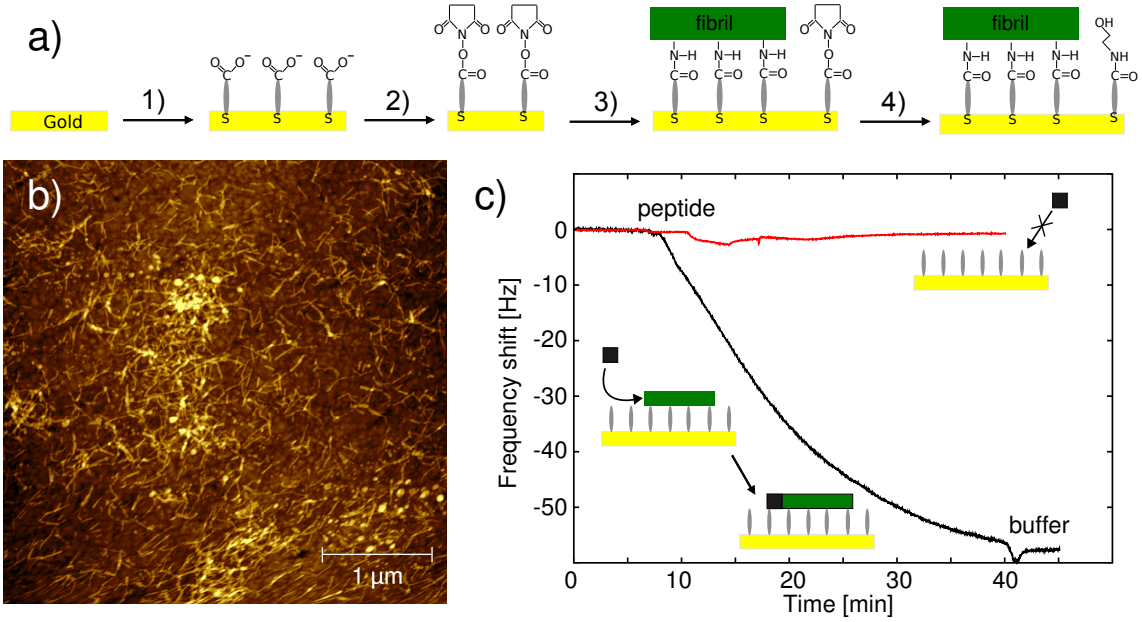

Figure 3.1: a) Covalent attachment of Aβ (1-42) amyloid fibrils to the gold surface of a QCM crystal (see protocol in text for details): 1) formation of a self-assembled monolayer (SAM) of mercaptoundecanoic acid (MUA); 2) activation of the SAM with a mixture of EDC and NHS; 3) coupling of Aβ (1-42) amyloid fibrils to the activated SAM; 4) passivation of the remaining surface with ethanolamine. b) AFM image of the QCM crystal after attachment of the amyloid fibrils. c) QCM experiment monitoring the growth of the surface bound Aβ (1-42) amyloid fibrils. After ca. 10 min, a 2 μM solution of the Aβ peptide in 100 mM phosphate buffer pH 7.4 was introduced and the elongation of the surface bound fibrils monitored via the decrease in resonant frequency (overtone at 15 MHz, corresponding to n = 3, is shown). After 40 min, the liquid cell was flushed with buffer, which stopped the elongation. For comparison, a typical frequency trace where soluble Aβ (1-42) is brought into contact with a QCM-chip with no attached fibrils, only covered by a passivated SAM, is shown as well (red line).

Protocol of attachment of Aβ (1-42) fibril attachment to a SAM of a mercap-

toacid:
All chemicals were from Sigma Aldrich (Gillingham Dorset, UK) unless stated otherwise. Gold coated QSX 301 QCM crystals (Q-Sense, Västra Frölunda, Sweden) were immersed in a solution of 0.5 mg/ml mercaptoundecanoic acid (MUA) in ethanol for 24h. The crystals were rinsed with ethanol and dried with nitrogen gas. Then, they were immersed in an aqueous solution of 0.3 mg/ml N-(3-dimethylaminopropyl)-N'-ethylcarbodiimide hydrochloride (EDC) and 0.5 mg/ml N-hydroxy succinimide for 20 min, rinsed with water and dried with nitrogen gas.
Aliquots of 50 μg Aβ (1-42) (Bachem, Basel, Switzerland) in 10 μl 0.01 M NaOH were diluted into 400 μl of 100 mM phosphate buffer pH 7.4 and 100 μl of the resulting solution were put onto each biosensor for ca. 15 min in an atmosphere of 100% humidity. Then the crystals were rinsed with water, and incubated with 100μl of a 0.7 M ethanolamine solution (pH adjusted to 9 with HCl) for 20 min. Finally, the crystals were rinsed with water and either put into the microbalance flow cell (Q-Sense E4) for a QCM measurement or they were dried for AFM imaging.
Before a measurement was performed, the sensors were left to equilibrate over night in 100 μM phosphate buffer pH 7.4. When a stable baseline was attained, the QCM-measurements were carried out.
For the dye-binding experiments described in Chapter 6, the surface coverage of fibrils had to be maximized, in order to obtain a measurable signal from the binding of the dye. In order to achieve this aim, the surface-bound seed fibrils were brought into contact with a solution of the Aβ (1-42) peptide for approx. 30 min (Figure 3.1 c), allowing the seed fibrils to elongate. Figure 3.1 shows the record of this growth period followed via the decrease in resonant frequency. The crystals with the Aβ (1-42) fibrils attached were then used for the study of the dye-amyloid interactions.

The common attachment methods for proteins, like the one described above, rely on the fact that side chain amines and carboxylic acids are usually abundant. A fundamental challenge, however, is that the reactivity of these groups is highly dependent on the pH value of the solutions involved. Thus, for example under acidic conditions, where many amyloidogenic proteins form fibrils particularly readily [40], the amine groups are mostly protonated and the number of accessible non-protonated nucleophilic amines available for amide coupling is very low. A change of solution conditions after fibril formation is not always possible, as pre-formed fibrils can dissociate if these conditions are changed [123]. Extensions to the commonly used methodologies are therefore required to establish general methods that cover a wide range of pH values. In addition, it is also advantageous to enlarge the toolbox of available attachment chemistries, at neutral pH in particular, because, as is demonstrated below, given methods of surface attachment can have very different efficiencies for fibrils assembled from different proteins.

3.1.1 Fibril attachment via naturally occurring cysteine residues

Attachment of amyloid fibrils to gold surfaces is straightforward and largely independent of solution pH when cysteine residues or disulphide bridges are present in

the polypeptide sequence, provided they are exposed on the surface of the fibril. The attachment efficiency is not likely to depend on the formation of disulphide links by the cysteine residues, even though it still is a topic of debate as to whether a disulphide bond remains intact when attached to gold or whether it is cleaved [124; 125]. This strategy has been used previously and its efficiency was shown in the case of amyloid fibrils formed from bovine insulin [76] (Figure 3.2 a) that contains three disulphide bonds in its native state. Hen lysozyme can form amyloid fibrils under similar solution conditions to insulin and possesses two additional cysteine residues, 8 in total, all present as disulphide bonds in the native state in solution. However, the surface coverage that can be achieved by simple incubation is generally lower for lysozyme than for insulin, when incubated at the same fibril concentration for the same length of time; this low coverage is indicative of weaker binding and the latter suggests that the cysteine residues in the lysozyme fibrils are less accessible for attachment than those in the insulin fibrils (3.2 b). A similar observation holds for bovine α-lactalbumin (Figure 3.2 d), a structural homologue of lysozyme, and for a cysteine mutant of the PI3K-SH3 domain (Figure 3.2 c) a protein which contains no cysteine residues in its natural sequence.
The covalent links between the fibrils and the gold surfaces are sufficiently stable such that the fibrils are not displaced from the surface even, for example, following a subsequent incubation with a thiol that forms self-assembled monolayers (SAM) on gold surfaces (Figure 3.2 e). This requirement is important for the attachment process, as the production of such a SAM on the regions of the surface not occupied by the fibril ends is important for biosensor measurements [76]. In particular, in the absence of such a layer, monomeric proteins are frequently capable of attaching directly on to the exposed gold surface, making it difficult to dissect the measured signal into the parts stemming from fibril elongation and from direct surface attachment of the monomeric building blocks.

3.1.2 Functionalization of fibrils that form under acidic solution conditions

In order to control the attachment of amyloid fibrils formed from proteins without natural cysteine residues to surfaces in acidic solution, minimally invasive chemical modification of pre-formed fibrils offers a convenient strategy. Low pH conditions are known to be favourable for the in vitro preparation and study of many amyloidogenic proteins. However, these conditions can present a particular difficulty for any reaction involving protein functional groups because any basic amino groups within a polypeptide chain (at the N-terminus or the side chains of lysine residues) are largely protonated and therefore not nucleophilic. Furthermore, the typically small quantity of amyloid fibrils that can be suspended acts to limit the maximal concentration of peptide amine groups in solution, resulting in a low attachment efficiency. In order to circumvent this problem, a strategy has been developed that is based on the well established attachment of cystamine [$H_2N(CH_2)_2SS(CH_2)_2NH_2$] molecules to monomeric proteins [126], where the aim is to introduce sulphhydryl groups into a specific molecular system (Figure 3.3). Reductive cleavage of the disulphide bonds

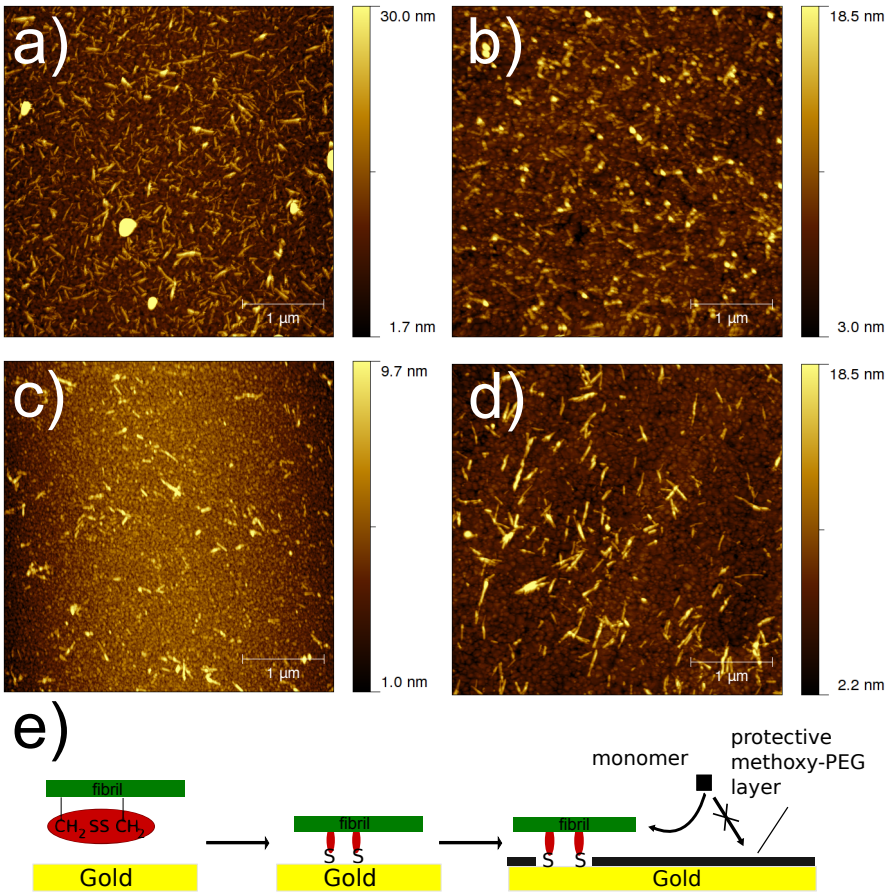

Figure 3.2: Attachment of amyloid fibrils from proteins containing cysteine residues/disulphide bridges in the amino acid sequence. In the case of bovine insulin a), good surface coverages can be achieved [76] with this strategy. However, hen lysozyme b), although having 8 cysteine residues compared to 6 for insulin, attains a lower surface coverage under similar experimental conditions, suggesting that the cysteines are largely buried inside the fibrils. Low surface densities of fibrils were also observed for a mutant of PI3K-SH3, where a cysteine residue has been artificially introduced (M1C) c), as well as for bovine α-lactalbumin d), containing 8 natural cysteines. Image size in all cases 4x4 μm. e) Schematic diagram of cysteine-attachment, including the subsequent passivation of the remaining gold layer.

within the attached cystamine molecule to form free thiol groups was omitted in the case of the fibrils, as disulphides appear to be as capable as free thiols of attaching to gold surfaces as discussed above.
The pH optimum for the initial step in the coupling reaction, the activation of carboxylic acid groups with N-(3-dimethylaminopropyl)-N'-ethylcarbodiimide hydrochloride (EDC), is at low pH values [127] as protonated carboxylic acids and not carboxylate ions attack the EDC. Nevertheless, acidic conditions are generally unfavourable for the formation of an amide bond as a result of the low reactivity

of amines at pH values several units below the normal range of pka values of amine groups (ca. 9-11). Under these conditions, only a small fraction of these functional groups is unprotonated and therefore nucleophilic enough to attack an activated carboxylate group before it is hydrolysed. This problem can be circumvented, however, with the approach described here, as a large excess of cystamine can be used to promote the coupling reaction. But even by using excess cystamine, the fraction of carboxylic acid groups in a given protein that reacts with cystamine molecules is small. Indeed, in the case of PI3K-SH3, only ca. 5% of the polypeptide molecules within a fibril are modified (see mass spectrum in Figure 3.3; estimates of relative populations based on the assumption of equal ionization efficiencies). Qualitative examination of mass spectra acquired from dissociated activated fibrils of other proteins (β-lactoglobulin, hen lysozyme) indicated similarly small reaction yields.

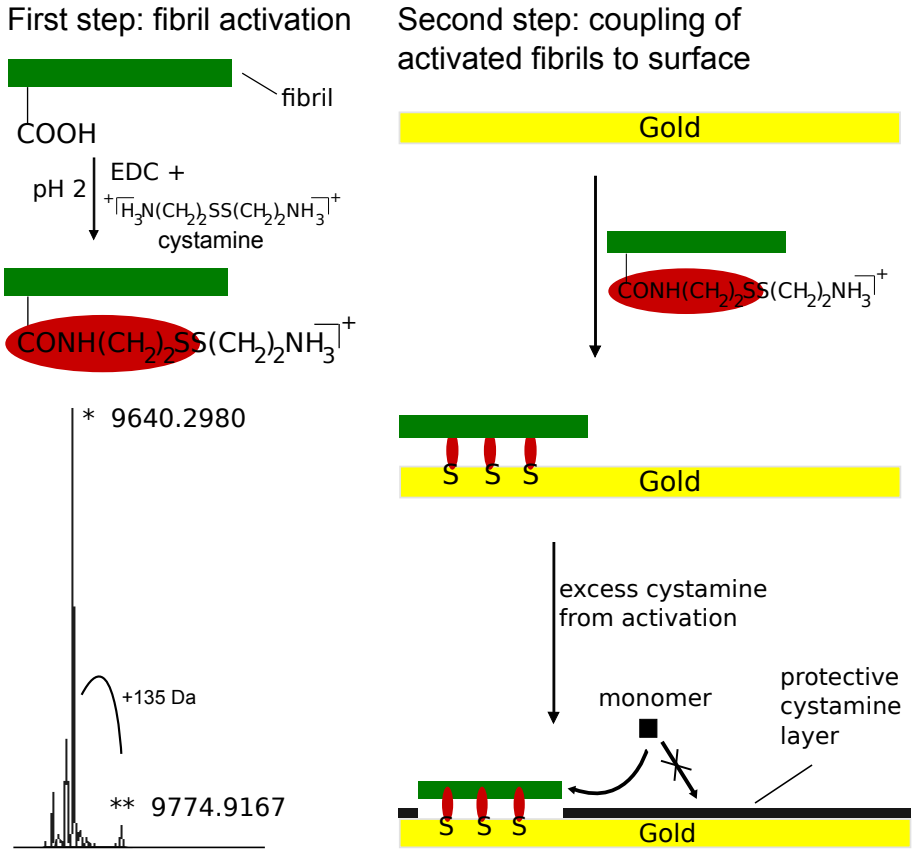

Figure 3.3: Schematic diagram of the surface attachment strategy that was used under acidic conditions where many proteins readily form amyloid fibrils [40]. The method uses a large excess of cystamine because almost the entire population of amine groups is protonated at pH 2. This fact explains the low yield ($\leq$ 5%) of functionalized molecules, as shown in the mass spectrum. [(*) is native protein, (**) corresponds to protein molecules carrying one cystamine molecule]. Nevertheless, even this level of modification enables stable interactions of the amyloid fibrils with the surface to be achieved.

Even though the yields are limited, they are sufficient to achieve efficient surface

attachment of the fibrils because not every protein molecule within the polymeric assembly needs to interact with the surface. Moreover, as the cystamine molecules can react only with those carboxylic acid groups that are exposed on the surface of the fibrils, the disulphide bonds that have been coupled to the fibrils are likely to be in ideal positions to interact with the gold surface as soon as the modified fibril fragments diffuse towards it. The number of available carboxylic acid groups per unit length of fibril is likely to be variable between different proteins, as a result of differences in the number of acidic amino acids in the sequence and of different fractions of such residues that are exposed on the fibril surface. In the present study, for example, the surface coverage achieved varied from a value of the order of 20 μm^{-2}) for bovine α-lactalbumin to one of ca. 100 μm^{-2} for hen lysozyme (see Figure 3.4 and Table 3.1.

Indeed, in the case of the B-chain of insulin, mass spectrometric analysis could not identify a population of cystamine-containing molecules and, in agreement with this observation, no statistically significant increase in surface coverage was achieved relative to that obtained with unmodified fibrils. In this 30 residue peptide, the naturally occurring cysteine residues had been oxidized to sulphonic acids that are unable to form covalent bonds with gold. The small number of carboxylic acid groups in this short sequence, two side chains and the C-terminus all of which are potentially buried in the fibril core, appears to be unable to react with the cystamine groups to a significant extent under these reaction conditions. In all cases, the presence of unmodified fibrils on the gold surface even after rinsing (see Figure 3.9) can be attributed to adsorption resulting from non-covalent interactions; this phenomenon will be discussed in detail below. The excess of cystamine and the hydrolysis-products of EDC generated during the reaction need to be removed after the reaction is complete, and this was achieved by repeated centrifugation and re-suspension cycles to isolate the now modified fibrils from the reaction medium. Fibril purification was terminated at a stage where approximately 10-50 μM of cystamine remained in solution (see protocol below) with the fibrils, as the residual cystamine molecules provide a source of a self-assembled monolayer (SAM) on the unreacted gold surface, analogous to the polyethylene glycol (PEG) layer produced in the case of attachment of fibrils via cysteine residues.

In conclusion, this method of covalent attachment of cystamine molecules to pre-grown fibrils can increase the surface coverages attained for the majority of amyloid fibrils generated from a range of different proteins compared to the surface coverages achieved with the non-modified fibrils (compare Figures 3.2 and 3.4, and see Table 3.1) under identical acidic conditions. The increase in surface coverage between the unmodified and modified fibrils is largest in cases where no cysteines are present (e.g. PI3K-SH3). However, even in cases where cysteine residues are naturally present, the increase in surface density of fibrils can be a factor of two or more as a result of the fibril modification process, reducing the quantity of protein needed for a given coverage. In addition, if a higher number of fibrils per unit surface is achieved, it will lead to higher signal-to-noise levels in experiments involving the study of the surface bound fibrils, especially in the case of species with a lower propensity to convert from the soluble into the fibrillar state.

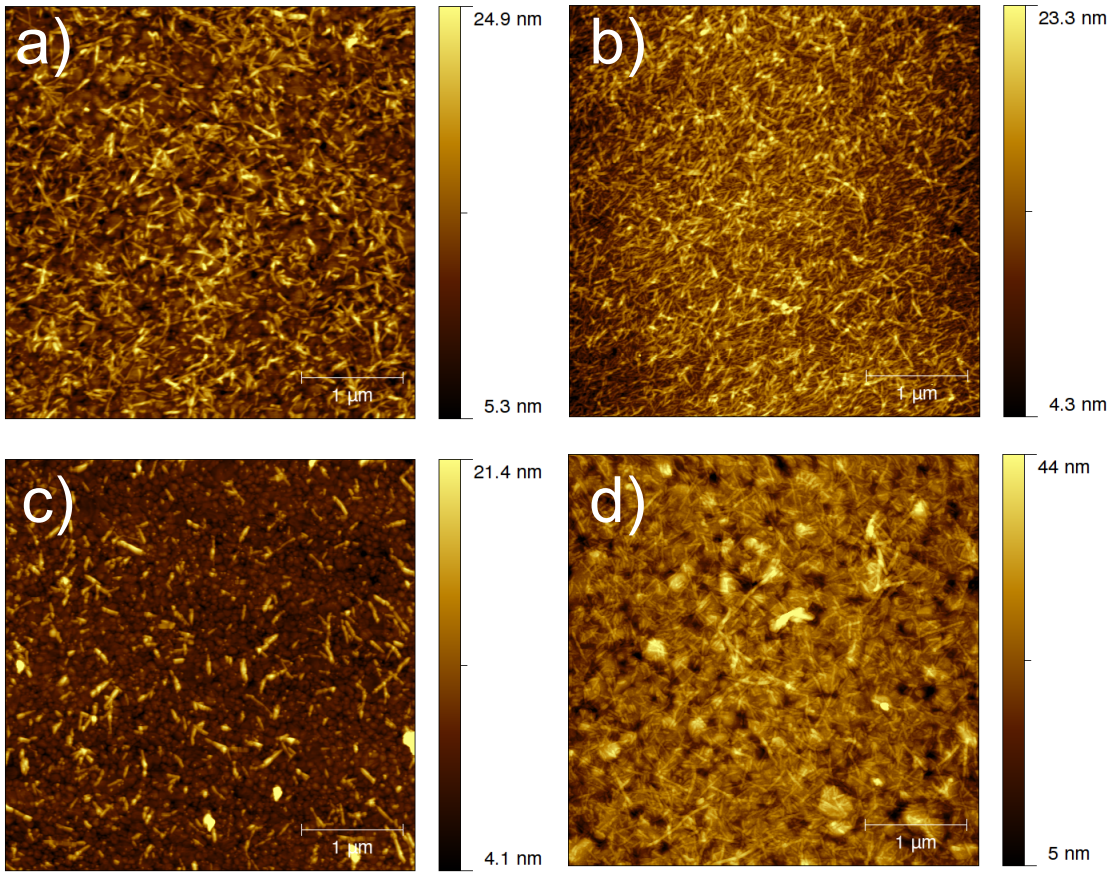

Figure 3.4: The attachment strategy presented in Figure 3.3 used for a range of amyloid fibrils formed at acidic pH. Examples are shown where sonicated (for details see protocol below) fibrils of a) PI3K-SH3, b) hen lysozyme, c) bovine α-lactalbumin, d) bovine β-lactoglobulin were functionalized and attached to gold-surfaces of QCM chips. The surface coverages achieved in this way, as well as their increase compared to non-functionalized fibrils, varied greatly between the different proteins. This result is likely to be a consequence of variations in the number and accessibility of carboxylic acid groups in the amyloid fibrils under study, as these groups are first activated by EDC and subsequently react with the added cystamine.

Protocols for fibril modification at acidic pH: The detailed protocol for modifying fibrils at low pH is illustrated for PI3K-SH3; the modification of bovine β-lactoglobulin, the α-lactalbumins and the lysozymes was carried out in an essentially identical manner. 100 μl aliquots of 1 mM fibril suspension (in 0.01 M HCl) were mixed with 100 μl of 1 M cystamine dihydrochloride (Sigma) solution and 1 mg of EDC (N-(3-dimethylaminopropyl)-N'-ethylcarbodiimide hydrochloride, Sigma), and then made up to 2 ml with 0.01 M HCl. The solution was centrifuged at 20°C for 2 h at 12 krpm (ca. 8500 g), the supernatant removed and the remaining pellet redissolved in 2 ml 0.01 M HCl. This procedure was carried out three times in order to minimize

any excess cystamine which could compete with the fibrils for surface attachment. The final pellet was re-suspended in 500 μl of 0.01 M HCl. In order to calculate the remaining cystamine and EDC in the final fibril suspension, it was assumed that in every centrifugation step 90% of these reagents were removed together with the supernatant (from estimated relative volumes of pellet and supernatant).

3.1.3 Fibril modification under physiological conditions

As discussed in detail above, if accessible natural cysteine residues are present in a sequence, amyloid fibrils could be attached to a surface via those thiol groups. Many amyloidogenic proteins, however, especially naturally unfolded polypeptides such as the Aβ peptide and α-synuclein that are implicated in disease, do not have cysteines in their sequence. The strategy that has been applied almost exclusively to date to attach amyloid fibrils under physiological conditions to gold surfaces is the coupling of unmodified amyloid fibrils to a chemically activated layer of molecules carrying a carboxylic acid group. This strategy has been applied several times successfully with the Aβ peptide ([96; 97; 128], and see Figure 3.1) and attachment to glass is also possible by using a similar procedure. It was shown above that the chemical functionalization of amyloid fibrils is a convenient strategy to enable their attachment to gold surfaces. As the surface coverages that can be achieved with a given attachment method can vary strongly, it is useful to investigate the applicability of the general approach of covalently modifying amyloid fibrils in such a way that they can be attached to a surface at physiological pH values and so studied under more biologically relevant conditions.
For this purpose a small molecule, 2-iminothiolane ("Traut's reagent"), was chosen that has previously been used to introduce thiol groups into monomeric proteins [126; 129]; this method is efficient and elegant because it is based on a one-step reaction (Figure 3.5). This cyclic electrophilic reagent is typically attacked by a nucleophilic amine group of the protein with good yield, resulting in the opening of the ring and the exposure of a free thiol group, ideal for surface attachment. It has been shown [130], however, that a subsequent reaction can occur that leads to the loss of ammonia and the formation of an N-substituted 2-iminothiolane, a species that is not capable of forming a gold-sulphur bond, a result in accord with studies on alkane sulphides that have been shown to adsorb only non-covalently to gold surfaces, and not to form covalent links as do thiols or disulphides [131]. The half life of the free thiol form of the attached Traut's reagent that is prone to this type of secondary reaction depends on the nature of the specific amine involved, and on the pH and the temperature of the solution [130].

In order to test whether this secondary reaction would interfere with the purpose of surface attachment, the interaction of Traut's reagent with fibrils formed from human α-synuclein and Amyloid β (1-42) was studied. A high fibril surface coverage (as shown in Figure 3.6) was achieved when the gold surface was incubated with fibrils shortly after functionalization (see protocol below), indicating that the re-

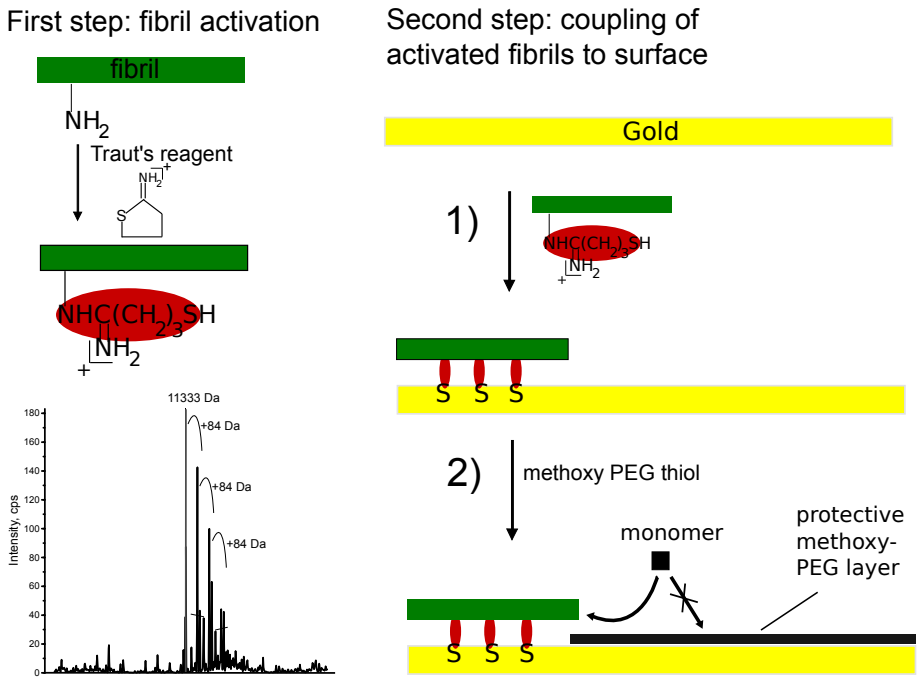

Figure 3.5: Attachment strategy, using 2-iminothiolane (Traut's reagent) to functionalized amyloid fibrils. Pre-grown fibrils were incubated with an excess of Traut's reagent (see protocol below for details), and then the fibrils were attached to gold surfaces. The mass spectrum shows α-synuclein fibrils functionalized for 15 minutes and then dissociated by suspension in HCl at pH 1.0. The spectrum shows an 11.3 kDa peak illustrating the truncation of the α-synuclein sequence (see text for a discussion) that can occur after prolonged time and a series of peaks differing by 84 Da corresponding to the masses of attached 2-iminothiolane-molecules after re-cyclization and loss of ammonia.

cyclization reaction does not occur within minutes and that the free thiol is available for a sufficient amount of time to ensure covalent attachment to the gold. The finding that a molecule of α-synuclein can carry several modifications (as can be seen in the cascade of peaks with ΔM= 84 Da in a mass spectrum of dissociated modified fibrils, Figure 3.5) is a consequence of the fact that the full length sequence contains 15 lysine residues and a considerable part of the sequence appears not to be in the fibril core [132]. AFM imaging shows in addition that the modified fibrils attached to the surface are essentially identical in morphology to unmodified ones and are still able to elongate after incubation with a solution of unmodified monomer, indicating that the modification does not interfere with the capability of the protein molecules to seed fibril growth (see Figure 3.6). In these experiments, sometimes amyloid fibrils that contained truncated sequences (see Figure 3.5) were found, probably due to starting protein degradation. The part of the protein sequence that is not burried within the core of an amyloid fibril has been shown for other proteins [133] to be readily cleaved off under certain conditions; in the present case, the strong decrease in pH used to dissociate the fibrils is likely to enhance this cleavage. However, the

fibrils containing truncated α-synuclein showed no detectable difference in surface attachment, morphology or seeding efficiency relative to fibrils consisting of full length α-synuclein; the two types of fibrils behave identically in all experiments carried out.

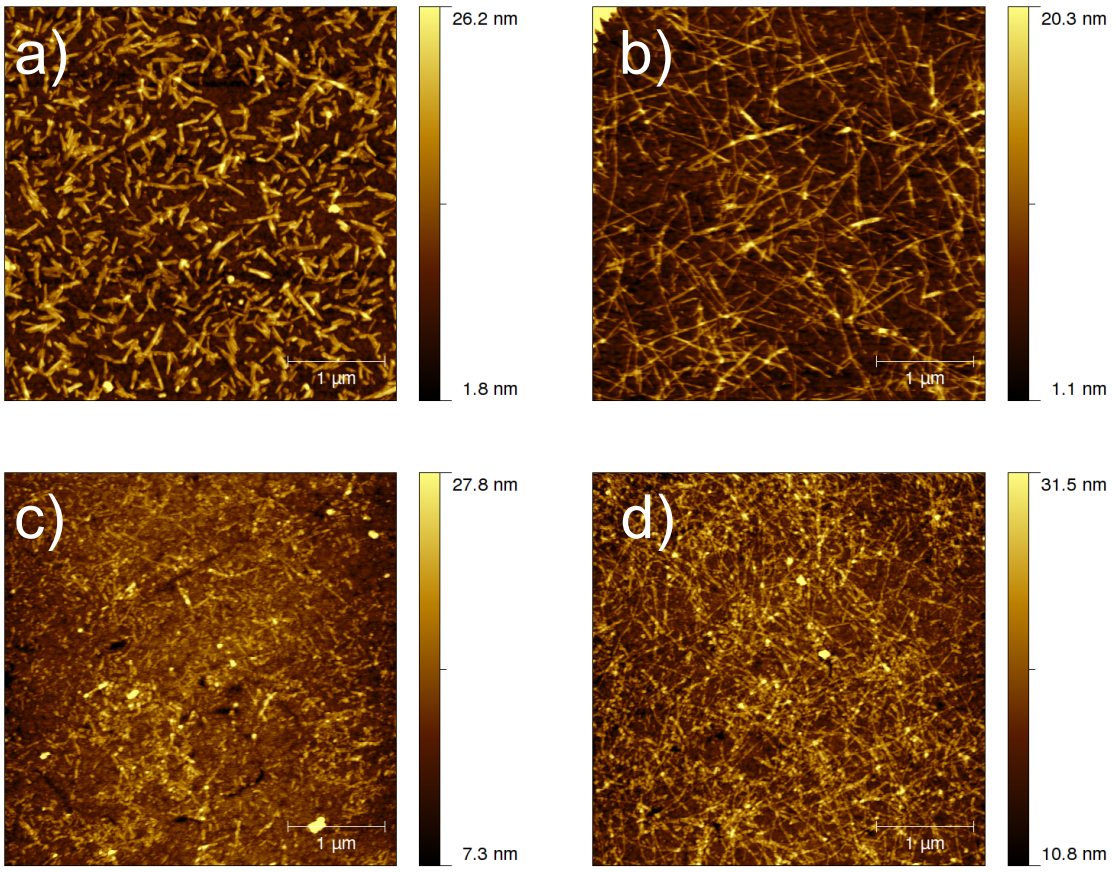

Figure 3.6: AFM images showing short fragments of amyloid fibrils of α-synuclein a) and Aβ (1-42) c) that were attached to a gold surface via Traut's reagent. The α-synuclein fibrils were then incubated with a 20 μM solution of monomeric α-synuclein in PBS for ca. 1 h. The Aβ-fibrils were brought into contact with a 7 μM Aβ monomer solution, also for ca. 1 h. The images demonstrate that, in both cases, the attachment of Traut's reagent did not interfere with the capability of the fibrils to elongate in the presence of monomeric protein (see b and d).

When a large excess of Traut's reagent is used, its hydrolysis product, a thiol, can react with the gold surface, even though it has been shown that the half-life of the intact cyclic compound at neutral pH is several days [134]. Therefore, in order to ensure complete passivation of the surfaces within a much shorter time scale, the gold surfaces were incubated with a methoxy-PEG-thiol after fibril attachment, in a manner analogous to that adopted with the natural cysteine attachment described above. This approach, where pre-grown amyloid fibrils were modified with Traut's reagent under physiological conditions, also yielded good results in the case of fib-

rils formed by the Amyloid β (1-42) peptide (Figure 3.6). As before, no differences in morphology or seeding efficiency were observed compared to fibrils attached via the well established amide coupling to an activated SAM [96; 97; 128]. In principle, therefore, comparable surface coverages can be achieved with both methods, although the relative mobilities of the activated groups are different. The coupling to an activated SAM requires a high surface density of activated groups, such that the fibrils, which have a limited mobility will come in contact with such an activated surface group. This requirement no longer applies if the fibrils are able to attach directly to gold via a sulphur-containing linker whenever they come in contact with the surface.
The reactivity of Traut's reagent is very strongly pH dependent, as it relies on reaction with an unprotonated amine group. This reagent is therefore ineffective in modifying fibrils which are only stable at acidic pH and another approach is required to achieve efficient functionalization of such structures (eg in the case of the B-chain of bovine insulin, where the modification with cystamine was unsuccessful). This observation led to the exploration of an alternative approach; monomeric peptides were modified at neutral pH with Traut's reagent and then, in a second step, preformed seed fibrils were elongated with these modified monomers at acidic pH (see Figure 3.7 and protocol below).

With this method, however, and in contrast to the functionalization of assembled fibrils discussed above, amino acid residues that are crucial to the self-assembly process can be modified and therefore the structure and mechanism of formation of the amyloid fibrils can potentially be altered. Indeed, it was found that in the case of hen lysozyme, the morphology of the fibrils formed from functionalized monomers can be different from the morphology of fibrils formed entirely from unmodified protein (Figure 3.7 c). These differences are highlighted by the finding that some functionalized fibrils (e.g. hen lysozyme fibrils where the monomer had been functionalized with a 3-fold excess of Traut's reagent) wind up into spirals, indicating that the monomer modification introduces stress into the amyloid scaffold, leading to lower persistence length or increased inherent curvature. This morphology is not normally observed. In many cases, however, the morphology of fibrils grown from functionalized monomers are indistinguishable by AFM from unfunctionalized structures; in such cases this approach represents a very effective strategy to achieve functionality in protein nanostructures. Indeed, using this method, the surface coverage of fibrils formed from the B-chain of bovine insulin was increased by 200-300% (compare Figures 3.7 d and e). The modified monomers (4-fold excess of Trauts reagent at pH 7.4) were analysed by mass spectrometry (Figure 3.7 c) and it was found that the population of modified monomer (M ca. 3600 Da) is small compared to the population of unmodified monomer (M ca. 3500), similar to the situation where fibrils were modified with cystamine. The Trauts reagent is likely to react with the N-terminus, as it represents the least basic amine within a protein. Therefore, the lack of apparent alterations in the morphology of the structures in this case can be readily understood as a consequence of the small proportion of modified monomers within the final fibrils. A further factor that is likely to reduce the effects of the modification on the filament structure stems from the fact that this modification

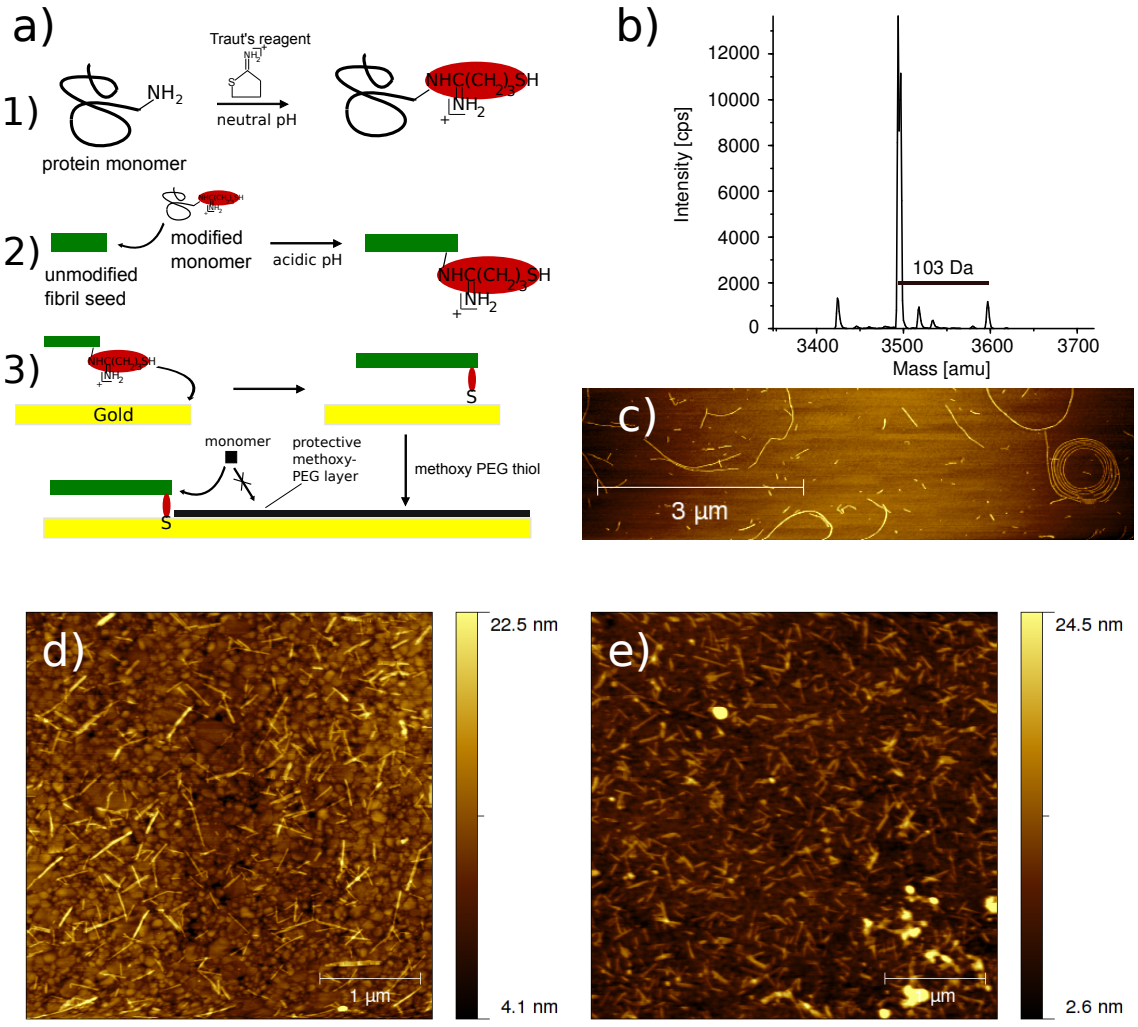

Figure 3.7: Covalent modification strategy involving attachment of Traut's reagent to monomeric protein at neutral pH followed by elongation of pre-grown fibril seeds with these modified monomers at acidic pH and then attachment of the modified fibrils to the gold surface. b) mass spectrum of the modified B-chain monomers, indicating the small yield of the modification (unmodified monomer around 3500 Da and modified monomer around 3600 Da). Due to the acidification of the peptide solution after incubation with Traut's reagent (see protocol), the Traut's reagent is still intact after more than one day, and has not undergone the subsequent rearrangement reaction described in the text. c) This strategy, however, can lead to alteration of fibril morphology, as residues crucial for the protein self assembly can be modified. This AFM image shows that in the case of hen lysozyme pre-modification of the monomer can lead to more highly curved fibrils, in extreme cases forming spirals (Fibrils modified and image acquired by Dr Christoph Meier). Despite this potential drawback, this method enabled to increase very strongly the surface coverage of bovine insulin B-chain fibrils: d) highest surface coverage achieved with unmodified fibrils; e) surface coverage achieved with modified fibrils.

predominantly occurs at the extremity of the polypeptide chain which is likely to be less important in the assembly mechanism than a position within the sequence. The mass spectrum acquired for the functionalized insulin B-chain monomer solution, shows only modified peptides where the attached Traut's reagent has not undergone the subsequent reaction leading to the elimination of ammonia, as shown by the measured masses of M + 103 instead of M + 84. The stability of this functional group is due to the lowering of the pH from 7.4 to 1 (see protocol below) 5 min after the addition of the Traut's reagent, conditions that quench the subsequent rearrangement reaction. This quenching stems from a significant decrease in the population of the thiolate, which is the nucleophile for the intramolecular nucleophilic attack.
Therefore, the covalent modification of pre-formed amyloid fibrils with a small molecule, 2-iminothiolane, under physiological conditions is a very convenient and effective strategy for surface attachment of fibrils formed from the naturally unfolded polypeptides Aβ (1-42) and α-synuclein. The modification is fast and efficient and does not normally alter the morphology or seeding capacity of the amyloid fibrils. Compared to the alternative method of coupling the fibrils to an activated SAM, this novel strategy involves less steps and can be controlled more accurately through variation of the concentration of Traut's reagent and the incubation time.

Protocol for activation of seed fibrils with Traut's reagent: For α-synuclein, 50 μl aliquots of a ca. 100 μM solution of fibrillar form of the protein were diluted with water to 1 ml and then 1 mg of 2-iminothiolane (Traut's reagent) was added. The solution was then left to react for at least 5 min. The extent to which the fibrils are modified depends on the relative concentration of Traut's reagent and the time of incubation. In fact, two hours of incubation of the α-synuclein fibrils with Traut's reagent led to complete disappearance of the unmodified peak in the mass spectrum. For Aβ (1-42), 100 μl aliquots of approx. 30 μM solutions of amyloid fibrils formed from Aβ (1-42) in PBS buffer were centrifuged at 90 krpm for 1h. The supernatant was removed and the remaining sample (no pellet was visible) was re-suspended in 200 μl of water. The fibril solutions were then reacted with 1.5 μg 2-iminothiolane for ca. 15 min.
Protocol for elongation of seed fibrils with modified monomeric protein: A solution of 10 mg (0.7 μM) hen lysozyme in 1 ml 100 mM phosphate buffer pH 7.5 was prepared, then 10 μl of 3 mg (22 μmol) 2-iminothiolane (Sigma-Aldrich) dissolved in 100 μl 100 mM phosphate buffer pH 7.5 were added. The solution was incubated for 1 h at RT, then acidified to pH 2 with 210 μl 1M HCl and incubated at 65 C for 6 days. (Protocol from Dr Christoph Meier)
1 mg of the B-chain of bovine insulin was diluted in 700 μl H_2O. First 20 μl of 100 mM phosphate buffer pH 7.4 and then 4 equivalents of Traut's reagent were added. After 5 min, the reaction was quenched with 10 μl of 1N HCl. To seed the fibril formation, 20 μl of pre-formed (see above) unmodified B-chain fibrils were added to the monomer solution which was then stirred overnight at 30℃.

3.1.4 Protocols for attachment of activated fibrils to the biosensor surface

Protocol for attachment under acidic conditions: The only step that differs in the protocols used for the various proteins that form amyloid fibrils particularly readily under acidic conditions is the duration of the ultrasonication that results from the different mechanical stability of the fibrils formed from different proteins. The sonication, that is carried out in order to maximize the number of growth sites was carried out in all cases after functionalization of the fibrils; longer fibrils can more readily be separated from the excess reagents (cystamine etc.) by centrifugation. The sonication was carried out with a 500 W ultrasonic homogenizer (Cole Parmer, Hanwell, UK), at 20% maximum power. Different numbers of identical cycles with 3 s pulses and 3 s breaks were used (in order to avoid excessive heating of the sample) and the total sonication times were: insulin, 10 min; insulin B-chain, 2 min; PI3K-SH3, 30 s; lysozymes, 15 s; β-lactoglobulin, 3 s; α-lactalbumins, 3 s. 100 μl aliquots of each fibril solution were then pipetted on to a biosensor surface that was kept in an atmosphere with 100% humidity. Then the surfaces were rinsed with 0.01 M HCl and the sensors were either inserted into the QCM for measurement or dried for AFM imaging. No additional passivation layers were required in this protocol, as it was found that non-specific attachment was small even after the first incubation of a biosensor with monomeric protein, suggesting that the excess cystamine forms a charged layer that is very effective in preventing monomeric protein from non-specific attachment.

Protocol for attachment under physiological conditions: The gold surfaces of biosensors were incubated for 1h in an atmosphere of 100% humidity with 100 μl of a solution containing freshly activated α-synuclein fibrils that had been sonicated for a total of 4 min. The chips were then rinsed with water. Even though Traut's reagent has been shown to have a slow hydrolysis rate at neutral pH [134], the high molar excess of the compound will lead to a partial coverage of the surface by its hydrolysis product, a thiol amide. In order to ensure complete passivation for the biosensor measurements, however, the surfaces was incubated with a 0.5 vol.% solution of an inert PEG thiol ($CH_3O(CH_2CH_2O)_6SH$, Polypure, Oslo, Norway) for 1 h, also at 100% humidity. Then the chips were rinsed with water and dried for AFM imaging. In the case of Aβ (1-42), the fibrils already had a length distribution appropriate for a biosensor measurement, and no sonication step was therefore required. A clean biosensor was incubated with 100 μl of the solution of re-suspended fibrils for 1 h in an atmosphere of 100% humidity. The sensor surface was rinsed with water and dried for AFM imaging.

3.1.5 Comparison between covalent and non-covalent surface attachment of amyloid fibrils

Non-covalent interactions between charged molecules and metal surfaces can be strong because of the high polarizability of metals; a charged compound in contact

with a metal surface can induce an opposite (mirror) charge which leads to strong Coulombic attractions [135]. Non-covalent interactions between the soluble forms of proteins and surfaces of different chemistry and topography have been studied in detail, especially in the framework of potential biomedical applications [136; 137; 138]. These interactions are likely to play an equally important role in the case of amyloid fibrils, as the protein monomers that form the fibrils are often very highly charged under the acidic denaturing conditions where many proteins most readily form amyloid structures (see Chapter 5). Figure 3.8 demonstrates that non-covalent interactions depend on the roughness of the surface by comparing the outcome of incubating of WT PI3K-SH3 fibrils on very smooth template-stripped gold [117] (RMS roughness ca. 0.5 nm) and on a gold substrate with a roughness comparable to that of commercially available biosensors (RMS roughness ca. 1.5 nm). As the fibrils are very stiff [20] and do not necessarily follow the features of a surface, the roughness determines the average distances between the charges and the polarizable surface and, in addition, the larger contact area between the fibrils and the surface with decreased roughness also increases van-der-Waals attractions and hydrophobic interactions.

It was found that rinsing the surface with a solution of high ionic strength ($\geq 10^{-1}$ M) detaches a larger proportion of non-covalently attached fibrils than occurs when rinsing with a solution of lower ionic strength (10^{-2}M) (Figure 3.8). This result indicates that the majority of the interaction energy in such cases is likely to result from electrostatic forces. The shear stress $\sigma = \eta \cdot \frac{\partial u}{\partial z}$ experienced by the fibrils during the rinsing can be estimated to be of the order of 1 N/m^2 (assuming maximum shear rates $\frac{\partial u}{\partial z}$ of 1000 s^{-1} and a dynamic viscosity of 10^{-3} Pa s). With a fibril diameter of roughly 10 nm, this leads to a force per unit length of fibril of 10^{-8} N/m. If this value is compared with an order of magnitude estimate of the unscreened electrostatic forces, $\mathrm{F/l} = \frac{\lambda \cdot q}{4\pi\epsilon_0\epsilon_r r^2} = \frac{n}{l} \cdot \frac{q^2}{4\pi\epsilon_0\epsilon_r r^2} \approx \frac{n}{l} \cdot 2.9 \cdot 10^{-12} N$ (where l is the unit length of fibril and $\lambda = \frac{Q}{l} = \frac{nq}{l}$ is the one-dimensional charge density, r is here taken to be 1 nm and the value of ϵ_r for water is used), the two opposing forces are only of the same order of magnitude for an unrealistically low charge density of 10^4 m^{-1}. A realistic charge density can be expected to be at least 10^5 times higher than this value[1], due to the high density of protein molecules within the amyloid fibrils, all of them carrying several charges. Therefore, the forces due to rinsing will not be sufficient to overcome the unscreened Coulomb attraction. If, however, oppositely charged counter-ions are present, as is always the case, although in varying quantities depending on the ionic strength of the buffer, these ions can diffuse into close proximity with the fibril/surface interface and thereby reduce the electrostatic forces via a Debye-type screening and the formation of ion pairs (see Chapter 5 for details). The remaining electrostatic, van-der-Waals and hydrophobic forces are then of a comparable order of magnitude as the forces from the mechanical action of rinsing, such that rinsing at high ionic strength is able to remove the fibrils (3.8). It is interesting to note that in the case of fibrils formed from bovine insulin and

[1] or $\sim 10^4$ times if ϵ_r of protein is used instead of the value for water in the calculation of the electrostatic force, but this variation does not change the qualitative conclusions

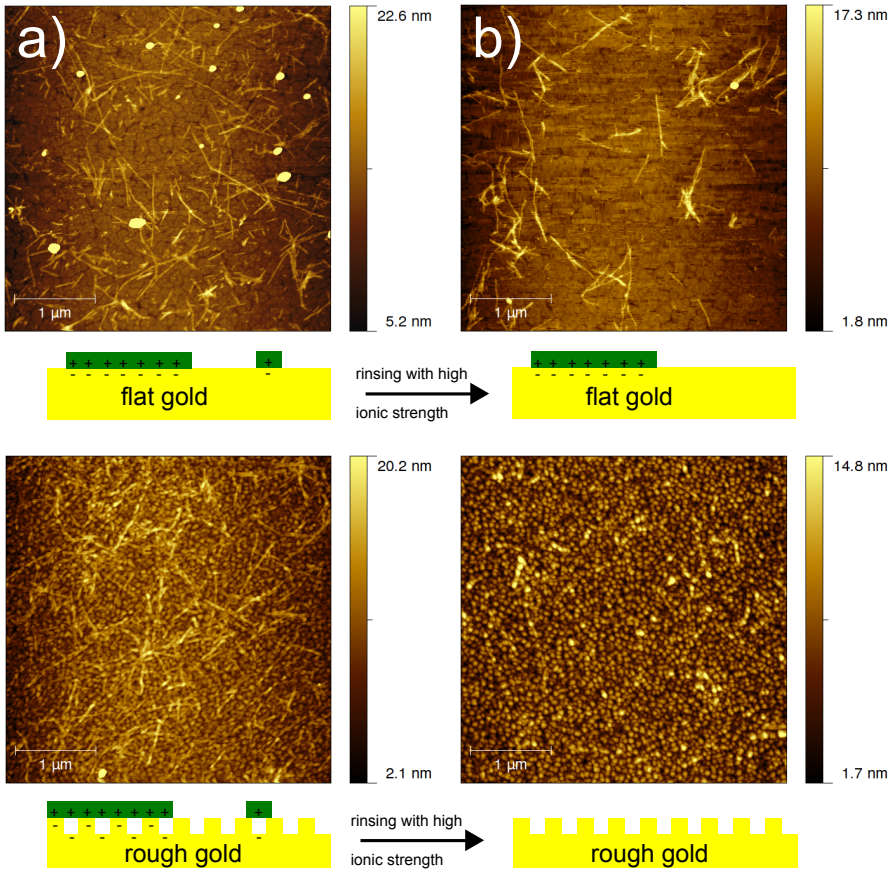

Figure 3.8: Stability of non-covalent interactions between gold surfaces of different roughness and PI3K-SH3 amyloid fibrils. In the case of the smooth (RMS roughness ca. 0.5 nm) template-stripped gold (top), the difference between rinsing with 10 mM HCl a) and 10 mM HCl + 100 mM NaCl b) is small, with only short fibrils in general being removed. However, the interaction forces are weaker in the case of the gold surface with higher roughness (RMS roughness ca. 1.5 nm, substrates prepared by Dr Tuomas Knowles) (bottom). Here, the fibrils were entirely displaced by rinsing the surface with a solution of high ionic strength (compare c and d).

its B-chain fragment, the charge density of the two types of fibrils is very similar (assuming that the monomeric building blocs carry the same charge within the fibrils as in solution; this assumption will be discussed in Chapter 5). The B-chain at pH 2.0 carries the same net charge as the intact protein (i.e. the combined A- and B-chain) assuming that the pK_a values of all residues are independent of each other, an assumption that is consistent with calculations with the protein pk_a calculator PROPKA [139]. The presence of two sulphonic acid residues in the oxidized B-chain decreases the charge from +5 to +3 at pH 2.0 but the sequence length of 30 residues compared to 51 in full length insulin and the similar fibril diameters imply that the overall charge density of the B-chain fibrils at acidic pH is likely to be very similar to that of fibrils formed from intact insulin under the same conditions. The large difference between the surface attachment of full length insulin amyloid

(3.2 a) and the isolated B-chain (highest surface coverage achieved is shown in Figure 3.7 c) can therefore unambiguously be attributed to the formation of covalent bonds with the gold surface in the case of full length insulin as a result of the presence of cysteines/disulphides compared to the sulphonic acid residues in the B-chain.

3.1.6 Applications of covalent surface attachment

In Table 3.1, a summary of the surface attachment methods presented above and their efficiencies is given.

Protein	**pH**	**Method**	**Surface Coverage Enhancement Factor**
bovine insulin	2	natural cysteine attachment [76]	no modification required to achieve high surface coverage
bovine PI3K-SH3	2	attachment via cystamine	> 10
HEW/human lysozyme, bovine β-lactoglobulin, bovine/human α-lactalbumin	2	attachment via cystamine	2-5
human A β 1-42, human α-synuclein	7.4	attachment via Traut's reagent	5-10
bovine insulin B-chain	7.4/1.0	pre-modification of monomer with Traut's reagent, subsequent elongation of seed fibrils with modified monomer	ca. 3-5

Table 3.1: Summary of attachment methods for the proteins under study. The surface coverage enhancement due to the covalent modification of fibrils is reported as a comparison between an incubation of the gold surface with a solution of modified and non-modified fibrils and extensive rinsing of the surface with the respective (buffer-)solution: PBS for Aβ 42 and α-synuclein, HCl pH 2.0 for all the others.

In order to demonstrate at this point the usefulness of these novel attachment methods, Figure 3.9 shows a comparison between QCM measurements carried out with non-covalently and covalently attached PI3K-SH3 amyloid fibrils. It can be seen in Figure 3.9 a) and b), that in the case of only non-specifically adsorbed fibrils, the fibrils are almost quantitatively removed when the sensor surface is flushed with a solution of moderate ionic strength, and a subsequent elongation measurement is made impossible. On the other hand, covalent attachment using cystamine enables

an experiment probing the influence of an increase in ionic strength on the rate of PI3K-SH3 amyloid fibril elongation (Figure 3.9). The AFM image in Figure 3.9 d) shows long fibrils of a surface density at least an order of magnitude higher than in Figure 3.9 c). These experiments were performed with the old QCM system D-300, where the protein solution is introduced into the liquid cell via a gravity flow system, reaching quite high flow rates (of the order of 10 ml per minute). The lower flow rates reached with the peristaltic pump of the newer system E4 make fibril detachment a slightly less dramatic problem. However, irreversible attachment is under any circumstances the preferable approach and in the remainder of this thesis, the high reliability of the covalent surface attachment methods described above will be explored. In particular, the opportunity to probe the influence of ionic strength on the elongation rate will be exploited extensively in Chapter 5.

3.2 Mass sensitivity calibrations for QCM experiments of amyloid fibril elongation

For the detailed analysis of the free energy barriers against protein aggregation presented in Chapter 4, the average absolute rate of addition of monomers to every fibril end has to be measured. It is important to note that with the analysis that will be described in the following, it is not possible to capture behaviour such as the stepwise growth of amyloid fibrils that has been reported for several amyloidogenic proteins [140; 141; 142]. Relying on the interpretation of ensemble kinetic experiments, the present analysis will yield an average over the active and inactive periods. In order to be able to estimate the numbers of protein molecules that incorporate into single fibrils per unit time with QCM experiments, the numbers of fibrils on the surface of each QCM sensor has to be estimated. This was achieved via AFM imaging of the sensor surface on several independent areas of usually 4 μm x 4 μm, manually counting the number of fibrils. Averages over the different areas on a single sensor were then taken. An example is given in Figure 3.10 a) where the fibril density was estimated to be 500$\pm$200 μm^{-2}. Figure 3.10 illustrates an experiment where the surface-bound seeds shown in a) had been exposed repeatedly to a solution of 0.2 mg/ml soluble insulin in 0.01 M HCl at 40℃. The rate of change of frequency due to the elongation of the seeds of this series of identical repeats is highly reproducible, a general characteristic of surface bound techniques, where a constant ensemble of seeds is repeatedly probed.

However, in order to determine the absolute elongation rate, the QCM frequency response needs to be calibrated, i.e. the observed rate of change of frequency has to be correlated with the equivalent rate of mass addition to the surface of the QCM sensor. The overall rate of mass addition divided by the number of fibrils then yields the property of interest. In the case of growing amyloid fibrils, that form a rough visco-elastic layer on the surface of the QCM sensor (see section on QCM experiments above), the proportionality constant between the changes in surface-bound mass Δm and resonant frequency ΔF is not simply given by the Sauerbrey equation ([99] and see Experimental section); indeed in some cases the normalized frequency

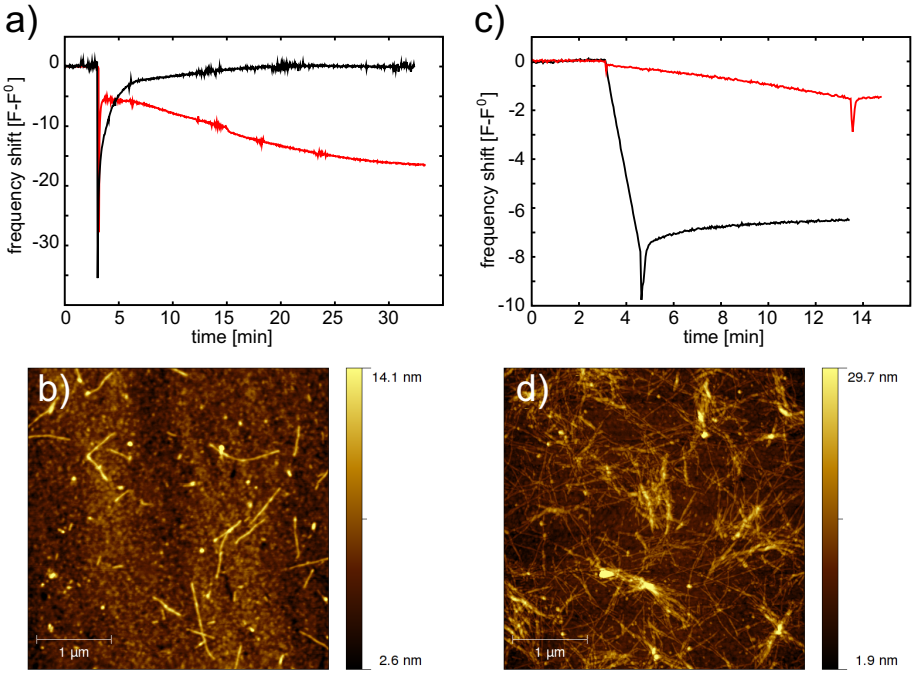

Figure 3.9: QCM measurements of PI3K-SH3 amyloid growth, illustrating the advantages of covalently attaching the fibrils to the biosensor surface. a) fibrils have been exposed to PI3K-SH3 monomer solution at pH 2.0: before (red line) and after (black line) flushing the cell with 40 mM NaCl solution at a flow rate of ca. 10 ml/min. The reversible spike in frequency at t = 3 min is due to the injection of sample into the QCM-cell. The frequency shift of the red line indicates growth of the surface bound fibrils, whereas the absence of a shift in resonant frequency for the black line is characteristic of a lack of any fibril elongation. Indeed, AFM imaging of the chip after the experiment revealed that very few fibrils were left on the surface; the contact of the chip with a solution of moderate ionic strength had removed most of them (see b). c) Similar experiment to the oen shown in a) with seed fibrils covalently attached via the modification scheme of Figure 3.3. Frequency shift due to fibril elongation in the absence of NaCl (red line) and in the presence of 20 mM NaCl, after having been flushed repeatedly with solutions of moderate ionic strength (black line). AFM-imaging reveals that at the end of the experiment, after repeated contact with solutions of different salts and of similar ionic strengths as in a), the surface coverage of fibrils remains high (see AFM image in d)). The reliable covalent attachment therefore allows for the probing of the influence of ionic strength on the elongation rate; this possibility will be explored in detail in Chapter 5.

response of the different overtones can differ by up to an order of magnitude, a feature not predicted by the Sauerbrey equation. An empirical calibration method that has been proposed earlier [76] relies on the determination of the proportionality factor between ΔF and Δm by AFM imaging and correlation of the observed length increase with a measured frequency increase. The method will be illustrated by car-

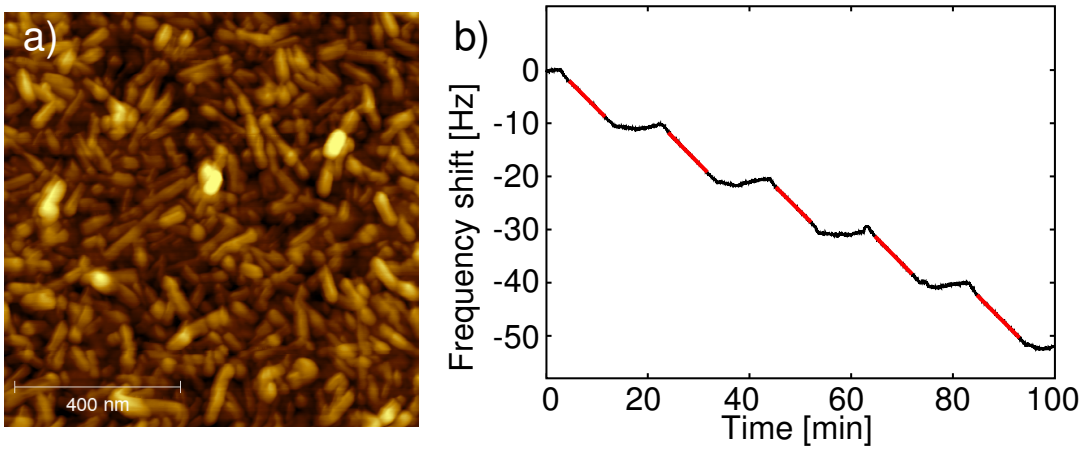

Figure 3.10: The AFM image on the left hand side shows seed fibrils of the protein insulin attached to a QCM sensor surface, before the series of experiments shown on the right hand side of the figure were carried out. The surface number density is estimated to be 500±200 μm^{-2}. On the right hand side a typical QCM experiment, in this case a test of the intrinsic reproducibility, is shown. The surface-bound seed fibrils are repeatedly exposed to a solution of 0.2 mg/ml insulin in HCl pH 2 at 40℃. The red lines indicate the sections of the frequency trace (here the frequency overtone with N = 5) that were fitted with a linear function in order to extract the rates of frequency change. The average rate of the five repeats shown here is 0.96±0.01 Hz/min.

rying out an example calculation. Figure 3.11 shows a gold substrate with attached sonicated insulin amyloid fibrils before a) and after b) having been incubated for the same duration of time at 40℃ with 0.2 mg/ml soluble insulin as the QCM chip that was used for the measurement in Figure 3.10. The average length increase per fibril is estimated from Figure 3.11 to be 200±100 nm. The number density of seed fibrils (Figure 3.10) is estimated to be 500±200 μm^{-2}. The diameter of a fibril is 5 nm, and the density is assumed to be 1.2 g/cm^3, as for a globular protein. The active area of a QSX-301 sensor is 1 cm^2. Therefore, the observed frequency shift of ca. 50 Hz corresponds to between 70 and 500 ng of added fibrillar protein, yielding a mass sensitivity coefficient of between 1.4 and 10 ng/Hz. If this value is compared to the Sauerbrey mass sensitivity of the sensor of 17.7 ng/Hz (as quoted by the supplier), it can be seen that an additional contribution to the frequency shift, not stemming from dry mass, occurs.

The accuracy of the calibration calculation outlined above is not very satisfying, and it would certainly be possible to improve on it, for example by increasing the number of measurements and analysing the fibril length increase automatically on a large number of fibrils. However, in the following, an alternative approach is presented that is more accurate, as it does not require estimation of the seed fibril density and of the fibril length increase. In the case of the very rapidly elongating fibrils formed from Aβ (1-42) and Ure2p Sc, it is possible to monitor the quantitative

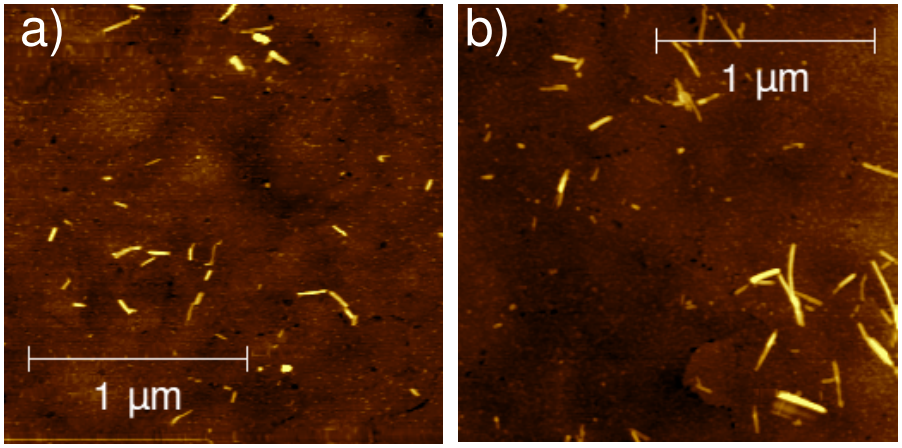

Figure 3.11: These two AFM images were used to estimate the length increase that the surface-bound insulin seeds had undergone in the experiment shown in Figure 3.10. Gold substrates had been prepared in a similar way to the QCM sensors, albeit with a much lower surface density, which greatly facilitates estimation of the length increase. For an actual QCM measurement, the elongation of surface-bound fibrils at such a low surface density would not give rise to a measurable signal. a) At the beginning of the experiment b) After incubation for 1h at 40℃ with an insulin solution of 0.2 mg/ml in HCl pH 2. The average length increase is estimated to be 200±100 nm.

depletion of monomer from the liquid cell of the QCM, as the measurements are performed in the absence of flow, and therefore no new soluble protein is supplied during the duration of a measurement. This was possible because the concentrations required to observe fibril elongation were of the order of 1 μM, a concentration so low that the total available precursor was consumed within ∼10 min (Aβ) to 1h (Ure2p Sc) (see Figure 3.12, where the rate of change of frequency decreases to almost zero over these durations). These different timescales are caused by the different diffusion coefficients of Aβ (1-42) ($\sim 2.4 \cdot 10^{-10} \frac{m^2}{s}$, estimated from the value reported in [143], and corrected for the temperature dependence of viscosity) and Ure2p Sc ($\sim 0.9 \cdot 10^{-10} \frac{m^2}{s}$, from DLS measurement of Ure2p solution, and conversion of the apparent hydrodynamic radius into a diffusion coefficient using Stokes formula). The diffusion of the protein from the bulk of the QCM liquid cell toward the sensor surface corresponds to a 1-dimensional diffusion current. The height of the cell is $4 \cdot 10^{-4}$m. The time it takes for a particle with the diffusion coefficient of an Aβ peptide to travel this distance, i.e. the square root of the mean square displacement can be estimated from $t = \frac{<r^2>}{D} \approx \frac{1.6 \cdot 10^{-7}}{2.4 \cdot 10^{-10}}$s $\approx$ 11 min. This time scale corresponds almost exactly to the observed time scale of depletion. This observation indicates that the fibril elongation of Aβ (1-42) proceeds without a significant free energy barrier. Indeed, it will be shown in Chapter 4 that this peptide has the lowest free energy barrier against aggregation of all studied peptides and proteins. Interestingly, the time scale of Ure2p Sc depletion is over-proportionally longer, suggesting that

its free energy barrier is higher, such that the formation of a concentration gradient away from the sensor surface is less pronounced, leading to a smaller flux of protein towards the surface. This qualitative observation is also confirmed by the accurate measurement of the free energy of activation for this protein in Chapter 4. In both cases, the sensor was incubated twice with the same protein concentration to probe if the observed decrease in the rate of change of frequency was indeed due to monomer depletion, as opposed to the fibril crowding phenomenon mentioned in the general section on QCM measurements above. The exact reproducibility of the frequency response confirmed that depletion was at the origin of this phenomenon.
These interesting depletion phenomena were not observed for any other peptide under study, due to the higher concentrations used in combination with higher free energy barriers. Indeed, a linear rate of change of frequency was usually observed, that was stable for up to hours, indicating a steady state situation in the cell without noticeable depletion. However, the clear signature of depletion in the case of Aβ (1-42) and Ure2p Sc was used to calibrate the mass sensitivity of the QCM for fibril elongation. Numerical simulations of the one-dimensional diffusion equation with a sink at the sensor surface confirmed that the content of the liquid cell was quantitatively (of the order of 90%) depleted; therefore the observed frequency shift (the average of the first three overtones n = 3,5,7) was taken to origin from the attachment of all the available peptide, the latter being calculated from the protein concentration and the known volume of the liquid cell (40 μl). Assuming that a negligible fraction of the peptide or protein is absorbed at the walls of the cells or elsewhere in the flow system, the values of the mass sensitivity coefficient for amyloid fibril elongation thus obtained therefore represent an upper bound of the mass sensitivity. It is unlikely that a significant amount of peptide is absorbed in the flow system, given the good reproducibility of the frequency shift traces shown in Figure 3.12.

Performing the analysis as described above, it was found that the mass sensitivity coefficients for both Ure2p ($\sim$10ng Hz^{-1}) and Aβ 42 ($\sim$7ng Hz^{-1}) are very similar. Given the fact that these two polypeptides differ considerably in size (4.5 compared to 40 kDa) and fibril structure, it is reasonable to assume that the mass sensitivity coefficients for amyloid seed fibril elongation by other polypeptides are similar to the ones measured here. Therefore, the average of the values measured for Aβ (1-42) and Ure2p Sc, (8.5$\pm$2 ng Hz^{-1}), was used as the global mass sensitivity coefficient for all proteins and peptides studied in this work. This value is included in the possible range from the AFM calibration experiments detailed above and corresponds to $\sim$50% of the Sauerbrey mass sensitivity coefficient, i.e. a mass sensitivity that is twice as high as expected from the dry mass of the protein. In conclusion, therefore, the typical underestimation of the absorbed mass that arises from the viscoelastic properties of the attached material [101] is not observed in QCM experiments of fibril elongation, but rather the hydration water of the protein, as well as the increase in surface roughness due to the growth of the fibril network on the QCM-chip (leading to additional frequency shifts from the drag of water trapped in the groves [104]) seem to play an equally important role.

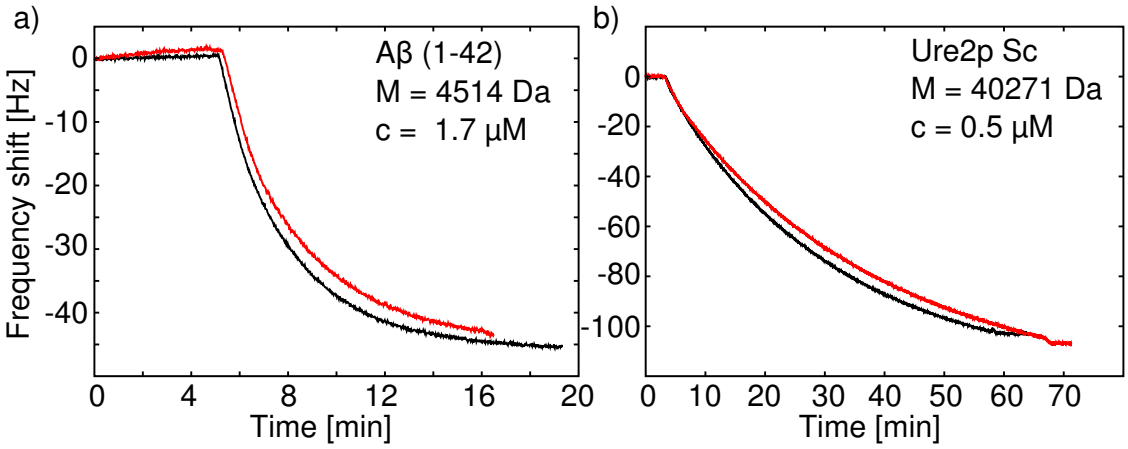

Figure 3.12: a) A QCM sensor covered with Aβ (1-42) seed fibrils was repeatedly incubated with a solution of 1.7 μM soluble Aβ peptide at 40°C and the cell was only flushed with PBS buffer when the rate of change of resonant frequency had levelled off. The black trace is from the first incubation, the red one from the second b) a similar experiment as in a), but with the yeast prion Ure2p Sc. The induced frequency shift scales with the molecular mass and concentration of protein, indicating that the mass sensitivity coefficients are very similar for these two polypeptides. Note also the different time scales of the depletion phenomena, that are due to the different diffusion coefficients of the two proteins (see text).

3.3 DLS measurements of fibril elongation

The most widely used assay for amyloid formation kinetics in bulk solution is based on the shift of the fluorescence spectrum of the dye Thioflavin T (see above). However, as mentioned there, the fluorescence intensity of ThT depends on factors other than just the quantity of amyloid fibrils present. In addition, as will be demonstrated in the last chapter of this thesis, this method is highly prone to artefacts, such as fluorescence quenching by small molecules etc. It is therefore desirable, to be able to follow the formation and growth of amyloid fibrils in solution without the use of a label. Light scattering has long been used for this purpose [70; 71; 144; 145], but the physical principles governing the scattering of light by small particles render this method difficult to employ. The scattering intensity scales with R^6 [112]; therefore, in solutions and suspensions with very inhomogeneous particle size distributions, larger particles contribute the majority of the detected intensity of scattered light, even if their number concentration is small. If this dominance is too strong, the multi-modal character of the correlation function cannot be properly resolved. In such cases, the overall size distribution of all particles in the solution cannot be determined, and even a quantification of the total amount of aggregated material is difficult. It shall be mentioned here only briefly, that a label-free determination of the total quantity of insoluble material can be determined via an ultra-centrifugation assay, as for example demonstrated recently in [146].
Despite these difficulties, the label-free nature of light scattering techniques has

potential for aggregation assays, and in Chapter 5, it is shown how the method described below can be used to probe the influence of ionic strength on the elongation rate of insulin amyloid. In the following, a detailed description of the method is given. The first important aspect to note is that the fibrils the elongation of which is studied are obviously not spherical, such that the most simple type of analysis of the data in terms of the Stokes-Einstein equation $D = \frac{k_B T}{6\pi\eta R}$, that relates the diffusion coefficient to the hydrodynamic radius of a sphere, cannot be employed. However, the problem of the apparent hydrodynamic radius of non-spherical objects has been solved for a range of simple shapes of biological relevance [147] and the results can be used in a straightforward manner. The relationship between apparent hydrodynamic diameter and fibril length is given for two fibril diameters (5 and 10 nm) in Figure 3.13 a).

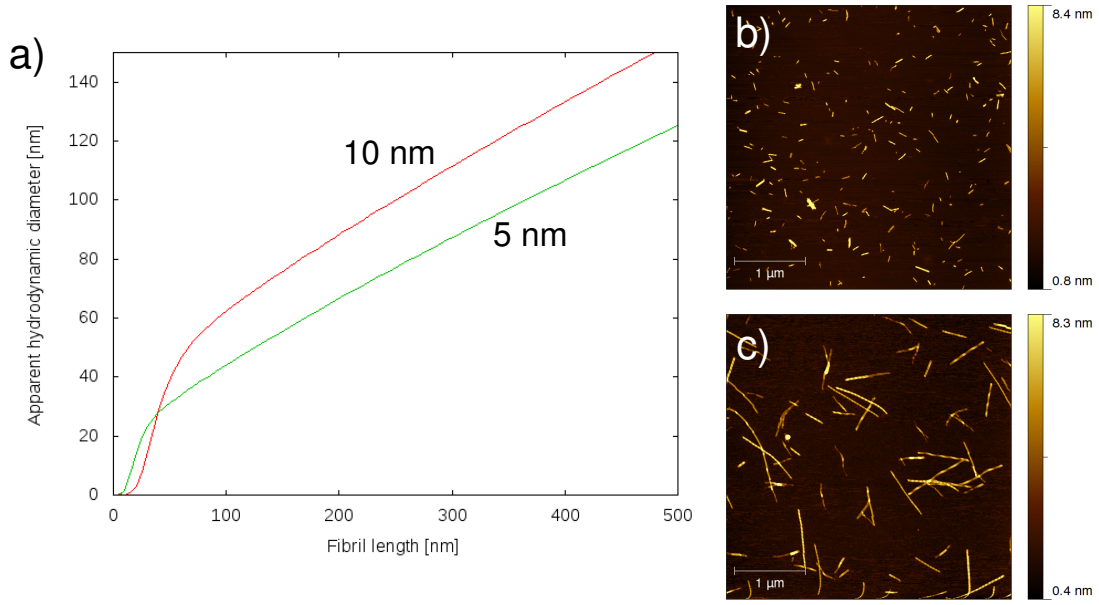

Figure 3.13: a) Curves relating the apparent hydrodynamic diameter with the fibril length for two fibril diameters (5 and 10 nm), calculated according to [147]. b) AFM image of the seed fibrils at the beginning of the assay c) AFM image of the insulin fibrils after 45 min growth at 45℃ with a monomer concentration of 0.15 mg/ml.

The key idea of the elongation assay is to start with a relatively narrow size distribution of seed fibrils that can accurately be determined with DLS. The evolution of this ensemble of seeds after addition of monomers is then monitored for a short time during which the initial narrow size distribution is projected onto a size distribution with larger average length, ideally equally narrow. The overall aggregation rates have to be adjusted such that the reaction is sufficiently fast in order to avoid sedimentation of the formed fibrils, but also sufficiently slow to be resolved with the limited time resolution of the instrument. In the case of the assay of the ionic strength dependence of the elongation rates, this adjustment was achieved by

varying the temperature. Figures 3.13 b) shows the initial length distribution of seed fibrils, and c) the result of incubation of these seeds at 45℃ for 45 min, in the presence of 0.15 mg/ml insulin monomer. The initial length of the seed fibrils is 100-200 nm (Figure 3.13 b), and the Z-average value of the size is 50-60 nm. Taking into account the thickness of the fibrils ($\sim$ 5nm), this result is in good agreement with the calculated prediction (Figure 3.13 a). Before being able to proceed, however, it must be established that the measured apparent diffusion coefficient is a purely translational one, as rotational diffusion can play a significant role in rod-like structures. It was shown by Pecora [112; 148], that the time-correlation function of the scattered field for a long rigid rod can be written as:

$$I(q,t) \propto [S_0(qL)e^{-q^2Dt} + S_1(qL)e^{-(q^2D+6\Theta)t} + ...] \tag{3.1}$$

where the right hand side of equation 3.1 is the so-called dynamic form factor of a single rod-like molecule, D is a unique diffusion coefficient for the translational diffusion of the rod, that can be calculated according to [147], Θ is the rotational diffusion coefficient, q is the scattering vector and L is the length of the rod. The "strengths" $S_{\frac{l}{2}}$ are defined in terms of the spherical Bessel functions j_l, according to:

$$S_{\frac{l}{2}}(qL) = (2l+1)\left|\frac{2}{n}\sum_{j=1}^{\frac{n}{2}} j_l(qb_j)\right|^2 \tag{3.2}$$

where n is the number of small segments the rod is divided into for the calculation of the form factor and b_j is the position vector of segment j with respect to the centre of mass of the rod. Pecora demonstrated that for $qL \leq 3$, $S_1(qL)$ is completely negligible. q is defined as: $q = \frac{4\pi n}{\lambda} sin\frac{\alpha}{2}$, where n is the refractive index of the medium (water, $\sim$ 1.33) and α is the scattering angle [112]. For the scattering geometry applied in the instrument used here, the Malvern "zetasizer nano" (see Experimental section for details), $\alpha = 173$ °, the laser wavelength $\lambda = 633$ nm and $q = 2.64 \cdot 10^7 \mathrm{m}^{-1}$. At the start of the experiment, the length of the seed fibrils is approximately 100 nm, therefore $qL = 2.64$. This calculation explains why the agreement between the length of the seeds as determined by AFM images and the value measured by DLS and converted according to the curve in Figure 3.13 a) is so good. However, at the end of the assay, the fibrils have clearly elongated several fold (Figure 3.13 c)), and the fibril length now varies between 300-1000 nm. The Z-average value measured at this point is ca. 100 nm. This value is an underestimation, as is apparent from Figure 3.13 a). It is clear that at these values of qL the rotational diffusion of the fibrils contributes significantly to the autocorrelation function of the scattered intensity. Therefore the interpretation in terms of a purely translational diffusion is not valid any more.

However, if the same range of Z-average values is explored under different conditions, e.g. with varying salt concentrations, it is a reasonable first order approximation that the ensembles of seed fibrils will be projected onto very similar final length distributions regardless of the slight change in conditions. Therefore, this assay can

then be used to compare relative elongation rates in a label-free manner. In order to improve on this approximation, it would be possible to fit the raw correlation data to a sum of two exponentials, or indeed use a different scattering geometry that minimizes the product qL.

Protocol for insulin elongation assay with DLS: The dynamic light scattering measurements were carried out using a Malvern zetasizer nano (see above). The kinetics were measured at 45℃, ensuring the right time scales, as discussed above, were met. As seeds, 500 μl a suspension of 0.1 mg/ml pre-grown insulin amyloid fibrils were used, that had been sonicated for 15 min at 125 Watts and filtered through a 220 nm filter. The length distribution of the fibril suspension was measured by DLS (Z-average value 50-60 nm) and was independently confirmed by AFM imaging to be quite narrow, and close to the minimum length that insulin fibrils can be broken down to [149]. Then 0.15 mg/ml soluble insulin were added and the evolution of the seed fibrils monitored through the change in Z-average size. The measurement was stopped when the Z-average value exceeded 100nm. The apparent hydrodynamic diameter was converted into a fibril length according to [147].

Chapter 4

Protein aggregation as a diffusive process on a free energy landscape

Having established the technical aspects of surface-bound kinetic measurements of amyloid fibril elongation, the next chapters will demonstrate how these techniques can be systematically applied to elucidate fundamental aspects of the parts of a protein's free energy landscape governing this self-assembly reaction.
Whereas structural studies by methods such as nuclear magnetic resonance (NMR) spectroscopy [150], X-ray diffraction [23], cryo-electron microscopy [28], or atomic force microscopy (AFM) [151] are applicable to the study of relatively deep minima of the free energy surface characterizing the degrees of freedom of a polypeptide chain, associated for example with the native state, folding intermediates, and the amyloid form of proteins, kinetic measurements are needed to gain insight into the energy barriers separating such minima. The extent to which variations in external conditions or differences in the intrinsic amino acid sequences influence the kinetics of amyloid assembly is a direct manifestation of the modified free energy surface. However, at the starting point of such studies, an appropriate physical picture and conceptual framework has to be established within which the acquired data can be analysed. A unifying framework for the interpretation of the wealth of data that links protein misfolding and aggregation to the extensively studied field of protein folding remains challenging to establish. In the first section of this chapter, a model considering Langevin dynamics of polymers on a characteristic energy surface is introduced, that establishes close connections between the phenomenon of amyloid growth and the current view of protein folding ([6; 152; 153], and see Introduction). Subsequently, this conceptual framework and the analytical expression for the rate law of amyloid formation derived from it are used to analyse an extensive set of measurements of the temperature dependence of amyloid elongation for a range of very varied polypeptides and proteins and the corresponding absolute elongation rates. This analysis provides insight into the molecular origin of the energy barriers that are responsible for the kinetic stability of many peptides against aggregation [34].

4.1 Amyloid formation as a diffusive process

This section is partly based on the article "Frequency factors in a landscape model of filamentous protein aggregation", Buell et al., Phys. Rev. Lett. 2010, [154]. The technical derivation of the frequency factor in the rate equation of amyloid formation is not reproduced here, as it was carried out by Dr Tuomas Knowles and Professor Eugene Terentjev.

As has been outlined in the introduction, in every kinetic theory of a molecular process the rate equation consists of two parts: a kinetic pre-factor and an exponential term, the exponent of which is interpreted as an energy of activation. In the framework of classical transition state theory, the pre-factor and the entropic part of the free energy of activation are intricately linked to each other:

$$k = \Gamma e^{\frac{\Delta S^{\ddagger}}{k_B}} e^{\frac{-\Delta H^{\ddagger}}{k_B T}} \tag{4.1}$$

where k is the rate constant, Γ the kinetic pre-factor, k_B the Boltzmann constant and $S^{\ddagger}$ and $H^{\ddagger}$ the entropy and enthalpy of activation respectively. [1] The frequency factor Γ is for simple gas phase reactions equal to $\frac{k_B T}{h}$, stemming from the quantum mechanical treatment of the motion along the reactive coordinate. The enthalpic part (per mol) can be measured from the temperature dependence of the rate r:

$$\Delta H^{\ddagger} = N_A k_B \frac{d\ln(r)}{d(\frac{1}{T})} \tag{4.2}$$

assuming that Γ is independent of temperature. Even though this is not normally the case, the weak linear dependence on temperature of the pre-factor can often be neglected if the temperature dependence is measured over a narrow temperature range. If in addition the absolute reaction rate can be measured, this measurement yields a combination of the free energy barrier and pre-factor:

$$\frac{r(T)}{e^{\frac{-\Delta H^{\ddagger}}{kT}}} = \Gamma e^{\frac{\Delta S^{\ddagger}}{k}} \tag{4.3}$$

Therefore it is useful to have an analytical expression for the pre-factor in the kinetic rate equation for amyloid formation that allows to compute this pre-factor from first principles. If this can be achieved, it allows in turn to use measurements of the absolute aggregation rate together with the enthalpy of activation from the temperature dependence measurements to determine the entropic part of the barrier as well.
As has been outlined in the introduction, the modern view of protein folding differs from the prevailing picture of small molecule reactions. Instead of a unique

[1] Compared to the equation presented in the historical overview, the quotient of partition functions has been identified with an entropy term here and the energy of activation is identified here with an enthalpy. This is approximately valid, as the difference between energy and enthalpy of activation is small.

and well-defined reactive trajectory all the way from reactants to products as pictured in a small molecule reaction, such as the prototypical gas phase reaction H-H + H $\rightarrow$ H + H-H, protein folding is more appropriately described by diffusive dynamics on a multi-dimensional free energy landscape. This energy landscape has in principle as many dimensions as the protein molecule has degrees of freedom. The number of degrees of freedom depends on the description of the polypeptide chain, and can range from course-grained descriptions that treat the polypeptide as a Gaussian chain (see below) to approaches that take the positions and momenta of each of the atoms into account. In order to fully construct such an energy landscape, one has to compute the energy of each of the possible conformations of the polypeptide chain. However, this has not been achieved to-date at any level of sophistication. Course-grained approaches, that do not rely on a complete description of the energy landscape, but that nevertheless capture key experimental features of the reaction under study therefore provide a promising route towards the ultimate goal of completely understanding protein dynamics.

Similar as in corresponding descriptions of protein folding in terms of diffusive dynamics, the polypeptides at the starting point of the aggregation process can be described as Gaussian polymers [155] with N segments, joint by Hookean springs. The number of segments is smaller than the number of amino acids of the polypeptide chain. In a Gaussian polymer, the relative orientation of the different segments is statistically independent, even though their dynamics are coupled. However, the geometry of the peptide bond leads to a correlation between the orientation of subsequent amino acid residues. Therefore, a sufficient number of amino acid subunits has to be taken together to form an ensemble that is statistically independent from the adjoint ensembles, and that provides the entropic elasticity for the springs joining the segments. As will be seen in the next section, most of the polypeptides and proteins under study here, and indeed a large part of all known amyloidogenic polypeptides are, at least partly, unfolded under the conditions where they form amyloid most readily. For these cases, the Gaussian chain model is likely to capture the characteristics of the soluble monomeric precursor to amyloid formation well. However, even the proteins, such as insulin or lysozyme that are still folded under amyloidogenic conditions will have to unfold considerably at some point on their reaction coordinate, given the large structural differences between the soluble and the aggregated protein subunit. The results of the next section show that this unfolding along the reaction coordinate is likely to take place before the transition state is reached.

The polymer segments evolve in a potential G_1 which results from the interactions with the fibril end. The physical origin of this potential is in the direct electrostatic interactions between the charged protein and the fibril end, as well as in contributions from van-der-Waals and hydrophobic interactions; in addition the breakage and formation of non-covalent contacts within and between polypeptide chains as well as with solvent molecules will contribute to this potential. In the second section of this chapter, as well as in the next chapter, the relative importance of these different energetic contributions will be studied in detail. The dynamics of such a system can be described by the Langevin equation, where the inertial term is neglected

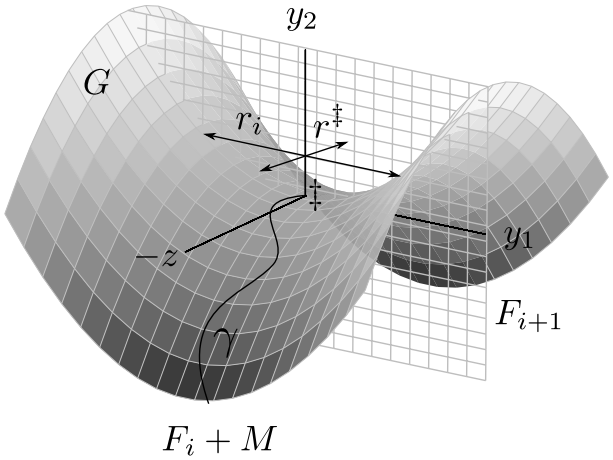

Figure 4.1: Amyloid growth through diffusive sampling of an energy surface G. The reaction rate is determined through the flux from the reactants ($A := F_j + M$) to the product ($B := F_{j+1}$). An arbitrary path γ from A to B in the proximity of the saddle point ‡ is shown in black. Drawing by courtesy of Dr Tuomas Knowles.

(overdamped case):

$$\zeta \partial_t x_i = -\partial_{x_i} G(x_1, \ldots, x_{3N}) + \xi_i(t) \tag{4.4}$$

where the $3N$ coordinates of chain segments undergo stochastic motion on the energy surface

$$G(x_1, \ldots, x_{3N}) = \sum_{i=1}^{3N} G_1(x_i) + \kappa/2 \sum_{i=1}^{3N-3} (x_i - x_{i+3})^2 \tag{4.5}$$

given by the connectivity-enforcing harmonic potentials and the external potential G_1. The thermal noise ξ_i satisfies the fluctuation-dissipation theorem $\langle \xi_i \xi_j \rangle = 2k_B T \zeta \delta_{ij}$. The reaction rate is then given by the total probability flux from one basin of the energy surface, corresponding to a fibril of length i and a separate monomer, $F_i + M$, to another basin describing the energetically more favourable fibril of length $i + 1$: F_{i+1} (Figure 4.1).

This flux can be computed by going from the Langevin to the corresponding Fokker-Planck equation [156]:

$$\partial_t \psi = -divJ \tag{4.6}$$

with

$$J_i = -D[\partial_{x_i} \psi + \beta \psi \partial_{x_i} G] \tag{4.7}$$

where $\beta = (k_B T)^{-1}$ and $\psi(x_1, \ldots, x_{3N}; t)$ is the probability density of the polypeptide chain in a configuration with the segment coordinates $[x_i]$. The complete derivation of the rate equation for amyloid fibril elongation starting from this stochastic

differential equation will not be given here. The analysis follows closely the methods employed by Kramers [56] and Chandrasekhar [157] and is described in detail in [154]. The final expression for the kinetic rate equation is:

$$\Phi = \frac{D r_{\text{eff}} c}{1 + (D r_{\text{eff}} c)\tau_R} e^{-\beta G^{\ddagger}} \tag{4.8}$$

where D is the diffusion coefficient of a chain segment (comprising ~ 3 amino acids) $D = \frac{k_B T}{\zeta} \sim 5 \cdot 10^{-10} \frac{m^2}{s}$ [158], c is the soluble protein concentration, r_{eff} is a length scale that depends on the reactive geometry of the transition state and τ_r is the average residency time of the monomer close to the fibril end, during which time no other monomer can attempt the barrier crossing. For small concentrations, this expression simplifies to

$$\Phi = D r_{\text{eff}} c e^{-\beta G^{\ddagger}} \tag{4.9}$$

An estimate of r_{eff} in terms of parameters of the Gaussian chain can be made through a self-consistency argument [154], relating the time scales of internal rearrangement of the Gaussian chain with its center of mass diffusion. r_{eff} can be computed according to:

$$r_{\text{eff}} = \frac{b_0}{\pi\sqrt{6N}} \tag{4.10}$$

where $b_0 \approx 1$ nm is the length of a segment ("Kuhn length") of three residues, and N is the number of segments. This relation is used to compute the kinetic prefactors for the computations of the free energies of activation in the next section. For example for a protein with 50 residues a value of $r_{\text{eff}} = 0.3$ $\mathring{A}$ is obtained.
As mentioned above, it can be easily seen that Equation 4.8 yields the limit $\Phi = Dc\, r_{\text{eff}} e^{-\beta G^{\ddagger}}$ at low concentrations and saturates at $\Phi = \tau_R^{-1} e^{-\beta G^{\ddagger}}$ at high concentration. It therefore reproduces the well-known sub-linear concentration dependence of amyloid fibril elongation [70; 76; 159; 160; 161]. The crossover between these two regimes occurs at $\tilde{c} = (D r_{\text{eff}} \tau_R)^{-1}$.
Having established this conceptual framework, that treats amyloid fibril elongation as a diffusive process, it can now be used in combination with the highly accurate and selective surface-based biosensor measurements described in the Methods section to gain fundamental insight into the molecular mechanisms of protein misfolding and aggregation.

4.2 Free energy barriers against amyloid formation

This section is mainly based on the article "The nature and origin of energy barriers against protein aggregation", Buell et al. 2011, in preparation. Contributions of co-authors are appropriately indicated.

The starting point for a quantitative determination of the free energy barriers associated with amyloid growth is the measurement of the temperature dependence of this process, that allows the determination of the enthalpy of activation, $\Delta H^{\ddagger}$. Raw data of a QCM measurement of the dependence of the elongation rate of PI3K-SH3 amyloid fibrils on temperature is shown in Figure 4.2 and used to illustrate the principle of the experiment. A change in temperature leads to a change in resonant frequency of the quartz crystal and before the growth rate can be probed at this new temperature, a new stable baseline needs to be established. The rate of decrease of frequency is proportional to the aggregation rate, and therefore a linear fit to the growth period is used to extract the aggregation rate. In all cases, the average of the rate for the 3 overtones N = 3,5,7 is used; a detailed explanation and justification of this analysis can be found in the section on mass sensitivity calibration in the Method development chapter.

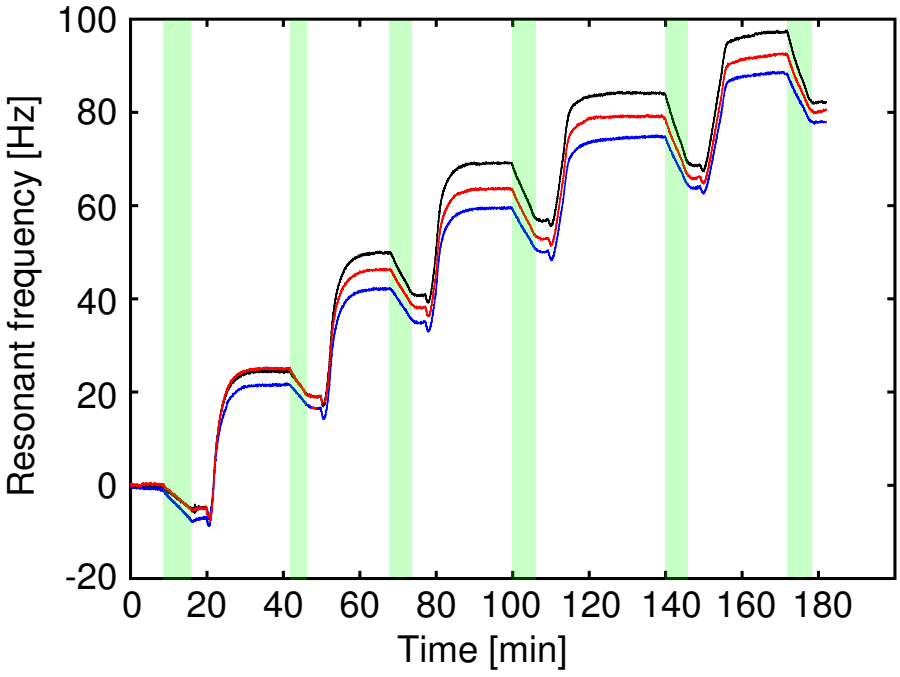

Figure 4.2: This figure illustrates the entire time course of a temperature dependence measurement of amyloid fibril elongation. In this case, seed fibrils from the protein PI3K-SH3 that forms amyloid in acidic solution, are repeatedly brought into contact with a protein solution of 1mg/ml in 0.01 M HCl (green bands). Subsequently, the liquid cell is flushed with HCl and then the temperature is increased. The increase in temperature leads to an increase in resonant frequency, and a new baseline will be established. The aggregation rates are extracted from the data by fitting the linear decrease of frequency due to fibril growth with a linear function and the average of the slopes of N = 3 (black), 5 (red), 7 (blue) was used as a measure of the elongation rate (see Method section for details). The temperature range studied here is 20-45°C.

If an Arrhenius plot of the logarithm of the reaction rate against the inverse abso-

lute temperature is linear over a certain temperature range, a well-defined energy of activation characterizes the pathway from the reactants to the products. It is known for protein folding, however, that this linearity is often not fulfilled, especially at higher temperatures, as a result of the difference in heat capacity between the initial state and the transition state of the reaction [162]. The temperature dependence of the enthalpy of activation can then be written as:

$$\Delta H^{\ddagger}(T) = \Delta H^{\ddagger}(T_0) + \int_{T_0}^{T} \Delta C_p^{\ddagger}(T) dT \approx \Delta H^{\ddagger}(T_0) + \Delta C_p^{\ddagger}[T - T_0] \tag{4.11}$$

where $\Delta H^{\ddagger}(T_0)$ is the enthalpy of activation at a reference temperature $\Delta C_p^{\ddagger}$ is the difference in heat capacity between the soluble state of the protein and the transition state. However, it was found in the present study that, for the peptides and proteins and the temperature range (15-45℃) investigated here, no strong deviations from linearity are observed (see Figure 4.3), indicating that $\Delta C_p^{\ddagger} \cdot \Delta T << \Delta H^{\ddagger}(T_0)$. Therefore, linear fits to the Arrhenius plots were performed in all cases to extract the enthalpy of activation $\Delta H^{\ddagger}$ (Figure 4.3)

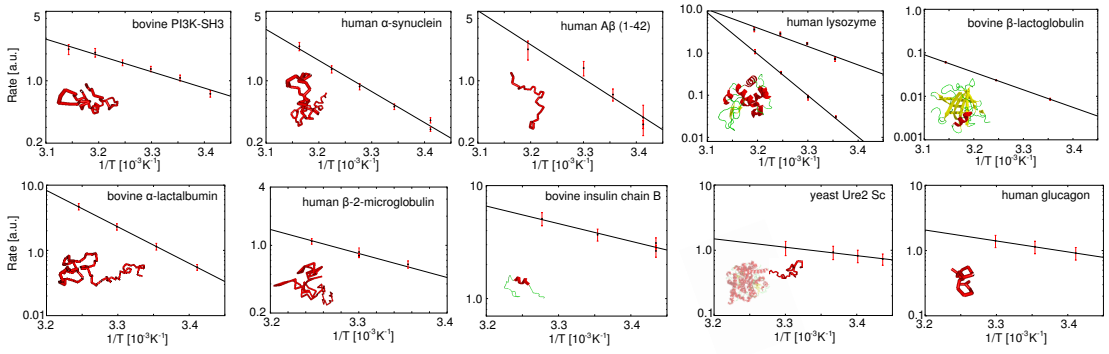

Figure 4.3: Representative Arrhenius plots for the peptides and proteins studied in this work. PDB structures are shown for the cases where the structure is relevant under the conditions where the experiments were preformed. For the unstructured amyloidogenic precursors, random coils were drawn with the persistence length of the respective polypeptide. These illustrations are intended to demonstrate the great structural and sequence-diversity of the amyloidogenic polypeptides studied here. In the case of human lysozyme, the Arrhenius plots for the native, non-reduced, form and for the form where the disulphide bonds have been reduced and blocked (see Method section for details) are shown in the same plot and the rates are normalized with respect to the concentrations of soluble protein and the fibril surface concentration, such that the absolute differences in rate are directly comparable (i.e. as vertical shift in the Arrhenius plots). The error bars are in this case not from repeated measurements, but have been determined from the deviation between the frequency harmonics with N = 3,5,7. The numerical values of the enthalpies of activation, $\Delta H^{\ddagger}$, are given in Table 4.2.

Representative Arrhenius plots for all the peptides and proteins examined in this study with QCM kinetic experiments are shown in Figure 4.3, and the corresponding numerical values of the enthalpies of activation are listed in Table 4.2. It can be noted that there is a considerable variation in this quantity, ranging from values close to the theoretical minimum for a diffusive reaction in water, stemming from the activation enthalpy of water viscosity ($\sim$ 16 kJ/mol, [163]), to values greatly in excess of 100 kJ/mol that are indicative of the need to disrupt a considerable number of interactions in order to reach the transition state.
A crucial point for the possibility to carry out these experiments was the toolbox of surface attachment methods the development of which is described in detail in the Method development chapter. Due to the large range of peptide sequences and solution conditions that were explored in these experiments, the full range of attachment strategies had to be exploited. It was an integral part of the design of this study to be able to investigate the largest possible range of amyloidogenic sequences and conditions, ranging from very short peptides to folded proteins and from non-physiological to physiological solution conditions. The reasoning behind this strategy was the hope that the common factors responsible for the tendency of many peptides and proteins to form amyloid could be distilled out of a large data set. However, the attempts to attach seed fibrils formed from the very short peptides TTR (105-115), GNNQQNY and Aβ (25-35) were not successful. The surface densities of seed fibrils that were achieved were in all cases too low to yield a measurable frequency change upon contact with soluble peptide. This finding could indicate that the parts of the polypeptide's sequence that are buried inside the fibril are not available for covalent surface attachment. Although no data is available on the proportion between buried and accessible amino acid residues for these short peptides, recent results show that the stability of the amyloid state per residue increases with decreasing sequence length [34]. This is indicative of an increasing proportion of buried residues for shorter sequences. In the case of the three very short peptides mentioned above, this effect could explain why the chemical functionalization of the fibrils formed from the short peptides is inefficient. In order to be able to measure the temperature dependence of a short peptide, therefore, an alternative route had to be explored. Thioflavin T fluorescence, despite the problems associated with its use (discussed in the Methods section), provides a possibility to carry out these measurements. However, even these measurements turned out to be impossible for the TTR and GNNQQNY peptides; for the former due to its lack of ThT binding and fluorescence and the latter due to its high tendency to form crystals instead of fibrils. Aβ (25-35) on the other hand did bind ThT and the temperature dependence of its fibril elongation reaction could therefore be probed (see Figure 4.4, and Experimental chapter for details).

In these experiments, a temperature dependence of the fibrillization could not be resolved. Therefore, and due to the difference in technique employed for this peptide, it is only included qualitatively in the following discussions.
The Arrhenius-plots shown in Figure 4.3 are all based on a single measurement. However, for the numerical values in Table 4.2, the averages of several repeated experiments are reported. The reproducibility (see errors in Table 4.2) was very

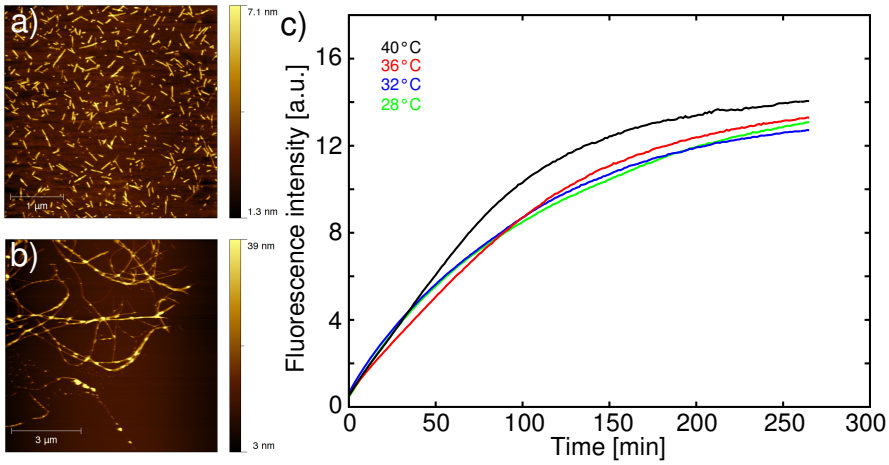

Figure 4.4: Thioflavin T fluorescence measurements to probe the temperature dependence of Aβ (25-35) amyloid fibril elongation. The increase in fluorescence with time at different temperatures was monitored. a) AFM image of the initial mixture of monomer and seed b) AFM image of an aliquot at the end of the experiment c) Fluorescence traces (raw data) at different temperatures between 28 and 40 ℃.

good in most cases. However, in the case of glucagon, the reproducibility was not very satisfying. Therefore, the temperature dependence of fibril elongation of this peptide was studied using ThT fluorescence in addition to the QCM experiments (Figure 4.5, Experimental chapter for details on the protocol). Interestingly, the ThT measurements yielded a stronger temperature dependence than suggested by the QCM measurements, hence the large error bars associated with this value.

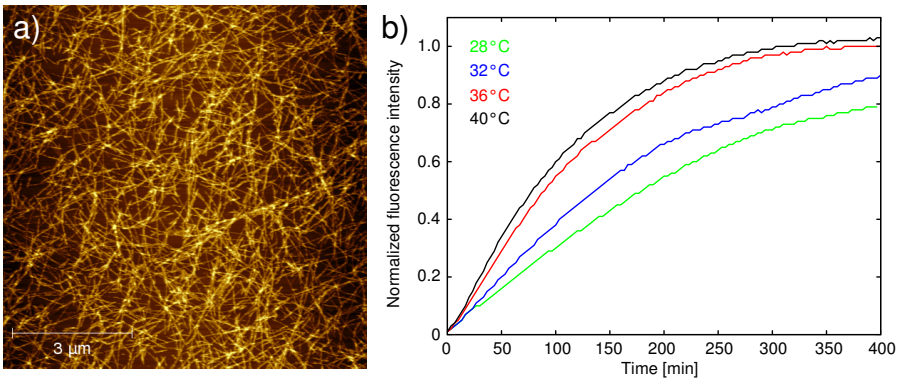

Figure 4.5: a) AFM image of the seed fibril used for the ThT measurements of glucagon amyloid fibril elongation b) normalized ThT traces (divided by final fluorescence level). The temperature dependence was measured from the slope of the initial linear part of the fluorescence traces.

As is thus demonstrated, the determination of the enthalpy of activation of amy-

loid fibril elongation does not require a knowledge of the absolute rate, but rather its relative change with temperature, this quantity is accessible with a variety of experimental techniques. Indeed it has been measured for protein aggregation of a variety of proteins [71; 75; 76; 161; 164; 165; 166; 167; 168]. These literature data have been included in Table 4.2 to give an overview of most of the values known to date along with the data measured in the present study. In general where enthalpic barriers were measured for proteins for which such data have been reported previously, the values reported here are in good agreement with the earlier values (legend to Table 4.2).

A unique feature of surface bound techniques such as QCM, however, is that the substrate can be imaged before and/or after the experiment by AFM (see Experimental and Method development chapters) and an estimate can be made of the absolute number of amyloid fibrils whose growth has contributed to the measured signal (see Figure 4.6). This analysis was in all cases carried out by hand, as it can not easily be automated; the reason is that in order for the elongation of the surface-bound fibrils to produce a measurable signal, the fibril density has to be so high that the fibrils overlap, which makes the use of standard algorithms that trace the fibrils [22; 169] impossible. An additional complication for this manual estimation of the fibril surface density is created by the relatively high average roughness of the QCM sensors. Therefore, especially in cases of very high fibril surface densities, there will be a considerable error associated with the determination of this quantity. However, due to the fact that for each individual measurement, the count was performed on several independent areas of the sensor surface and that the surface fibril density enters logarithmically in the calculation of the free energy, these errors do not affect the determination of the desired quantities to an appreciable extent. In addition, the free energy of activation was calculated separately for several individual measurements and the average of these individual calculations is quoted in Table 4.2.

This feature of surface-bound measurements therefore enables an estimate of the absolute elongation rate, ϕ_{obs}, the flux of amyloidogenic precursors adding to a single fibril end per time unit, to be made. Comparison between the theoretical, diffusion-limited maximum of the aggregation rate ϕ_{max} (see previous section for the computation) and its measured value then permits to calculate the free energy of activation according to $\Delta G^{\ddagger} = RT \log(\frac{\phi_{max}}{\phi_{obs}})$. This, in turn, allows to calculate the entropic contribution to the total free energy barrier according to $T\Delta S^{\ddagger} = \Delta H^{\ddagger} - \Delta G^{\ddagger}$; the results of these calculations are shown in Figure 4.7.

As the entire data set shown here has been acquired with the same experimental technique, these thermodynamic parameters for each system can be easily compared and correlated with the physical properties of the precursor polypeptides. The solution conditions had been chosen in each case such as to generate a high amyloidogenicity for each polypeptide, and therefore variations in pH (acidic to neutral) and ionic strength (10-200 mM) exist between the reaction conditions for the different systems (see Table at the end of the chapter for details). These factors are known to be able to modulate the rates of amyloid formation by up to two orders of magnitude ([170; 171] and in particular see Chapter 5), and therefore the free energy barriers

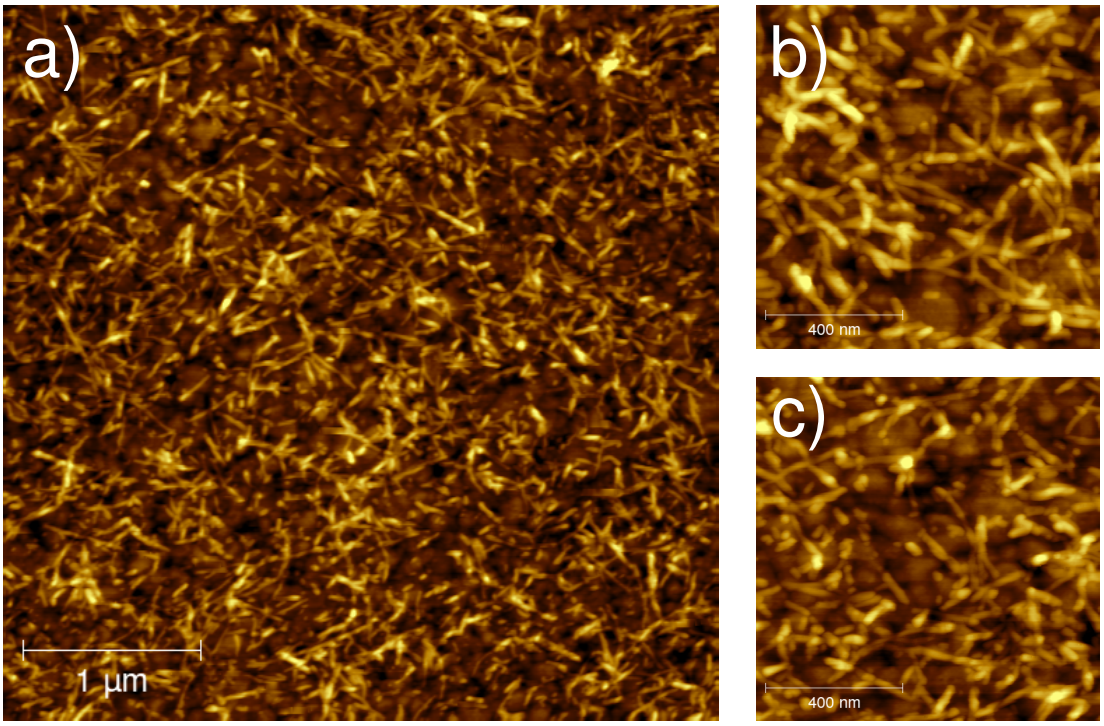

Figure 4.6: These AFM images were used to calculate the absolute elongation rate of PI3K-SH3 amyloid fibrils in the experiment shown in Figure 4.2. The surface fibril density is estimated to be on average 150±50 μm^{-2}.

by several k_BT; these effects have to be kept in mind when identifying the physical origins of these energy barriers.

Several important points can be noted when comparing different polypeptide systems. First, while the enthalpic contribution to the total free energy barrier is unfavourable in all cases, the transition state is favoured entropically relative to the precursor state for all the peptides and proteins in this study, a finding that is qualitatively different from previous reports in terms of the sign of the entropic contributions [172]. This difference stems in most cases from the use of different physical models for amyloid formation, in particular leading to very different expressions for the frequency factor in the kinetic rate equation, such as the expression $\frac{k_BT}{h}$, which was derived for simple gas phase reactions. The diffusive model that is outlined in the previous section, however, is a natural development of the widely accepted model for protein folding, namely stochastic dynamics on a free energy landscape [174; 175]. The second observation, that the differences in the enthalpy and entropy of activation between different proteins are much larger than the differences in the overall free energy barriers, reveals an interesting analogy between protein folding and misfolding, the so called enthalpy-entropy compensation ([9] and see Table 4.2). These quantities are intricately linked, most likely as a result of the important contribution of solvation and desolvation of proteins during the folding and aggregation processes. Hydration phenomena generally lead to both enthalpic (through breaking

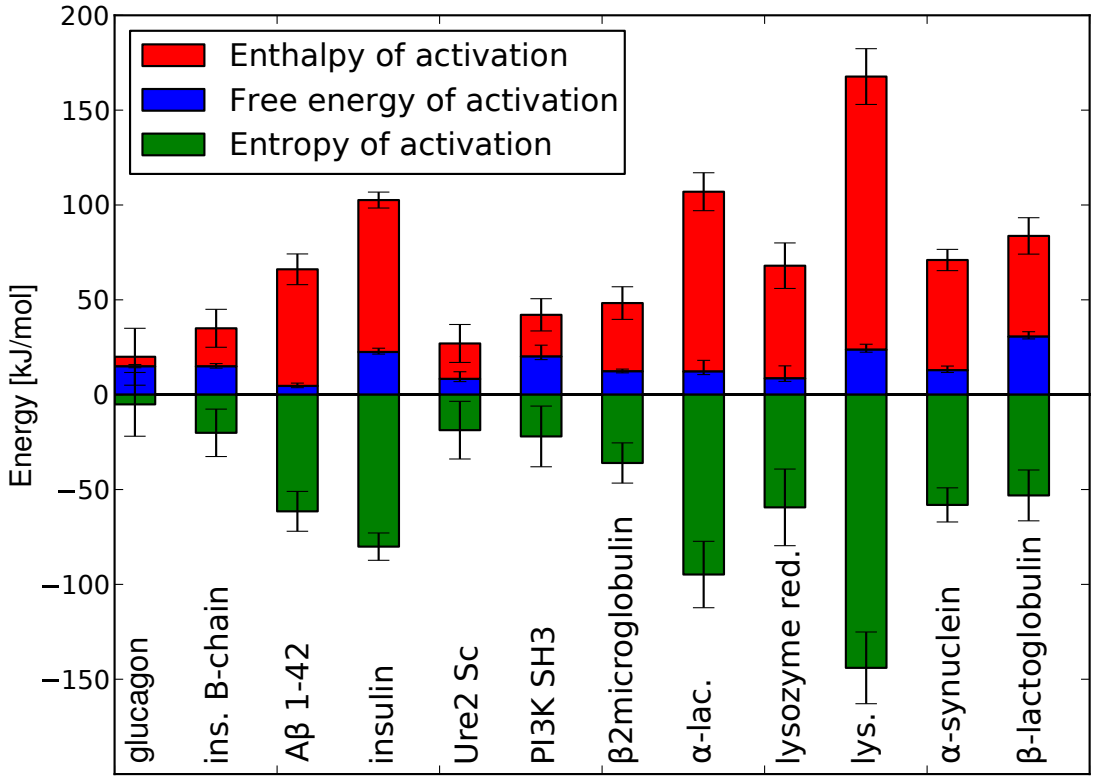

Figure 4.7: Overview of the measured enthalpies, entropies and free energies of activation for amyloid growth. The data reveal that all measured proteins have a positive enthalpic barrier for this process (the enthalpy of activation of the water viscosity has not been subtracted), whereas the entropy of activation is favourable in all cases. The phenomenon of enthalpy-entropy compensation is clearly apparent, as the overall variability in the free energies of activation is much smaller in absolute terms than the variability in the enthalpies of activation, that range from values close to the theoretical minimum for a diffusive reaction in water (16 kJ/mol) to values clearly above 100 kJ/mol, indicative of a major structural reorganization.

and formation of hydrogen bonds) and entropic (due to the lower degree of order of water molecules in bulk solution compared to a hydration shell) contributions [176]. Therefore, this compensation phenomenon is not restricted to protein reactions, but rather is a common feature of many chemical reactions in water, e.g metal complex formation [177]. It should be mentioned at this point that the observation of a generally rather narrow range of free energies is due to a certain bias of the limited sample taken in this work from the whole sequence space of known proteins; a study of the elongation rate is only possible for proteins that have relatively small free energy barriers for aggregation. Many proteins are in principle capable of forming the amyloid state, but in some cases the high barriers to conversion prevent them from doing so on measurable time scales.

peptide/protein	**free energy of activation $\Delta G^{\ddagger}$ [kJ/mol]**	**lower bound of free energy of activation [kJ/mol]**	**upper bound of free energy of activation [kJ/mol]**	**enthalpy of activation $\Delta H^{\ddagger}$ ± std [kJ/mol]**	**entropy of activation $T\Delta S^{\ddagger}$ ± std [kJ/mol] (at 298K)**
bovine PI3K-SH3	20.1	18.5	26.1	42.1±8.5	22.0±16.0
human α-synuclein	12.9	11.8	15.2	71.0±5.6	58.1±9.0
human Aβ (1-42)	4.6	3.7	6.1	66.1±8.1	61.5±10.5
human lysozyme (reduced)	8.6	7.0	15.2	68±12	59.4±20.2
human lysozyme (native)	23.7	22.4	26.6	167.7±14.7	144.0±18.9
bovine β-lactoglobulin	30.6	29.4	33.2	83.7± 9.6	53.1± 13.4
bovine insulin	22.5	21.4	24.4	102.5±4.2 [76]	80.1±7.2
bovine α-lactalbumin	12.22	10.6	18.1	107±10	94.8±17.5
bovine insulin B-chain	14.9	14.0	16.4	35.0±10.0	20.1±12.5
yeast Ure2p	8.3	6.9	12.1	27±10	18.7±15.2
human glucagon	14.9	14.1	15.9	20±15	5.1±16.8
human β-2-microglobulin	12.3	11.5	13.5	48.3±8.6	36.0±10.6
yeast Het-S	n/a	n/a	n/a	16±2 [172]	n/a
human Ig light chain	n/a	n/a	n/a	153±12 [165]	n/a
human stefin B	n/a	n/a	n/a	112.9±20.9 [168]	n/a
human α-chymotrypsin	n/a	n/a	n/a	208±17 [167]	n/a

Table 4.1: Summary of the thermodynamic parameters of activation measured for all the proteins examined in this study, along with additional data taken from the literature. In some cases, the parameters have been reported before and also measured in this study; the enthalpies of activation agree well with reported data: human α-synuclein: 84.1±3.3 kJ/mol (from [164]); bovine β-lactoglobulin: 100.4 kJ/mol (from [161]); human Aβ peptide: 95.4±4.6 kJ/mol (from [71], for the less aggregation prone peptide Aβ (1-40) at acidic pH), 61.9±1.3 kJ/mol (from [166]; also Aβ (1-40) at acidic pH), or 42.9 kJ/mol (from [75], Aβ (1-40) at neutral pH). The enthalpy of activation of water viscosity is not subtracted from the measured overall activation barrier, as some authors in protein folding studies suggest [173] as it is an arbitrary separation, given that the thermodynamic system is formed by the protein and the interacting water molecules together. In this table, published values for the entropy of activation are not quoted, as this quantity is strongly model-dependent and difficult to compare between different studies.

At this point, it is instructive, to compare the measured values for the different energetic contributions to the barriers against aggregation with the corresponding values for protein folding and therefore to put the present work into a wider context. To this aim a set of equivalent parameters for protein folding and unfolding have been collected from the available literature (see Table 4.2). To achieve maximal comparability with the data on energy barriers for amyloid formation, the enthalpy of activation of water viscosity (ca. 16 kJ/mol, [163]) was added in the cases where the authors of the respective study have subtracted it. In the study of Akmal et al. [178] from which about half of the values are taken, the viscosity of water is assumed to have a polynomial dependence on temperature rather than an exponential one with an enthalpy of activation. Nevertheless, in these cases 16 kJ/mol were also added to the values for the enthalpies of activation of folding and unfolding. As a consequence, the values for the entropies of activation need to be altered as well. Only studies were included, where the authors have analysed the kinetic data in the framework of a diffusive kinetic theory [173]. In cases where the authors have proposed an upper and lower bound of the diffusional pre-factor, the resulting upper and lower bounds for the free energies and entropies of activation are quoted. As the numerical values for the diffusional pre-factors span several orders of magnitude, the results of different studies have to be compared with care. The picture that emerges from this comparison is that the process of folding seems to be less homogeneous than misfolding and aggregation, with both positive and negative values for both the enthalpy and entropy of activation having been reported for folding; this result can be understood from the fact that protein folding is a more complex process with a multitude of possible folds, and therefore the data from different proteins will differ as a result of the varying nature of the interactions within the structures. In amyloid formation by contrast, the similarity in the structures of fibrils formed from completely unrelated primary sequences is striking [179], and it is therefore plausible to expect a more homogeneous set of transition state ensembles.

Protein	**ref.**	**temp. [°C]**	**free energy of activation of unfolding $\Delta G_u^\ddagger$ [kJ/mol]**	**enthalpy of activation of unfolding $\Delta H_u^\ddagger$ [kJ/mol]**	**entropy of activation of unfolding $T\Delta S_u^\ddagger$ [kJ/mol]**	**free energy of activation of folding $\Delta G_f^\ddagger$ [kJ/mol]**	**enthalpy of activation of folding $\Delta H_f^\ddagger$ [kJ/mol]**	**entropy of activation of folding $T\Delta S_f^\ddagger$ [kJ/mol]**
RNase A WT	[180]	45	61.6	440	378.4	41.9	-44	-85.9
Lpp-56	[181]	60	84	501	417	35	-140	-175
M2V GCN4-p1	[182]	25	51.8	128.7	76.7	17.1	-6.7	-79.6
Hisactophilin	[183]	20	79.8	65.2	-14.7	52.7	51.0	-1.6
IgG domain of prot. L	[184]	22	75.2	112.0	36.8	51.8	39.3	-12.3
NTL9	[185]	25	58.5	90.3	31.1	40.1	51.4	11.8
CspTm	[173]	n/a	n/a	n/a	n/a	10-27	28	1-18
CI2	[178]	25	58.1-69.8	194.9	125.1-136.8	25.5-37.2	74.9	37.7-49.0
CSPB	[178]	25	26.8-38.0	106.3	68.3-79.5	19.2-30.5	60.7	30.2-41.5
protein L	[178]	25	33.4-44.7	102.5	69.5-71.2	27.2-38.5	56.1	17.7-29.0
FKBP12	[178]	25	56.0-67.3	65.7	-1.6-22.3	32.2-43.9	69.1	25.2-36.9

Table 4.2: This table gives an overview over the range of free energies, enthalpies and entropies of activation that were measured for protein folding and unfolding. In some cases, the reported data had been altered by addition of the enthalpy of activation of water viscosity, in order to facilitate comparison between the studies, as well as with the values for the barrier of amyloid elongation reported here (see text for details). Due to the dependence of the entropy of activation on the model used to analyse the data, only data has been included, where the authors have analysed their results in the framework of a diffusive theory.

The next step in the analysis of the origin of the free energy barriers against aggregation is to try and correlate any particular contribution to the barriers with structural and sequence properties, such as hydrophobicity and charge of the respective soluble amyloid precursors.

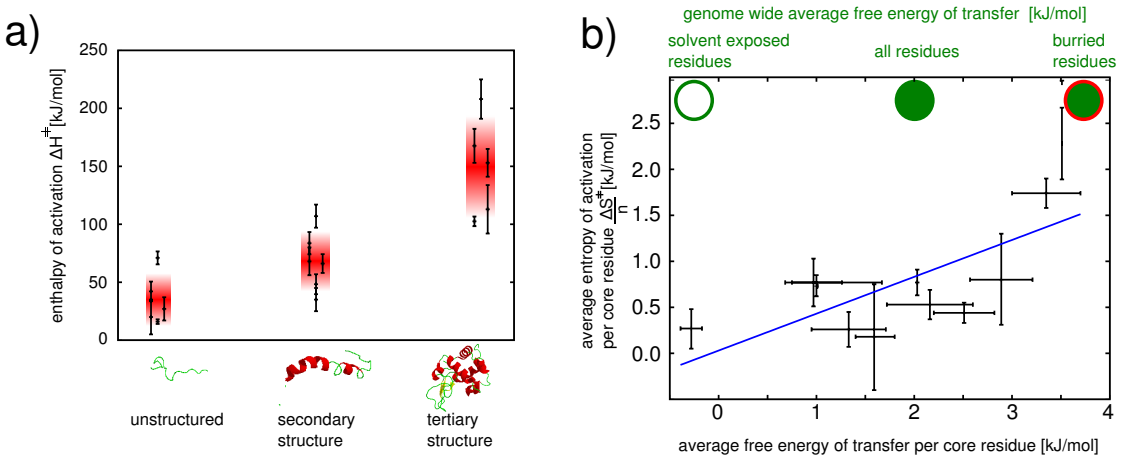

Figure 4.8: a) Correlation between the height of the enthalpic part of the free energy barrier, $\Delta H^{\ddagger}$, and the structure in the protein prior to aggregation. Values above 100 kJ/mol for $\Delta H^{\ddagger}$ are only observed for systems with persistent tertiary structure in the precursor state. The red zones indicate the means and the standard deviations respectively (values in Table 4.2). b) The average entropy of activation per core residue is plotted against the average free energy of transfer (from octanol into water, values from [88]), error bars in the x-dimension stem from the fact that part of the data set was acquired under conditions other than the ones in [88], and that in the case of reduced human lysozyme, cysteine residues were modified with respect to the reference in [88]) of the core residues. This plot suggests that the physical origin of the main favourable contribution of the entropy term to the free energy of the transition state is likely to be the (hydrophobic) collapse of the precursor protein onto a fibril end and resembles the transfer of a significant portion of its amino acids into a hydrophobic environment. A linear fit yields a slope of ca. 0.4 and a y-intercept of 0.03. As an illustration and for comparison, the average free energies of transfer of the exposed, buried and all residues of proteins from mesophilic bacteria were included on top of b) (see Experimental chapter for the computation).

The degree of residual structure in the amyloidogenic precursor varies strongly between the various polypeptides studied here. The majority do not possess persistent tertiary structure under the conditions of the experiments, and in general these peptides have much lower enthalpies of activation than the group of structured proteins (see Figure 4.8 and Table 4.2, which include data measured in this work along with data from the literature).
In order to probe this connection between structure and enthalpy of activation in more detail, not only the native state of human lysozyme was included into the

analysis, but also the reduced state where the four disulphide bonds are broken (see Experimental chapter for the protocol). Reduction and alkylation of human lysozyme gives rise to a monomeric state that lacks a well defined tertiary structure; indeed, the wavelength of maximum fluorescence emission, λ_{max}, shifts from 337 $\pm$ 2 nm to 346 $\pm$ 2nm upon reduction and alkylation, and the near-UV CD spectrum shows that tertiary contacts are no longer native-like (see Figure 4.9 a and d). The far-UV CD shows that the secondary structure is characterized by a shift to a larger random coil component after reduction (Figure 4.9 e). In the native form of this protein, a major unfolding transition is observed by calorimetry and spectroscopy very close to the temperature range of the experiments described in this chapter (see Figure 4.9) [186]. The effect of reducing the disulphide bonds, however, is a complete disappearance of the structural transition of the monomeric protein, as is evident from DSC and fluorescence experiments (Figure 4.9), accompanied by a substantial decrease in the enthalpy of activation for amyloid growth. This finding indicates that unfolding and aggregation are at least partly linked: lowering the energy required to unfold the protein also lowers the barrier for aggregation [187].

Interestingly, a physico-chemical parameter that is known to contribute to barriers against aggregation, namely charge [39; 188], does not appear to be a major contributor to the overall value of the enthalpy of activation. Thus, bovine PI3K-SH3 has a significantly higher net charge (+12) than bovine insulin (+5) and yet a much lower barrier under identical conditions (pH, ionic strength, temperature range). Similarly human lysozyme and β-lactoglobulin carry comparable charges at pH 2 ($\sim$+20), but their enthalpic barriers are very different. This finding does not, however, contradict the earlier results [39; 188] that show a strong modulation of aggregation rate with charge. Rather, it reveals that this alteration in the energy barrier is small compared to the contribution associated with residual structure. Indeed, in Chapter 5, the dependence of the fibril elongation rate on the ionic strength of the solution will be investigated in great detail. This dependence is a very sensitive measure for the importance of electrostatic interactions in the transition state ensemble of amyloid formation.

Another noteworthy observation is that two of the lowest values measured for the enthalpy of activation are for the two yeast prions HET-s (from [172]) and Ure2p (this work). Both proteins contain an unstructured prion-forming domain and a folded globular domain; the latter, however, does not contribute to the amyloid formation mechanism but rather provides function to the protein. Even though no fully definitive conclusion has been drawn as to whether yeast prions are best classified as yeast diseases [189] or functional traits [190], there is strong evidence that they have been optimised to form amyloid structures and a very low enthalpic barrier to their formation is completely consistent with this picture.

In order to complete the elucidation of the molecular origin of the free energy of activation, it is necessary to gain an understanding of the origin of the favourable entropy of the transition state. Intuitively, one might expect an unfavourable entropy of activation for an association reaction, as conformational and translational degrees of freedom are lost. The translational contribution, however, is much less important in the solution state than in gas phase reactions, as the mobility of a free

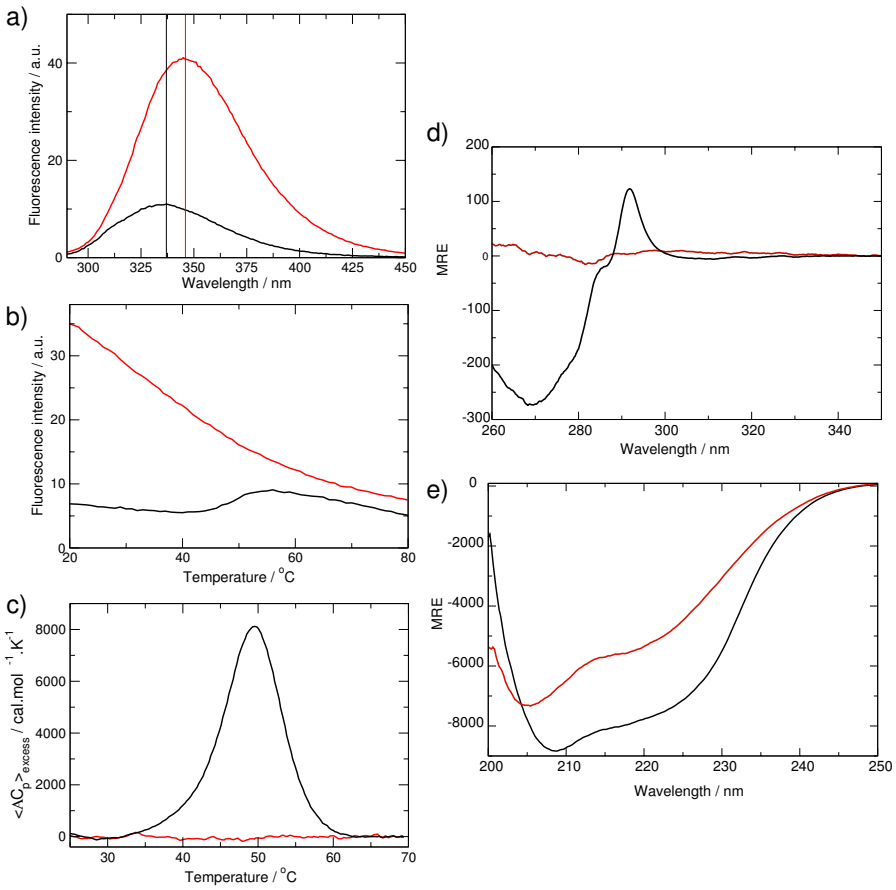

Figure 4.9: Comparison of structural properties and unfolding behaviour of the reduced and native forms of WT human lysozyme. The reduced form of human lysozyme is shown in red and the native form in black. a) Fluorescence spectra recorded at 20°C show that the tryptophans are in more hydrophobic environments in the native form than in the reduced form (lower λ_{max}, see text). b) Thermal unfolding monitored by fluorescence: an unfolding transition is only observed in the case of the native form of human lysozyme. c) Differential Scanning Calorimetry shows a peak in heat capacity for the native form only. d) Near-UV CD spectrum recorded at 35°C. e) Far-UV CD spectrum recorded at 35°C. In d) and e), 'MRE' stands for Mean Residual Ellipticity and is expressed in degrees.cm^2.dmol^{-1}. These experiments were performed with the help of Dr Anne Dhulesia and Dr Nunilo Cremades.

macromolecule in water is substantially restricted by viscosity effects [191]. Despite this restriction, this contribution to the entropy is likely to be non-negligible, but close to constant for a class of very similar reactions such as amyloid formation, as it is independent of the chemical nature of the polypeptide chain, and depends only on the size of the soluble precursor. This contribution is therefore not considered further in the analysis. The conformational entropy change of the polypeptide backbone, however, is known to be a major factor in the overall energetics of pro-

tein folding [9]. Therefore the native, disulphide-bond containing form of human lysozyme will be excluded from the following analysis, as it is the only polypeptide studied here that undergoes a major cooperative unfolding transition close to the temperature range of the experiments described above, associated with a large increase in conformational entropy. A very important contribution to the total entropy of fibril growth stems from the fact that both the precursor polypeptide and its fibril counterpart are solvated. When hydrophobic patches of up to 1 nm in diameter are exposed to water, they induce order in the water molecules in their immediate vicinity, leading to a loss of entropy of the system, whereas for larger hydrophobic surfaces, the effect is mainly enthalpic and not entropic in nature [192]. When a protein molecule attaches to the fibril end, part of this ordered water is expected to be released to bulk solution and to contribute favourably to the overall entropy of the system. In order to investigate whether this contribution can account for the sometimes very large value of TΔS (Figure 4.7 and Tables at the end of the chapter), the average entropy of activation per core residue ($\frac{T\Delta S}{n}$, where n is the number of amino acid residues that are located in the most highly structured region of the amyloid fibrils; this information is taken from the literature, see Tables at the end of this chapter) was plotted against the average free energy of transfer from water to octanol (after Fauchere and Pliska, [88]) of these core amino acids (Figure 4.8 b), and see Experimental chapter for details). This free energy of transfer of a solute from aqueous solution to a hydrophobic solvent is a measure of its hydrophobicity, and as the hydrophobic effect is thought to be mainly entropic in nature under the conditions of the experiments [192], a correlation of these hydrophobicity values with the measured entropic values might therefore be expected. Indeed, a correlation between hydrophobicity and favourable entropy of activation seems to exist (Figure 4.8 b); this finding indicates that the transition state ensemble, corresponding to the very first interactions between the soluble precursor and the fibril end, shows characteristics of a favourable transfer of the hydrophobic segments of the precursor sequence into the fibril core. This reasoning is valid even when the likely presence of some residual water in the amyloid core [193] is taken into account, as any such bound water molecules are likely to have a very different behaviour from molecules in the bulk solution. The correlation observed here is all the more remarkable for the fact that the data plotted for the different polypeptides were acquired under very different solution conditions, as mentioned before.
In order to give an additional illustration of the plausibility of the argument, that entropy associated with water plays a prominent role as one of the major determinants of the free energy of aggregation, the average free energy of transfer and therefore hydrophobicity, for surface exposed residues, for all residues, and for residues in the interior of proteins of mesophilic bacteria were indicated on the top of Figure 4.8 (see Methods section for the computation). The core residues of all polypeptides examined in this study, apart from the yeast prion Ure2p, are more hydrophobic than the typical amino acids located on the surface of a native protein, therefore making the tendency to bury these residues inside the fibrils a strong driving force for amyloid growth, similar to the situation observed in protein folding, and this effect appears already to be strongly developed in the transition state of the reaction.

The fact that it was possible to discover this correlation between hydrophobicity and the entropy of activation, while neglecting any contributions stemming from conformational entropy, strongly indicates that the degree of conformational freedom must be very similar in the amyloidogenic precursor and the transition state ensemble.
However, this reasoning raises the following question. Correlations are observed between residual structure and the enthalpy of activation of amyloid growth on the one hand, and between hydrophobicity and the entropy of activation on the other. It appears therefore that the two determining quantities of the overall free energy barrier of amyloid growth $T\Delta S^{\ddagger}$ and $\Delta H^{\ddagger}$, are strongly coupled through entropy-enthalpy compensation (see Figure 4.7), but have different physical origins, structure and desolvation. In order to investigate this apparent paradox further, and also to exclude the possibility that the correlation between enthalpy and structure is in fact only a correlation between size and structural stability [11], the 3-dimensional plot shown in Figure 4.10 was produced.

In this plot, the enthalpy of activation has been divided by the total number of residues in the sequence, therefore normalizing the data for the size of the protein. This quantity is now plotted against the same coarse structure parameter (differentiating only between systems without significant residual structure and those with secondary structure and with tertiary structure) as in Figure 4.8 a), and against the hydrophobicity of the core residues (as in Figure 4.8 b), the free energy of transfer [88] is used) of the polypeptide sequences in the second dimension. An overall trend of increasing $\frac{\Delta H^{\ddagger}}{n}$ is observed in both dimensions, even though the contribution of structure is less dominant after the normalization step, revealing the well-known correlation between protein size and structure-forming propensity [11].
Despite the difficulty to obtain a numerical value for the enthalpy of activation of the small peptide Aβ (25-35), the results that indicate a small temperature dependence and therefore a small value for $\Delta H^{\ddagger}$ can still be compared with a prediction made from the ensemble of conclusions drawn above. A low enthalpy of activation would be expected due to the complete lack of structure and the moderate hydrophobicity (the fragment (25-35) of Aβ is considerably less hydrophobic than the entire core region of the (1-42) peptide), in agreement with the experimental data.
The enthalpy of activation for amyloid fibril elongation therefore stems in large part from the breakage of interactions (presumably mainly hydrogen bonds) associated with the solvation and internal structure of the polypeptide chain. The generation of entropy-enthalpy compensation can be understood in a straightforward manner, as both desolvation and breakage of structure lead to enthalpic and entropic contributions to the free energy. This finding leads back to the intrinsic character of the presented data set, namely that amyloid formation can only be observed from those polypeptides that show clear evidence of compensation, i.e. those systems where the entropic gain from desolvation is large enough to make up for the unfavourable enthalpic contributions to the transition state ensemble.
These findings therefore readily explain and quantify in large part which physicochemical parameters govern the overall amyloidogenicity of amino acid sequences [39; 194] and build connections between protein folding on the one hand and misfolding

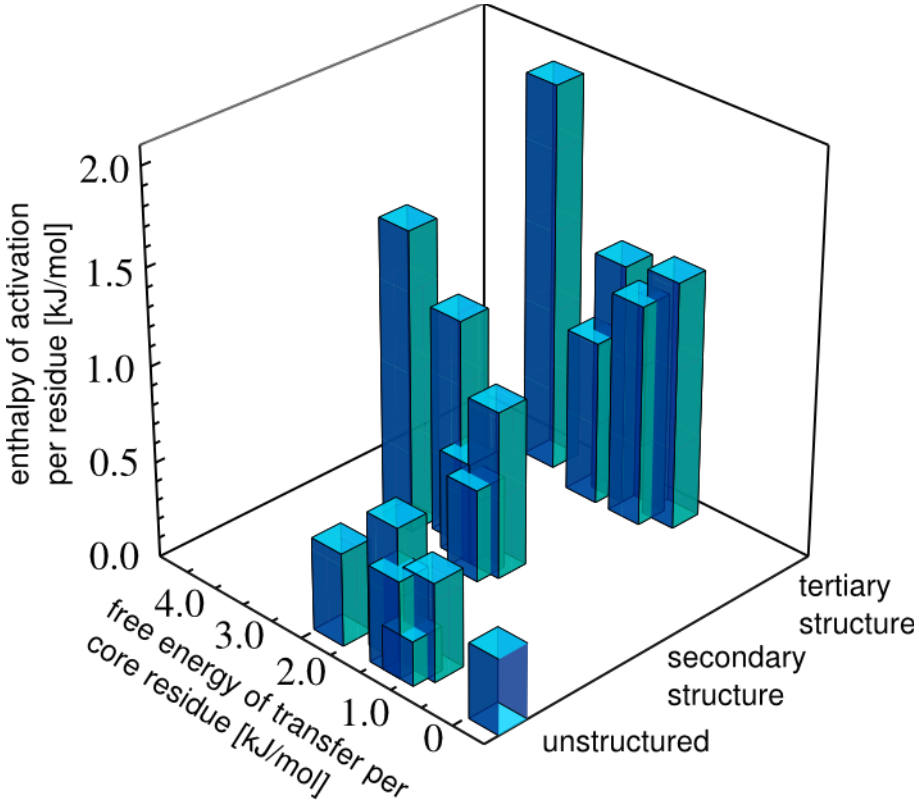

Figure 4.10: Three dimensional plot illustrating that both the degree of residual structure and the hydrophobicity of the soluble precursor polypeptide contribute to the overall enthalpic barrier for amyloid formation. The average free energy of transfer is plotted as a measure of the hydrophobicity of the residues that form the core of the amyloid structure in one dimension and the structural category in the other dimension. The average enthalpy of activation per residue is in large part determined by these two factors, at least for the proteins investigated in the present study.

and aggregation on the other. These processes can be described in terms of dynamical behaviour on the same overall free energy surface, governed by the same fundamental driving forces.

The tables on the following two pages give the full list of important parameters for the proteins of this study, such as sequence length, charge, solution conditions employed etc. In additon, it gives the kinetic pre-factors calculated according to Equation 4.10 and the measured values for the actual fluxes of monomer onto the fibril ends. From these quantities, the free energy barriers are computed.

Peptide/Protein	**number of residues**	**pH**	**ionic strength [M]**	**structure of amyloidogenic precursor**	**charge of amyloidogenic precursor**	**r_{eff} [m]**	**diffusional prefactor at 1 mM [s^{-1}]**	**flux at 298K ± std [s^{-1}]**
bovine PI3K-SH3	84	2	0.01	unfolded [195]	+12	2.46E-011	7394.5	2.2 ± 2.0
human α-synuclein	140	7.4	0.15	unfolded [196]	-9	1.90E-011	5727.7	30.9 ± 18.3
human Aβ (1-42)	42	7.4	0.1	some secondary structure [197]	-3	3.47E-011	10457.4	1622.9 ± 727.2
human lysozyme reduced	130	1.2	0.2	secondary structure [Fig. 4.9]	+21	1.97E-011	5943.9	182.8 ± 170
human lysozyme native	130	1.2	0.2	tertiary structure [Fig. 4.9]	+21	1.97E-011	5943.9	0.42 ± 0.29
bovine β-LG native	162	2	0.2	secondary structure [198]	+21	1.77E-011	5324.6	0.023 ± 0.015
bovine insulin	51	2	0.01	tertiary structure [199]	+5	3.15E-011	9489.9	1.1 ± 0.6
bovine α-LA	123	ca. 1.2	0.2	molten globule [200]	+17	2.03E-011	6110.7	44.1 ± 40
bovine insulin B-chain	30	2	0.01	some secondary structure [201]	+3	4.11E-011	12373.3	30.3 ± 14.0
Yeast Ure2p Sc	70 (354)	8.4	0.25	prion domain unfolded [202]	0 (-7)	2.69E-011	8100.2	285.8 ± 223.7
human glucagon	30	2	0.03	unfolded [203]	+5	4.11E-011	12373.3	22.4 ± 15
human β-2-microglobulin	100	2	0.04	molten globule like [204]	+18	2.25E-011	6777.1	47.3 ± 18
Yeast Het-s	ca. 70 (289)	7	0.12	prion domain unfolded [205]	0 (-6)	n/a	n/a	n/a
human IG light chain	122	7.4	0.11	tertiary structure [206]	+1	n/a	n/a	n/a
human stefin B	98	4.75	0.165	tertiary structure [207]	+8	n/a	n/a	n/a
human α-chymotrypsin	245	7.0	0.15	tertiary structure [208]	+4	n/a	n/a	n/a

Peptide/Protein	**free energy of activation [kJ/mol]**	**lower bound of free energy of activation [kJ/mol]**	**upper bound of free energy of activation [kJ/mol]**	**enthalpy of activation ± std [kJ/mol]**	**entropy of activation TS at 298K ± std [kJ/mol]**	**number of core residues**	**entropy of activation per core residue ± std [kJ/mol]**	**free energy of transfer per core residue**
bovine PI3K-SH3	20.1	18.5	26.1	42.1±8.5	22.0±16.0	84 [25]	0.26±0.19	1.33
human α-synuclein	12.9	11.8	15.2	71±5.6	58.1±9.0	79 [132]	0.76±0.11	1
human Aβ (1-42)	4.6	3.7	6.1	66.1±8.1	61.5±10.5	27 [27]	2.34±0.39	3.86
human lys reduced	8.6	7.0	15.2	68±12	59.4±20.2	77 [84]	0.79±0.28	0.97
human lys native	23.7	22.4	26.6	167.7±14.7	144.0±18.9	77 [84]	1.89±0.25	1.33
bovine β-LG native	30.6	29.4	33.2	83.7± 9.6	53.1± 13.4	122 [133]	0.45±0.12	2.51
bovine insulin	22.5	21.4	24.4	102.5±4.2 [76]	80.1±7.2	46 [209]	1.71±0.15	3.35
bovine α-LA	12.22	10.6	18.1	107±10	94.8±17.5	123 [210]	0.80±0.11	2.03
bovine insulin B-chain	14.9	14.0	16.4	35.0±10.0	20.1±12.5	25 [209]	0.88±0.50	2.89
yeast Ure2p	8.3	6.9	12.1	27±10	18.7±15.2	70 [211]	0.29±0.22	-0.28
human glucagon	14.9	14.2	16.0	20±15	5.1±16.8	29	0.18±0.57	1.59
human β-2-microgl.	12.3	11.5	13.5	48.3±8.6	36.0±10.6	68 [212]	0.53±0.16	1.59
yeast Het-S	n/a	n/a	n/a	16±2 [172]	n/a	n/a	n/a	n/a
human IG light chain	n/a	n/a	n/a	153±12 [165]	n/a	n/a	n/a	n/a
human stefin B	n/a	n/a	n/a	112.9±20.9 [168]	n/a	n/a	n/a	n/a
human α-chymotrypsin	n/a	n/a	n/a	208±17 [167]	n/a	n/a	n/a	n/a

Chapter 5

Electrostatic effects in protein aggregation

This chapter is based to a large extent on the article "Non-specific electrostatic effects in protein aggregation", Buell et al., in preparation. Contributions of co-authors will be appropriately indicated.

In the last chapter, it was shown that accurate kinetic measurements of amyloid fibril elongation can yield fundamental insight into the regions of a protein's free energy surface that form the barriers between the soluble and the aggregated state of a protein. The free energy of activation of amyloid elongation was decomposed into its enthalpic and entropic contributions. The physical origin of large parts of these energetic contributions was identified and the major determinants of the amyloidogenicity of a polypeptide defined. However, it was already outlined that electrostatic interactions, that were not taken into account in the previous chapter, do play an important role in protein aggregation. In this chapter, a systematic approach will be outlined that allows for the complex effects of salts on protein-protein interactions to be studied by kinetic measurements of protein aggregation. Indeed, as in the last chapter, the work presented here has relevance that goes beyond the specific reaction of amyloid fibril elongation, due to the identification of general principles that govern the interaction between proteins and the influence of solution ionic strength on these interactions.
The seminal contributions of Debye and Hückel [113] on the one hand and Derjaguin, Landau [213], Verwey and Overbeek [214] on the other hand to the understanding of the interactions of particles (ions, molecules or colloids) in solutions containing salts are still largely unchallenged in terms of their use in the toolbox of the practical scientist working on the interface between physics, chemistry and biology. An outline of Debye-Hückel theory will be given in the appendix at the end of this chapter, due to reference to this concept in the remainder of the chapter. Over the last decades, it has become clear that these theories fail to account for many observed effects that are clearly due to the presence of certain ions in solution, or do so only when several fitting parameters are invoked (see extensive discussion in [215]. The deviations between simple theories and experiments are particularly

obvious for biologically relevant salt concentrations where purely electrostatic interactions are largely screened [215]. Despite the strong screening in this regime, the presence of the ions cannot be neglected and other types of interactions such as dispersion or hydration forces can become important [216]. For proteins the study of electrostatic interactions has proven to be particularly challenging, even in solutions where screening is less efficient than under physiological conditions. Proteins are polyelectrolytes that can carry many charges of both signs simultaneously at a large range of pH values and therefore their interaction with any given type of ion is not straightforward to predict [215]. As an example, specific interactions between certain proteins and salts can even change the overall sign of the protein charge [217; 218]. For protein misfolding and aggregation salts have been shown to influence various stages on the pathway from soluble protein to insoluble aggregates. The reported results of systematic studies of the effects of various salts on amyloid formation differ qualitatively, ranging from reported acceleration of the reaction [170; 171; 195; 219; 220; 221; 222] to a decrease in rate [66; 223]. Also, in some cases, salts seem to follow the Hoffmeister series [219; 224], and in other cases rather the electroselectivity series [221; 225]. This multitude of findings makes the search for general features in the electrostatics of protein aggregation appear to be a daunting task. The origin of this confusing appearance of the field is the fact that most of these studies treat different proteins, under different pH conditions, and exploring very different concentration ranges of salts. In this chapter, it will be shown how a very systematic approach, starting from the simplest possible situation, namely protein aggregation under condition where the proteins only have positive charges in the presence of small concentrations of simple halide salts, can yield insight into the importance of electrostatics in protein aggregation, and can identify common features that are independent of the protein and the salt under study. The use of seed fibrils from the same batch or even of a constant ensemble of seeds in series of experiments at different ionic strength ensures that the observed differences in kinetics can directly be related to a modulation of the electrostatic forces acting between the seed and the soluble precursor, as the seed imposes the structure of the aggregate to the soluble protein in most cases [226; 227]. In addition, this approach also minimizes complications stemming from the observation that different solution conditions can induce the formation of structurally very different aggregates [195; 221].

5.1 The effect of changes in ionic strength on protein aggregation

In the previous chapter, it was established that quartz-crystal microbalance measurements can provide highly accurate data on the elongation rates of amyloid fibrils. Surface-bound seed fibrils can be incubated with solutions of soluble protein under different conditions (variable temperature in the previous chapter) and relatively subtle effects on the kinetics of elongation can be measured to high accuracy. These results suggest that the same measurements could be used as well in order to study

the influence of small variations in ionic strength on the elongation rate. At the same time, the full equivalence of the surface-bound methods, such as QCM and SPR and of the solution based assays, such as ThT fluorescence and light scattering has not been clearly established before. The present study presented an excellent opportunity to do that and the influence of low concentrations of NaCl (concentration range 0-20 mM, not far from the region of strict validity of the simple Debye Hückel theory [228]) on the elongation of pre-grown bovine insulin seed fibrils was therefore probed with the four different experimental methods mentioned above (Figure 5.1).

Experimental details for each of these four different assays of insulin fibril elongation are presented in the Experimental chapter. Here just the main characteristics are given. The first experimental difficulty arose from the fact that the final fluorescence levels were not the same for samples containing identical quantities of fibrillar and monomeric protein, but different salt concentrations. In the Experimental chapter, it is demonstrated that this phenomenon arises from an enhanced binding of ThT to insulin amyloid and/or enhanced fluorescence efficiency of bound ThT due to an increase in ionic strength, rather than a difference of the final free monomer concentration due to a change in thermodynamic stability induced by the presence of salt. The origin of this enhanced binding is presumably itself the screening effect of the salt; both the protein and the ThT molecules are charged positively under these acidic solution conditions. Therefore, in order to be able to use ThT fluorescence to study the elongation rate of insulin amyloid at different ionic strengths (Figure 5.1 a), the raw fluorescence data has to be normalized to the same final fluorescence level. As a label free alternative kinetic assay in bulk solution, the elongation of a homogeneous population of very short, pre-sonicated seed fibrils (ca. 100 nm, see section on Method development) was monitored by dynamic light scattering (DLS). Under the scattering conditions in our DLS set-up (Malvern zetasizer), and the aspect ratio of the seed fibrils (see Methods), rotational diffusion can be neglected [112] and the correlation function is quasi mono-modal. In this case, the apparent hydrodynamic radius from the fit to a single exponential, together with the thickness of the fibrils from AFM measurements, can be converted into the length of the fibrils in a straightforward manner [147]. At the end of the experiment, this conditions is not fulfilled any more; however, as discussed in the relevant section in the Method development Chapter, this does not render the assay impossible. It is crucial to optimize the experimental condition such that the initial ensemble of seed fibrils has a relatively narrow length distributions that is projected onto a similarly narrow distribution of final lengths, the average length of which does not differ by more than an order of magnitude from the initial average length. The minimal length of insulin fibrils that can be achieved by sonication is determined by the mechanical strength of the fibrils [149]. Therefore, this parameter cannot be minimized beyond the limits imposed by the high strengths of amyloid fibrils. The rate of elongation of the seed fibrils in the length interval from ca. 100 to 500 nm, corresponding to an increase in apparent hydrodynamic diameter from ca. 60 to 100 nm (Figure 5.1 b) was measured.

As surface based methods, not only QCM was explored, but also surface plasmon resonance (SPR), a technique that has been employed previously for the study of

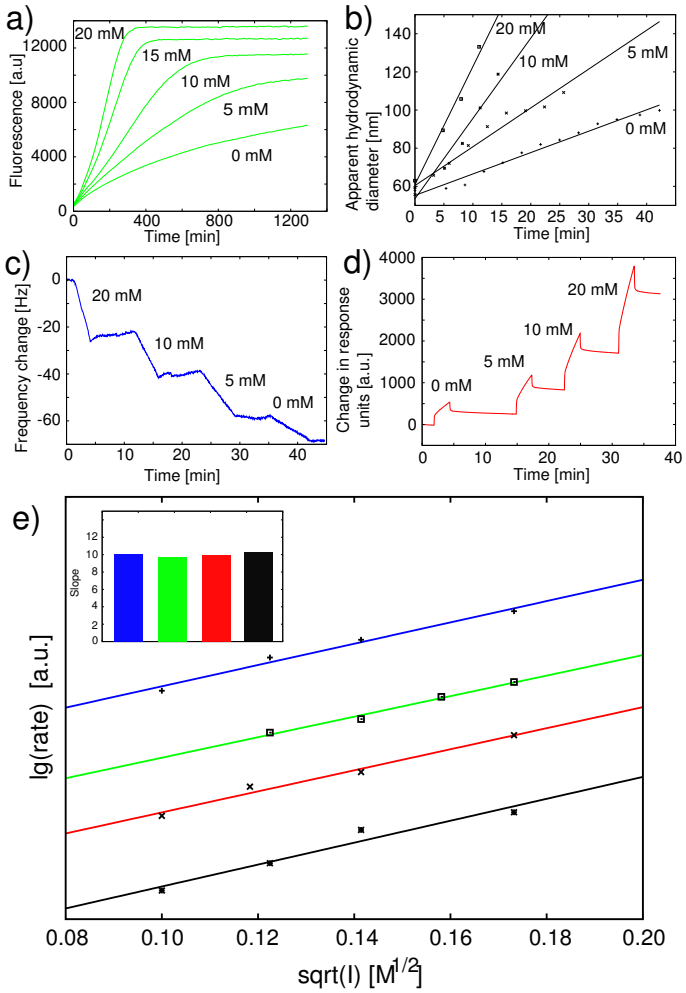

Figure 5.1: Raw data of experiments designed to study the influence of sodium chloride concentration on insulin amyloid fibril elongation rate in 0.01 M HCl, and 35-45 ℃, using 4 different experimental techniques: a) Thioflavin T (ThT) fluorescence (raw data, not normalized on the final fluorescence level), 40℃ b) dynamic light scattering (DLS), 45℃ c) quartz crystal microbalance (QCM) measurement, 35℃ d) surface plasmon resonance (SPR) measurement, 40℃. e) Debye-Hückel (DH) plot (lg of the reaction rate [in arbitrary units] against the square root of the ionic strength of the solution) of the effect of sodium chloride on the amyloid fibrils elongation kinetics of bovine insulin in 0.01 M HCl. The fibrils elongate faster at higher ionic strength. The kinetics have been measured using 4 different experimental techniques, two surface-based (QCM, SPR) and two solution based (ThT fluorescence and DLS). The good agreement between all 4 techniques (see inset for a comparison of the slopes) confirms that the process of fibril elongation along a surface is indistinguishable from the equivalent process in bulk solution, validating the surface-based biosensing approach. The linearity of the plots indicates that the salt induced screening of the positive charges operates according to a simple mechanism.

protein aggregation [96; 98; 229]. For both QCM and SPR, the same protocol was used for the attachment of the seed fibrils to the gold coated sensors, and that is described in detail in the section on Method development. The elongation of the surface-bound seeds was then monitored via their increase in hydrodynamic mass, using the QCM devices D300 and E4 (Figure 5.1 c) (Q-Sense, Västra Frölunda, Sweden) or the shift in resonance angle of surface plasmon excitation ("response units", see Figure 5.1 d), using a Biacore 3000 (see Experimental chapter).
A summary of the results of these experiments is shown in Figure 5.1 e), where the logarithm to the basis 10 of the fibril growth rate is plotted against the square root of the ionic strength of the solution, taking into account the hydrochloric acid, but neglecting the contribution from the protein itself. In the following, it will be demonstrated why this is a natural way to present such data of the reaction rate of ionic species in solution. It follows from a simple combination of the analytical expression of the rate equation for amyloid elongation (see Chapter 4) with the Debye-Hückel theory of electrolytes in solution ([113] and see appendix to this chapter). The starting point for the derivation is the rate equation of amyloid elongation:

$$\Phi = \frac{Dr_{\text{eff}}c}{1 + (Dr_{\text{eff}}c)\tau_R} e^{-\beta G^{\ddagger}} \tag{5.1}$$

To first order approximation, the frequency factor $\frac{Dr_{\text{eff}}c}{1+(Dr_{\text{eff}}c)\tau_R}$ is independent of ionic strength and will therefore be called Γ for simplicity. The free energy barrier can be decomposed into an electrostatic and a non-electrostatic part (which was discussed in detail in the last chapter). The influence of salt on the non-electrostatic contribution to the free energy of activation is neglected and the expression derived by Debye and Hückel is used for the electrostatic part of the interaction energy:

$$G^{\ddagger} = G^{\ddagger}_{ne} + V_e = G^{\ddagger}_{ne} + \frac{z_1 z_2 e^2}{4\pi\epsilon_0\epsilon_r r^{\ddagger}} e^{-\kappa r^{\ddagger}} = G^{\ddagger}_{ne} + V_C e^{-\kappa r^{\ddagger}} \tag{5.2}$$

Further, the assumption is made that the separation between the fibril end and the soluble precursor in the transition state, $r^{\ddagger}$, is smaller than the Debye length, κ^{-1}, such that the exponential function can be expanded for small $\kappa r^{\ddagger}$:

$$e^{-\kappa r^{\ddagger}} \approx 1 - \kappa r^{\ddagger} \tag{5.3}$$

This assumption seems reasonable, as the Debye length $\lambda = \kappa^{-1}$ varies between 3 and 1.7 nm for the range of ionic strength employed in the present measurements. The lower end of this range is comparable in size with the hydrodynamic radius of the proteins used here; the transition state separations can be expected to be of the same order as the radii. This reasoning, however, does not put the general contribution of a Debye-Hückel type screening mechanisms into question, as the transition state separation is unlikely to be small enough to exclude ions entirely from the contact region of the protein monomer and fibril end. One therefore obtains for the rate of amyloid formation:

$$\Phi = \Gamma e^{-\beta(G^{\ddagger}_{ne} + V_C(1-\kappa r^{\ddagger}))} \tag{5.4}$$

The unscreened Coulomb part V_C of the potential energy is to first order approximation independent of solution ionic strength (see further below for an extension of this simplified model), and can be summarized with all other independent factors into a constant C:

$$\Phi = Ce^{\beta\kappa V_C r^{\ddagger}} \tag{5.5}$$

The inverse Debye screening length κ is given by

$$\kappa = \sqrt{\frac{2N_A e^2 I}{\epsilon_0 \epsilon_r k_B T}} \tag{5.6}$$

Therefore the exponent $\beta\kappa V_C r^{\ddagger}$ can be written as:

$$\beta\kappa V_C r^{\ddagger} = \frac{1}{k_B T}\sqrt{\frac{2N_A e^2 I}{\epsilon_0 \epsilon_r k_B T}}\frac{z_1 z_2 e^2}{4\pi\epsilon_0\epsilon_r r^{\ddagger}} r^{\ddagger} = \sqrt{\frac{2N_A I}{\epsilon_0^3 \epsilon_r^3 (k_B T)^3}}\frac{e^3 z_1 z_2}{4\pi} \tag{5.7}$$

which makes the square-root dependence on ionic strength apparent. Hence we obtain the following expression for the natural logarithm of the aggregation rate:

$$\ln(\Phi) = \ln(C) + \sqrt{\frac{2N_A}{\epsilon_0^3 \epsilon_r^3 (k_B T)^3}}\frac{e^3 z_1 z_2}{4\pi}\sqrt{I} = D + E z_1 z_2 \sqrt{I} \tag{5.8}$$

with the numerical value of the constant $E = \sqrt{\frac{2N_A}{\epsilon_0^3 \epsilon_r^3 (k_B T)^3}}\frac{e^3}{4\pi} = 0.075\frac{m^{3/2}}{mol^{1/2}}$ at 298K. We therefore recover the same expression as in the theory that simply combines the activity coefficients of the reactants and the transition state [230]. Usually, the logarithm to the basis of 10, log_{10}, is used, and the units of concentrations are mol/l. Carrying out this conversion yields $E = 1.03\frac{l^{1/2}}{mol^{1/2}}$. As predicted by this simple derivation, linear behaviour is found (Figure 5.1 e) and, importantly, the slopes of the straight lines are the same within error for the data sets acquired with all four different techniques (see inset of Figure 5.1 e). This finding confirms that all four techniques are indeed probing the same molecular process, and that this process can be modelled as a bimolecular reaction between two charged species and is therefore strongly influenced by solution ionic strength. The absolute values of the rates have no importance here, and they were not determined, in contrast to the study described in the previous chapter. Only the relative change in rate with a change in ionic strength is considered in the following analysis. According to equation 5.8, the slope of such a plot is proportional to the product of the effective charges of the two reacting species: $log_{10}k = D + 1.03 \cdot z_A \cdot z_B\sqrt{I}$, as derived above. As a first order approximation, it will be assumed that the fibril end carries the same charge as the soluble pre-cursor and the square root of the product $z_A \cdot z_B$ will be taken as the effective charge of the protein. In this case, we obtain 10.0±1.0 for the slope and therefore 3.16± 0.17 for the effective charge. This is less than the absolute charge of insulin at this pH (+5, calculated under the assumption of independent pka's), consistent with the idea that only part of the total charge is relevant in the aggregation mechanism. In order to get some independent insight into the overall charge

state of both soluble and fibrillar insulin under these conditions, ζ-potential measurements were performed (see Experimental chapter). The ζ-potential of sonicated fibrils and soluble protein was measured in the absence of any added salt and values of +35.5±10.0 mV for monomeric insulin and +40.0±5.0 mV for sonicated fibrils were obtained, in support of the assumption that soluble protein and aggregates have similar charge densities. This finding is in disagreement with recent reports that proteins have to be neutral in order to incorporate into amyloid aggregates [116]. In the case of the soluble insulin molecules, we can roughly estimate the surface charge of the molecule (bovine insulin is mainly monomeric under the mildly acidic conditions employed here) from the ζ-potential, given the effective hydrodynamic radius of the soluble protein ($\sim$ 1.7 nm), according to the formula [231]: $Q = 4\pi\epsilon r_p(1 + \kappa r_p)\zeta_p$, where ϵ is the dielectric constant of the solution, r_p is the hydrodynamic radius of the protein and κ is the inverse Debye screening length ($\sim$ 3 nm at I = 0.01 M). This calculation, which is strictly valid only for $\zeta < \frac{k_B T}{e} \approx +25$ mV, yields a rough estimate for the surface charge of $\sim$+4-5, a value close to the absolute charge of the molecule. Together with the finding that the ζ-potentials of fibrils and soluble protein are not significantly different, we therefore have strong evidence that the protein does not change its charge state significantly when incorporating into an amyloid fibril.

5.2 Non-specific electrostatic screening

The satisfactory establishment of the equivalence of the two solution-based and the two surface-based experimental techniques for the study of amyloid elongation, therefore allowed to acquire the data shown in the remainder of this chapter by means of surface based measurements due to their accuracy, rapidity and ease of use. In order to test how general the screening mechanism described in the first section is, equivalent experiments to the ones shown in Figure 5.1 c) were performed to study the influence of small concentrations of a range of different simple halide salts on the amyloid fibril elongation of bovine insulin and of another protein that forms amyloid fibrils under very similar solution conditions, bovine PI3K-SH3. A series of mono-valent and also some di- and trivalent halides were tested (Figure 5.2 a) and b), and the picture that emerged from these measurements is that the mechanism of screening of electrostatic repulsion identified here is not restricted to insulin. Indeed, for PI3K-SH3 a qualitatively very similar behaviour is found, with indistinguishable slopes (within error) of the Debye-Hückel (DH) plots for all mono-valent salts. The slopes are higher than in the case of insulin by a factor of 2 (20±2), leading to an effective charge of 4.5±0.3, consistent with a higher maximum net charge (+12). The difference between the effective charge for the aggregation reaction and the total charge is much larger for PI3K-SH3 compared to insulin, suggesting that the existing charges could be placed in such a way as to have a smaller impact on the aggregation mechanism. Indeed, it was shown previously for this protein that subtraction of a charge only accelerates the kinetics by a factor of two; addition of a charge, however, can slow down the reaction to a much larger

degree [188].

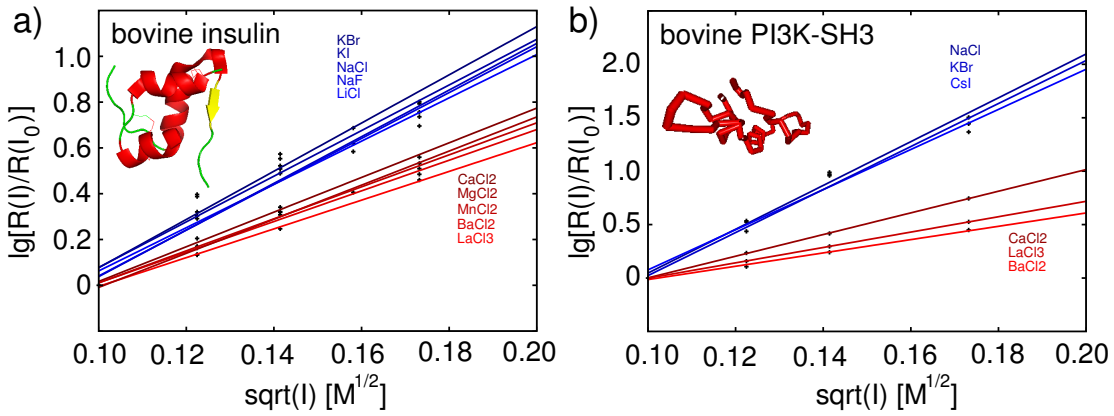

Figure 5.2: Debye-Hückel-plots plots for a) bovine insulin and b) bovine PI3K-SH3, obtained from QCM and SPR measurements. The data confirm that a non-specific screening mechanism exists that does not depend on the chemical nature of the anions and cations studied, but only on the valency of the cation. The dependence on the valency is opposite to the predictions of theory, where multivalent salts are predicted to be more efficient screeners than mono-valent salts at a given ionic strength [232]. Such a behaviour can most readily be explained by chemically non-specific ion pair formation (see detailed discussion in text).

Most interestingly, when probing the effect of simple multivalent salts, it is found that for both proteins, the corresponding DH plots are less steep than for the mono-valent salts, with the difference in slopes being more pronounced in the case of PI3K-SH3. Therefore, the multivalent salts are less efficient in screening the intermolecular repulsion that forms part of the energy barrier for the bimolecular reaction of amyloid fibril elongation. This finding, which is opposite to what an extension of Debye Hückel theory to multivalent electrolytes predicts [232], indicates that an analysis of the slope as the square of the effective charge for aggregation is an over-simplification. Assuming that the mechanism of aggregation does not change when the valency of the salt is changed, an explanation of the observed trend requires the inclusion of an additional term into the expression for the rate equation of amyloid elongation as a function of ionic strength. The simplest extension is to include binding of the salt ions to the protein in such a way as to change the global charge of the protein without interfering with the non-electrostatic contribution to the free energy landscape. It has been known for many decades, that ions can bind to proteins more tightly than the loose association of the ionic cloud interacting with the surface charges of the protein according to the Debye-Hückel mechanism [233; 234]. In the following, it will be demonstrated, how the inclusion of non-specific ion binding can lead to the observed behaviour. As a simple approach, it is assumed that the change in charge of the protein in the presence of an ion can be described by a single average "binding constant", neglecting any dependence of the binding on the

charge state of the protein. For the general case of a salt AB_i, one obtains for the charge of the protein:

$$Q = Q_0 + ieK_i[A^{i+}] - eK_-[B^-] \tag{5.9}$$

where Q_0 is the (hypothetical) charge in the absence of any ion binding, K_i and K_- are the binding constants for the cations (with charge +i) and anions (with charge -1), e is the elementary charge and [X] are the concentrations. Before proceeding further, it needs to be established why it is justified to write the variable charge in this form, using the K_i as defined above. Assume that there are n independent binding sites on the protein where ions can attach. These binding sites are taken to be non-interacting, excluding even simple electrostatic interactions. The following treatment will therefore only be valid for a small total number of bound ions. At each binding site the equilibrium:

$$K = \frac{[PX]}{[P][X]} \tag{5.10}$$

exists, where [P] is the protein concentration, [X] the concentration of the ion, and [PX] the concentration of ion pairs. The fraction f of ion pairs can then be written:

$$f = \frac{[PX]}{[P] + [PX]} = \frac{K[P][X]}{[P] + K[P][X]} = \frac{K[X]}{1 + K[X]} \tag{5.11}$$

Therefore, the protein charge changes due to these n binding equilibria by:

$$\delta q = nief = nie\frac{K[X]}{1 + K[X]} \tag{5.12}$$

This expression can be written for small $K[X]$ as $\delta q = nieK[x]$, where i is the charge of the ion. The K_is from equation 5.9 can therefore be identified with nK. But under what circumstances is it legitimate to simplify equation 5.12? The answer is if there are many binding sites (n large) and if the binding to each binding site is weak (K[X] small). This situation is probably fulfilled, as the lack of chemical selectivity of the observed ion binding suggests that the ions are unlikely to attach to fixed, well defined binding sites with a high affinity, but rather are loosely attached to varying parts of the protein.
All the experiments have been conducted in 0.01 M HCl, and the chloride anions from the HCl will be taken into account for the total concentration of anions, together with the anions from the added salt. Any hypothetical binding of the free protons will be ignored as, even if there is an interaction between protons and the protein other than direct protonation, the extent of this binding will be the same for all samples of one protein and the effect will be a shift in Q_0. In order to have only one independent variable, the concentrations of the ionic species are expressed as a function of the total ionic strength of the solution, I. There is a unique relationship between I and [X] for each of the valencies. Mono-valent:

$$[A^+] = I - 0.01; [B^-] = I \tag{5.13}$$

$$Q(I) = Q_0 + eI(K_1 - K_-) - e0.01K_1 = Q_0 + eI(K_1 - K_-) - eI_0K_1 \tag{5.14}$$

where $I_0 = 10^{-2}M$ is the concentration of HCl.
divalent:

$$[A^{2+}] = \frac{I - I_0}{3}; [B^-] = \frac{2(I - I_0)}{3} + 0.01 \tag{5.15}$$

$$Q(I) = Q_0 + eI(\frac{2}{3}K_2 - \frac{2}{3}K_-) - eI_0(\frac{2}{3}K_2 + \frac{1}{3}K_-) \tag{5.16}$$

and trivalent:

$$[A^{3+}] = \frac{I - I_0}{6}; [B^-] = \frac{3(I - I_0)}{6} + 0.01 \tag{5.17}$$

$$Q(I) = Q_0 + eI(\frac{1}{2}K_3 - \frac{1}{2}K_-) - eI_0(\frac{1}{2}K_3 + \frac{1}{2}K_-) \tag{5.18}$$

Next the expression of the variable charge is inserted into the equation 5.1 that describes the aggregation rate:

$$\Phi = \Gamma e^{-\beta(G^{\ddagger}_{ne} + V_{el})} \tag{5.19}$$

with

$$V_{el} = \frac{Q(I)^2}{4\pi\epsilon\epsilon_0 r^{\ddagger}} e^{-\kappa r^{\ddagger}} \tag{5.20}$$

In this expression, both the charge Q and κ are functions of ionic strength. In order to simplify that expression, the normalized rates will be considered:

$$\log(\frac{\Phi(I)}{\Phi(I_0)}) = \frac{Q(I_0)^2}{4\pi\epsilon\epsilon_0 r^{\ddagger} k_B T} e^{-\kappa(I_0) r^{\ddagger}} - \frac{Q(I)^2}{4\pi\epsilon\epsilon_0 r^{\ddagger} k_B T} e^{-\kappa(I) r^{\ddagger}} \tag{5.21}$$

The experimental data suggests a linear dependence of the rate on the square root of ionic strength for all valencies, therefore $\frac{Q(I)^2}{4\pi\epsilon\epsilon_0 r^{\ddagger} k_B T} e^{-\kappa(I) r^{\ddagger}}$ can be expanded around I_0 in $\sqrt{I}$ and only the linear term will be kept. This expansion has to be done separately for each valency, due to the different relationships between ionic strength and ion concentration. The detailed calculation is shown for the mono-valent case, the higher valencies are treated analogously. It is convenient at this point to make a variable change from I to x=$\sqrt{I}$:

$$V_{el}(I) = \frac{(Q_0 + eI(K_1 - K_-) - eI_0K_1)^2}{4\pi\epsilon\epsilon_0 r^{\ddagger}} e^{-\kappa(I) r^{\ddagger}} = \frac{(Q_0 + ex^2(K_1 - K_-) - eI_0K_1)^2}{4\pi\epsilon\epsilon_0 r^{\ddagger}} e^{-axr^{\ddagger}} = g(x) \tag{5.22}$$

where $\kappa = a\sqrt{I}$. The series expansion is then given by:

$$g(x_0 + \delta x) = g(x_0) + \frac{\partial g(x)}{\partial x}\Big|_{x_0} \cdot \delta x + \frac{1}{2}\frac{\partial^2 g(x)}{\partial x^2}\Big|_{x_0} \cdot (\delta x)^2 + ... \tag{5.23}$$

Evaluating $g(x)$ and $\frac{\partial g(x)}{\partial x}$ at $x = x_0 = \sqrt{I_0}$ yields:

$$g(x_0) = \frac{(Q_0 - eI_0K_-)^2}{4\pi\epsilon\epsilon_0 r^\ddagger} e^{-a\sqrt{I_0}r^\ddagger} = \frac{Q(I_0)^2}{4\pi\epsilon\epsilon_0 r^\ddagger} e^{-a\sqrt{I_0}r^\ddagger} \tag{5.24}$$

and

$$\frac{\partial g(x)}{\partial x}\Big|_{x_0} = \frac{2(Q_0 + ex^2(K_1 - K_-) - eI_0K_1)2ex(K_1 - K_-)}{4\pi\epsilon\epsilon_0 r^\ddagger} e^{-axr^\ddagger}\Big|_{x_0} \tag{5.25}$$

$$+ \frac{(Q_0 + ex^2(K_1 - K_-) - eI_0K_1)^2 ar^\ddagger}{4\pi\epsilon\epsilon_0 r^\ddagger} e^{-axr^\ddagger}\Big|_{x_0} \tag{5.26}$$

$$= \frac{e^{-a\sqrt{I_0}r^\ddagger}}{4\pi\epsilon\epsilon_0 r^\ddagger}[4Q(I_0)e\sqrt{I_0}(K_1 - K_-) - Q(I_0)^2 ar^\ddagger] \tag{5.27}$$

Therefore:

$$\log(\frac{\Phi(I)}{\Phi(I_0)}) = \frac{Q(I_0)^2}{4\pi\epsilon\epsilon_0 r^\ddagger k_B T} e^{-a\sqrt{I_0}r^\ddagger} - \frac{Q(I)^2}{4\pi\epsilon\epsilon_0 r^\ddagger k_B T} e^{-a\sqrt{I}r^\ddagger} \tag{5.28}$$

$$\approx \frac{e^{-a\sqrt{I_0}r^\ddagger}}{4\pi\epsilon\epsilon_0 r^\ddagger k_B T}[Q(I_0)^2 ar^\ddagger - 4Q(I_0)e\sqrt{I_0}(K_1 - K_-)] \cdot (\sqrt{I} - \sqrt{I_0}) \tag{5.29}$$

and analogously for divalent salts:

$$\log(\frac{\Phi(I)}{\Phi(I_0)}) \approx \frac{e^{-a\sqrt{I_0}r^\ddagger}}{4\pi\epsilon\epsilon_0 r^\ddagger k_B T}[Q(I_0)^2 ar^\ddagger - 4Q(I_0)e\sqrt{I_0}(\frac{2}{3}K_2 - \frac{2}{3}K_-)] \cdot (\sqrt{I} - \sqrt{I_0}) \tag{5.30}$$

and trivalent salts:

$$\log(\frac{\Phi(I)}{\Phi(I_0)}) \approx \frac{e^{-a\sqrt{I_0}r^\ddagger}}{4\pi\epsilon\epsilon_0 r^\ddagger k_B T}[Q(I_0)^2 ar^\ddagger - 4Q(I_0)e\sqrt{I_0}(\frac{1}{2}K_3 - \frac{1}{2}K_-)] \cdot (\sqrt{I} - \sqrt{I_0}) \tag{5.31}$$

Comparing these expression with the experimental data, it can be noticed that the slopes on the DH plots for divalent and trivalent ions are very similar, and smaller than for mono-valent ions, and that the only difference between the terms above for the different valencies is the expression involving the K_i. Hence, the following inequalities result from the above expressions:

$$\frac{2}{3}(K_2 - K_-) > K_1 - K_- \tag{5.32}$$

and

$$\frac{1}{2}(K_3 - K_-) > K_1 - K_- \tag{5.33}$$

From the experiments, it is clear that the binding constant of any given ion does not depend on its chemical nature, but only on its charge. *A priori*, none of the 4 binding constants K_i (i = 1,2,3) and K_- can be neglected. However, two extreme scenarios can be distinguished:
1) $K_- >> K_i$. Here, the difference between the K_i becomes irrelevant, and the less efficient screening of poly-valent salts is readily explained by the smaller number concentration in anions at any given ionic strength, compared to mono-valent salts.
2) $K_- << K_i$. In this case, we deduce from the above inequalities that $K_2 > K_1$ and $K_3 > K_1$. Therefore, the less efficient screening is explained by an increase of the charge of the protein by a binding of multivalent ions. This *a priori* counter-intuitive possibility of an efficient binding of a multiply positively charged ion to a multiply positively charged protein could be rationalized by the presence of neutral, polarizable patches even in globally positively charged protein molecules.
In Figure 5.3, linear fits for both proteins are shown where all the data points for one valency are taken together. The fits are forced to go through $(\sqrt{I_0}, 0)$, the point around which the expression for the rates was expanded.

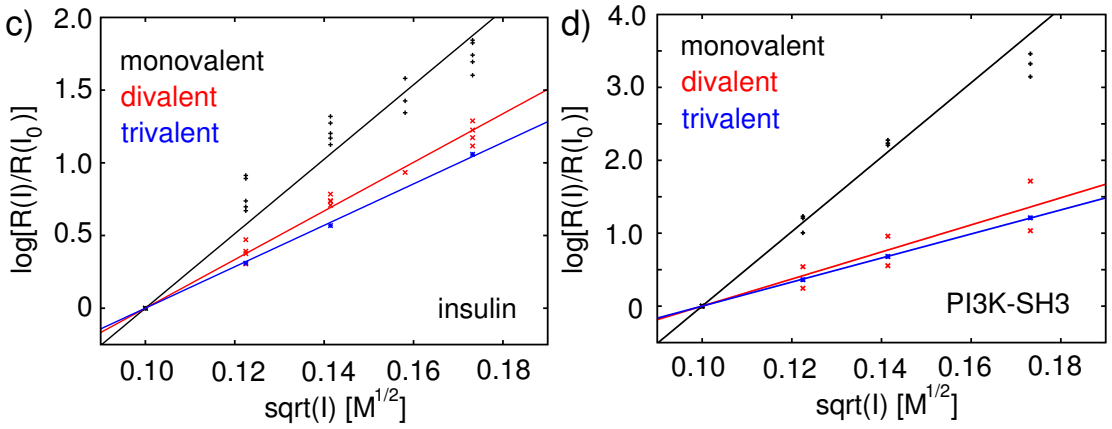

Figure 5.3: According to the theoretical analysis described in the text, the three data sets for mono-, di- and trivalent salts are separately fitted to linear functions that are forced to go through $(\sqrt{I_0}, 0)$, where I_0 is the ionic strength of the HCl and around which the rate was expanded in $\sqrt{I}$. a) bovine insulin b) bovine PI3K-SH3.

Based on the kinetic data only, it is not possible to unambiguously discriminate between the two alternatives, anion or cation binding. At the end of the next section, this problem will be discussed based on previously published data.

5.3 Specific effects

The results described in the previous section were qualitatively confirmed for two additional polypeptides that both form amyloid under similar solution conditions (HCl 0.01 M), human glucagon and human β2-microglobulin: in both cases, divalent chlorides were less efficient in screening than mono-valent chlorides. However, it

has been reported before for both glucagon [221] and β2-microglobulin [220], that iodide ions are more efficient in accelerating amyloid growth than chloride ions. This result suggests a difference between the proteins described in detail in this chapter and glucagon and β2-microglobulin. In order to confirm this difference, experiments were performed with these two proteins. The published results could be confirmed even for the smaller, less polarizable bromide ions (see QCM raw data in Figure 5.4 a and b); it can thus be concluded that chemically more specific ion binding must start to play a significant role here, as opposed to the combination of Debye screening and non-specific binding described above. In order to explain this difference between insulin and PI3K-SH3 on the one hand and glucagon and β2-microglobulin on the other hand, the charge density of the four proteins was computed in the simplest possible way: the theoretical maximum charge at this pH (in $10^{-2}M$ HCl, the difference to the actual charge should not be large) was divided by the total number of amino acids. The following values are obtained: bovine insulin: $+5/51 = 0.10$; bovine PI3K-SH3: $+12/84 = 0.14$; human glucagon: $+5/29 = 0.17$; human β2-microglobulin: $+18/100 = 0.18$. Therefore the resolvable specific interactions with bromide coincide in both cases with a higher average charge density. This difference in charge density might also rationalize the finding that systematically higher ionic strengths had to be used for both glucagon and β2-microglobulin in order to observe growth rates comparable to insulin and PI3K-SH3. In the absence of any added salt for example, fibril elongation could not be detected with the QCM for both glucagon and β2-microglobulin. The bromide ion is softer and more polarizable than the chloride ion and therefore has a stronger tendency to associate with soft alkylammonium groups on proteins. Potentially, the overall charge density determines the extent to which this association, which seems to be chemically more specific than the type of interaction described above for insulin and PI3K-SH3, can manifest itself. It cannot be excluded that subtle differences exist in the association of simple halides to insulin and PI3-SH3 as well, that we cannot resolve with our kinetic measurements. Future studies will establish if there really is a qualitative difference between these groups of proteins.

In order to further bridge the gap between this study and existing literature on the effect of salts on protein aggregation that is discussed in the introduction to this chapter, the effect of the more complex anions nitrate and sulphate on the elongation of PI3K-SH3 fibrils (Figure 5.4 c) was also investigated. In agreement with studies on other proteins, it was found that sulphate is by far the most efficient anion in accelerating amyloid growth. This effect can easily be explained through a tight binding between the structured sulphate ion (and to a lesser extent the nitrate ion) and the protein. However, such effects will be very susceptible to the particular protein under study and are therefore less well suited to identify very general principles governing the electrostatic interactions of macromolecules. The overall findings of this study are summarized in the schematic representation of Figure 5.5.

This chapter will be ended with a short discussion of the most likely origin of the less efficient screening of poly-valent salts compared to mono-valent salts at identical ionic strength. The question of ion binding to proteins has been under

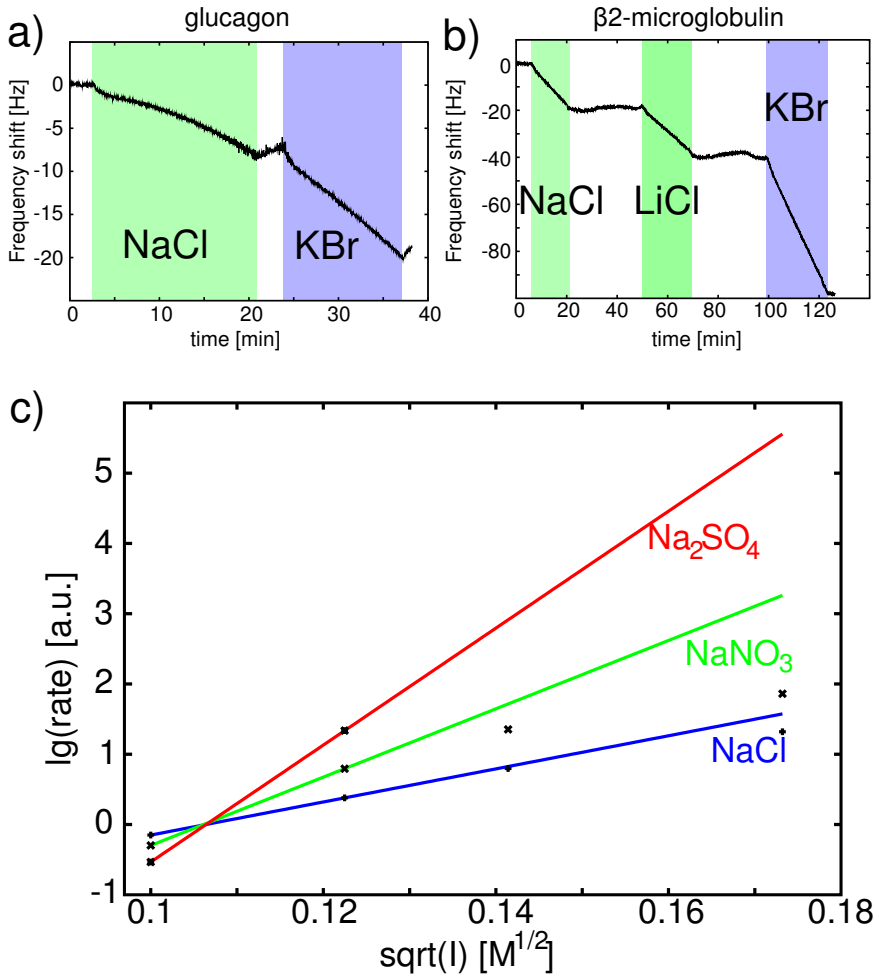

Figure 5.4: QCM-measurements, confirming that for a) human glucagon and b) human β2-microglobulin, specific electrostatic effects can already be observed for simple halides, here bromide. c) Strong specific effects are exhibited for more complex ions, such as nitrate and sulphate. Debye Hückel plots are shown for PI3K-SH3. The lines are in this case not fits, but connect the first two points, for comparison and due to the lack of data points at higher sulphate concentrations.

study for many decades now. It is interesting to put the work described in this chapter into context with the early work of two great protein scientists, George Scatchard and Charles Tanford. It has been known for a long time that the pH of solutions containing protein can be changed by adding a salt that does not change the pH of pure water. It was understood that the origin of this effect was the direct electrostatic effect of bound ions on the protonation equilibria of acidic and basic groups on the protein. Many experimental efforts have been undertaken to quantify this binding and to determine a protein's effective charge. The methods used were conductometric [233], or potentiometric [233], later also ultracentrifugation [235] and

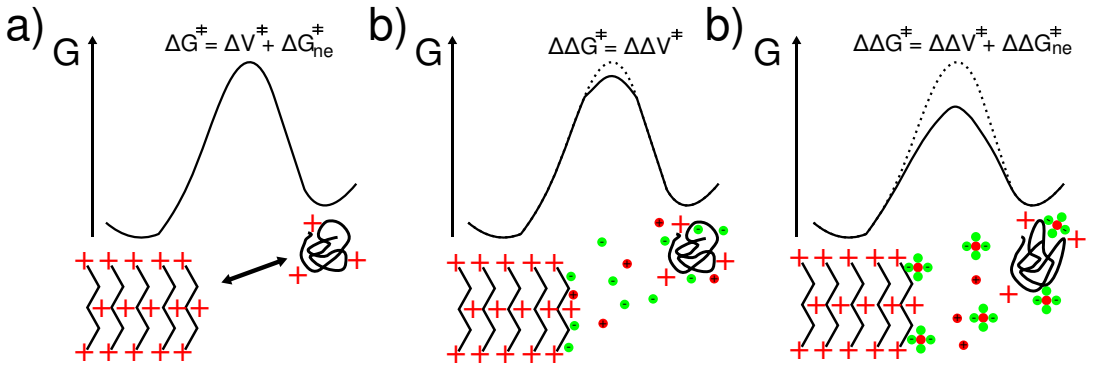

Figure 5.5: Schematic illustration of the proposed mechanisms of acceleration of amyloid fibril elongation by dissolved ions. a) Hypothetical unscreened mechanism, characterized by high repulsive electrostatic forces in addition to a non-electrostatic contribution to the free energy barrier. b) Debye Hückel type mechanism in conjunction with chemically non-selective binding. The electrostatic repulsion is screened by a diffuse cloud around the charged macromolecules, the charge of which can be modulated by ion pair formation that does not depend on the chemical nature of the ion, but only on its charge. c) Specific binding of some anions, such as sulphate, to the positively charged proteins decreases the effective charge more efficiently, and may even be able to change the structure of the precursor protein, and therefore also of the non-electrostatic part of the free energy barrier.

capillary electrophoresis [236] were used. The most recent experimental advance is to measure the ζ-potential from dynamic light scattering in the presence of rapidly oscillating AC fields, such as the measurements described in the Methods section. One of the main conclusions from these experiments was that ion binding can lead to a substantial alteration of the protein's net charge, with dozens of ions being able to bind to a single protein molecule [233]. It was demonstrated that anions have in general a higher affinity to proteins than cations, even under conditions where the protein carries charges of both signs. It should be noted, however, that in cases where proteins require the strong binding of ions to be functional, cations are more often the binding partners, such as is the case for iron and haemoglobin and magnesium and chlorophyll. This established knowledge on preferential non-specific anion binding, together with the fact that the proteins used in the present study carry only positive charges strongly suggests that the data discussed above is most readily explained by the smaller number concentration of anions at equivalent ionic strength of poly-valent salts.

The work presented in this chapter, apart from being a systematic study of the influence of salt on amyloid formation can also be regarded as an extension of the ground breaking work of Scatchard and Tanford. Whereas their experiments, being measurements of transport properties (conductivity), depended in a linear manner on the charge of the protein, the measurements of aggregation rates presented in this

chapter rely on the exponential dependence of the aggregation rates on the square of the net charge of the protein. This strong dependence allows to resolve very subtle differences in the overall charge state of a protein in the presence of different salts. Therefore, the results from these experiments have relevance that extends beyond the medically relevant question of ordered protein aggregation into the more general field of electrostatic interactions in protein science.

5.4 Appendix: Debye-Hückel-theory

A derivation of Debye-Hückel theory is given below. The derivation follows closely the one described in [237].
In a solution of ions, around an arbitrarily chosen central ion, there will always be statistically more ions of opposite charge than of equal charge, due to the electrostatic interactions between the ions. Due to the condition of overall electroneutrality of the solution, the excess of opposite charge around the central ion is equal in magnitude to the charge of the central ion. Under the following assumptions, the variation of the electrostatic potential around the central ion can be calculated:

- only electrostatic interactions are considered. The inclusion of other interactions, such as van-der-Waals interactions is considered in extended theories, such as DLVO theory [213; 214]
-in the range of concentrations considered, the electrolyte is entirely dissociated (strong electrolyte)
-the dielectric constant of the solvent is not perturbed by the presence of the ions
-ions are rigid spheres with a spherically symmetric potential at all times
-the electrostatic interactions are smaller than k_BT

The number density $N_i(r)$ of the ionic species i at a distance r from the central ion is given by the Boltzmann distribution:

$$N_i(r) = N_i^{\infty} e^{\frac{-z_i e\Phi(r)}{k_B T}} \tag{5.34}$$

where $\Phi(r)$ is the electrostatic potential at a distance r from the central ion, and $\Phi(\infty)$ has been set to 0. N_i^{∞} is the average number density of ions i. Then the overall charge density around the central ion is the sum over all ionic species in solution:

$$\rho(r) = \sum_i z_i e N_i(r) = \sum_i z_i e N_i^{\infty} e^{\frac{-z_i e\Phi(r)}{k_B T}} \tag{5.35}$$

if the last of the above-mentioned hypotheses is valid (i.e. $z_i e\Phi << k_BT$), Equation 5.35 can be linearised to become:

$$\rho(r) = \sum_i z_i e N_i^{\infty} \left(1 - \frac{z_i e\Phi(r)}{k_B T}\right) \tag{5.36}$$

The condition of electroneutrality of the solution, $\sum_i z_i e N_i^\infty = 0$ leads to the desired linear relationship between the potential and the charge density:

$$\rho(r) = -\frac{e^2}{k_B T}\left(\sum_i N_i^\infty z_i^2\right)\Phi(r) \tag{5.37}$$

The Poisson equation is the differential equation relating the spatial variation of the potential to the charge density:

$$divE = -\nabla^2\Phi = \frac{\rho}{\epsilon_0\epsilon_r} \tag{5.38}$$

In spherical coordinates, the natural coordinates for this problem, this differential equation reads:

$$\frac{\partial^2\Phi(r)}{\partial r^2} + \frac{2}{r}\frac{\partial\Phi(r)}{\partial r} = -\frac{\rho}{\epsilon_0\epsilon_r} \tag{5.39}$$

Using Equation 5.37, this equation can be written:

$$\frac{\partial^2\Phi(r)}{\partial r^2} + \frac{2}{r}\frac{\partial\Phi(r)}{\partial r} = \frac{e^2}{\epsilon_0\epsilon_r k_B T}\left(\sum_i N_i^\infty z_i^2\right)\Phi(r) = \kappa^2\Phi(r) \tag{5.40}$$

where

$$\kappa^2 = \frac{e^2}{\epsilon_0\epsilon_r k_B T}\sum_i N_i^\infty z_i^2 \tag{5.41}$$

In order to solve Equation 5.40, the following identity can be used:

$$\frac{\partial^2[r\Phi(r)]}{\partial r^2} = \frac{\partial}{\partial r}\left(\frac{\partial[r\Phi(r)]}{\partial r}\right) = \frac{\partial}{\partial r}\left(r\frac{\partial\Phi(r)}{\partial r} + \Phi(r)\right) = r\frac{\partial^2\Phi(r)}{\partial r^2} + 2\frac{\partial\Phi(r)}{\partial r} \tag{5.42}$$

Hence

$$\frac{\partial^2[r\Phi(r)]}{\partial r^2} = \kappa^2[r\Phi(r)] \tag{5.43}$$

Setting $y = r\Phi(r)$ yields the simple differential equation:

$$\frac{\partial^2 y}{\partial r^2} = \kappa^2 y \tag{5.44}$$

with the solution $y = r\Phi(r) = C_1 e^{-\kappa r} + C_2 e^{\kappa r}$. It remains to calculate the two integration constants C_1 and C_2. As $\lim_{r\to\infty}\Phi(r) = 0$, $C_2 = 0$. The total integral of the charge density around the central ion has to be equal to the charge of the ion:

$$\int_0^\infty 4\pi r^2\rho(r)dr = -z_c e \tag{5.45}$$

where the minimal distance of approach of the other ions to the central ion has been set to 0. Combining Equations 5.37 and 5.41 yields:

$$\rho(r) = -\Phi(r)\epsilon_0\epsilon_r\kappa^2 = -\frac{C_1\epsilon_0\epsilon_r\kappa^2}{r}e^{-\kappa r} \tag{5.46}$$

Therefore:

$$4\pi C_1\epsilon_0\epsilon_r\kappa^2\int_0^\infty e^{-\kappa r}rdr = z_c e \tag{5.47}$$

from where $C_1 = \frac{ze}{4\pi\epsilon_0\epsilon_r}$. Finally, this leads to the expression for the potential:

$$\Phi(r) = \frac{z_c e}{4\pi\epsilon_0\epsilon_r}\frac{e^{-\kappa r}}{r} \tag{5.48}$$

which is the expression used in the analysis and discussion of this chapter.

Chapter 6

Interactions between small molecules and amyloid

This chapter is based to a large extent on the article "Interactions between amyloidophilic dyes and their relevance to studies of amyloid inhibitors", Buell et al., Biophys. J. 2010, [238]. Contributions of co-authors will be appropriately indicated.

The results of the last two chapters demonstrate, that the surface based biosensing methods described in detail in the Experimental chapter can provide kinetic data of amyloid formation accurate enough to obtain new insight into the factors governing protein-protein interactions. In this final chapter, the field of kinetic measurements of amyloid formation will be left, and some characteristics of amyloidophilic dye molecules that still serve as the most widely used labels in bulk solution kinetic studies of amyloid formation will be more closely examined.
The question about the interactions between small molecules and amyloid fibrils is not only of interest due to the use of such molecules as labels, but also because of the therapeutic potential that small molecule inhibitors of amyloid formation possess. In the last decade, a multitude of studies have been published on the inhibitive effect on amyloid formation of various synthetic and naturally occurring small molecules. However, for most of these compounds, the evidence that they interact with the fibrillar form of the proteins is scarce. In cases where inhibitory effects have clearly been demonstrated, the origin of such effects can be different from the intended selective binding to the amyloid scaffold that blocks further elongation. Indeed, recent studies clearly demonstrate, that in many cases, the reported inhibitory effects can be explained by a colloidal aggregation of the small molecule compound and an interaction between the soluble amyloidogenic molecule and the colloidal aggregates [239; 240]. The therapeutic use of such effects is obviously very limited.
In Table 6, a few examples are given of small molecules that have been specifically reported to bind to amyloid. This table serves the purpose to illustrate that not many methods exist that can unambiguously demonstrate an interaction between amyloid structures and small molecules, and that therefore the development of such methods is a useful contribution to the applied aspects of protein misfolding and aggregation studies.

Molecule	**effect of binding to be exploited**	**experimental techniques used in the characterization of the compound**
PiB (derived from ThT)	radiolabelling of amyloid in vivo for PET [241]	filtering assay with radioactively labelled (^{125}I) [242]
Chrysamine G (derived from CR)	radiolabelling of amyloid in vivo	competition experiment with other radioactively labelled (^{14}C) compounds [243]
small aromatic molecule RO-47-1816/001	accelerates aggregation	compound fluorescence upon binding and kinetics of incorporation of biotinylated peptide [244]
Crystal violet	discrimination between τ and Aβ (1-42) aggregates	Thioflavin S fluorescence and TEM analysis of τ filaments [245]
NYGAILSS peptide	inhibition of human islet amyloid polypeptide aggregation	membrane binding assay, ThT fluorescence, turbidity, CD, TEM [246]
Propranolol	inhibition of PrP polymerization	SPR binding assay and anti-prion activity assay in scrapie-infected neuroblastoma (ScNB) cells [229]

Table 6.1: A short list of some small molecules (plus a short peptide) that have been reported to bind to amyloid structures.

In many cases, where the interactions of small molecules with amyloid has been examined, label molecules, such as ThT and Congo red (CR) are used, that presumably often bind to amyloid according to a similar mechanism as (potentially) the molecule under study, occupying the very same binding sites on the fibrils. This reasoning stresses further the need for label-free approaches to the study of amyloid.

6.1 Fluorescent probes of amyloid

The use of fluorescent probes to measure chemical and physical processes in biological systems is well established [247]. The fluorescent entities can be intrinsic to the molecule under study, for example tryptophan in proteins [248], covalently attached to it, as in fluorescence resonant energy transfer (FRET) experiments [249] or can interact non-covalently with the structures of interest, as in Thioflavin T (ThT) fluorescence assays of amyloid fibril formation and growth [250]. In order to gain insight into any process under study using fluorescence probes, knowledge is required of the fundamental steps that link the observed fluorescence signal with the molecular events that are taking place. The study of amyloid fibril formation

is a particular case where fluorescent dyes, such as ThT have been used as probes for many decades, although despite extensive experimental [251; 252; 253; 254] and computational [255; 256; 257] studies, there is no final definitive agreement as to the exact mechanism, stoichiometry and mode of binding to these supra-molecular proteinacious fibrils [258]. Several distinct binding sites for ThT on amyloid fibrils have been identified that can differ in their affinities and binding modes. For example, it has been reported that ThT binds in the forms of large micelles [251], but also that it binds in monomeric form [252]. Molecular dynamics simulations [256; 257] seem to suggest that the binding occurs in monomeric form. However, it is difficult to simulate high concentrations of dye molecules which might lead to a bias towards monomeric forms of the dye. In the last two years, efforts have increasingly focused on the study the origin of the increased fluorescence efficiency of ThT upon binding to amyloid [259; 260; 261; 262]. The origin of this enhanced fluorescence quantum yield of the dye when bound [261] or confined in viscous solution [259] seems to be a hindered rotation around the central C-C bond; this movement is responsible for the efficiency of non-radiative decay of the excited state [262].
Whereas the shift in Congo red (CR) absorption spectrum and its induced birefringence upon binding is commonly used as a qualitative test for the presence of amyloid structures [263], ThT fluorescence assays have been established as a more quantitative method for kinetic studies in particular (see Experimental chapter and data in Chapters 4 and 5). When ThT binds to β-sheet rich amyloid fibrils, its absorption maximum and fluorescence spectrum undergo a red-shift [67] and the fluorescence emission at 480 nm upon excitation at 440 nm is within certain limits commonly assumed to be proportional to the quantity of amyloid fibrils present. This property can then be used to follow time-courses of amyloid growth and such kinetic studies give valuable insight into the molecular mechanism of amyloid formation. Moreover, reduction in ThT fluorescence is often taken to be an indication of the inhibition of this macromolecular self-assembly process. The quest for potent inhibitors is a very active research direction [239], due to the close connection between amyloid formation and neurodegenerative and other diseases([40] and see introduction). Congo red is an example of a compound the inhibitory properties of which have been studied, but published results on its effects have given rise to very different conclusions [80; 240; 264; 265; 266; 267]. Moreover, in the context of studies of potential inhibitors of amyloid formation, it has been shown recently that inhibitor candidates that are themselves fluorescent can interfere with the ability of dye fluorescence to reflect accurately the quantity of amyloid present [268].
In order to explore avenues that avoid such interference effects, the label-free biosensing approaches to studying amyloid growth and that are described in the previous chapters have been developed. SPR has also been used to study the binding of amyloidophilic dyes to surface-bound protein aggregates [229; 269]. Equilibrium binding constants describing the interaction between amyloidophilic dyes and protein aggregates, as well as their kinetics of binding have been widely studied [251; 258; 270; 271; 272]. In the following, the binding of ThT and Congo red to surface-bound amyloid structures will be studied, in order to probe if the binding of these dyes is really independent and to elucidate the origin of the conflicting results

on the inhibitory effects of Congo red.

6.2 Interactions between amyloidophilic dyes and binding of the dyes to amyloid fibrils

In order to study the binding of small molecules to amyloid fibrils, short, freshly grown Aβ (1-42) amyloid fibrils were attached to the gold surface of a QCM-crystal, following established protocols ([97], and Method development chapter). The AFM images in Figure 3.1 suggest that the surface bound protein is mainly fibrillar in nature; however, it cannot be excluded that in this step, small oligomers could also attach to the QCM-sensor surface. However, in order to maximize the signal resulting from the binding of the dye molecules specifically to fibrillar material, the surface was further incubated with a solution of soluble Aβ (1-42) to increase the length of the attached fibrils and therefore the mass of fibrillar material on the sensor. During this step, it is highly likely that the peptide predominantly adds on to the pre-existing seed fibrils as opposed to creating new aggregates; indeed, the incubation of a sensor surface that has no attached fibrils shows less than 5% of the frequency shift of a sensor with attached seeds (Figure 3.1).
Figure 6.1 a) shows the result of a QCM measurement probing the binding of the dye CR to amyloid fibrils formed from Aβ (1-42). Contact of the biosensors with a dilute solution of the dye (50 μM in 100 mM PB pH 7.4) leads to a frequency shift of several Hz. In a control experiment where no fibrils were attached to the surface (top AFM-image in Figure 6.1), no change in resonant frequency was observed upon contact with the dye solution.

The observed frequency shift in the presence of fibrils, therefore, stems from the binding of dye molecules to the amyloid fibrils. With the Sauerbrey mass sensitivity of 17.7 ng Hz^{-1} cm^{-2}) of the QCM crystals this shift would formally correspond to a surface density of approximately one dye molecule per nm^2. Considering that, according to the AFM images, only part of the surface is coated with amyloid fibrils, this result indicates either that the dye binds in the form of large clusters or that a significant part of the frequency shift arises from a change in the hydrodynamic mass of the crystal (i.e. from coupling to the liquid [105]) rather than simply in the inertial mass of the bound dye molecules. Indeed, it was demonstrated in the Method development chapter that this latter mechanism contributes significantly to the signal stemming from fibril elongation. The binding of CR is saturable, as the change in resonant frequency is complete within 2 min, and the frequency remains constant even when the injection of dye solution is continued. The finding that the binding of CR to surface-bound amyloid fibrils can be monitored in real time led to the design of the sequence of experiments in Figure 6.1 b). These experiments allow first the binding of ThT to surface-attached amyloid fibrils to be probed and second, any competition between the two dyes for binding sites on the protein fibrils to be detected. Previous studies have reported that ThT and CR have very different stoichiometries of binding to fibrils [273] and occupy different binding sites [242]. It can be seen that binding of ThT (100 μM solutions in 100mM PB pH 7.4) to the

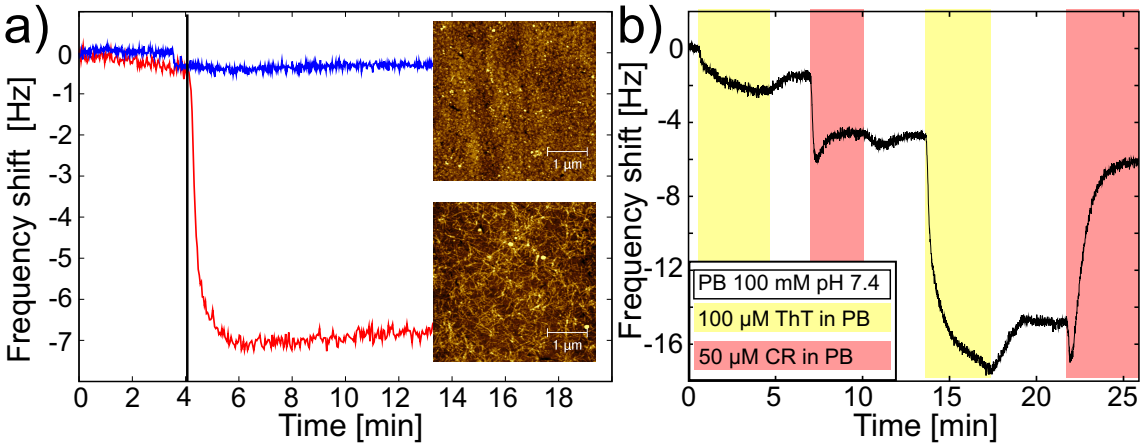

Figure 6.1: a) QCM measurements probing the binding of the amyloidophilic dye Congo red to surface-bound Aβ (1-42) fibrils (the vertical line indicates the injection of dye solution). The binding gives rise to a frequency shift of several Hz (red trace; shown is the frequency response of the overtone N=3). In the absence of amyloid fibrils (the AFM image above), no frequency response is detected (blue trace). b) The binding of ThT to the surface-bound fibrils can be detected in an analogous way. The presence of bound ThT does not prevent the binding of CR. Renewed contact with a ThT-solution leads to a drastically increased drop in resonant frequency, compared to the response to the initial contact with ThT; this decrease in frequency can be reversed by subsequent contact with CR solution. These observations strongly suggest that ThT and CR do not bind independently to the fibrils.

fibrils can also be detected and gives rise to a smaller frequency shift than that from CR binding. The corresponding control experiment, where a sensor without fibrils was exposed to a solution containing ThT was carried out and confirmed that the presence of fibrils is necessary to observe a significant change in the resonant frequency. The observed difference in the magnitude of the frequency shifts between CR and ThT binding can be rationalized based on several factors. The signal is dependent on the surface density of fibrils, as well as the stoichiometry of binding. Also, the exact mode of binding is likely to influence the frequency response of the QCM: if the dye binds in the form of large micelles, the overall roughness of the surface increases more strongly compared to the situation where the dye binds in monomeric form. The dye concentrations in these QCM experiments were for both CR [274] and ThT [251; 252] above the critical concentration for the formation of supra-molecular structures; however, the size of the dye molecule clusters can differ, leading to a different increase in roughness for an equivalent amount of binding and therefore to a differential QCM-response [105]. The raw frequency shifts can therefore not readily be converted to accurate stoichiometries.
The binding of ThT can be seen from the present data to be partly reversible, as revealed by the increase in frequency upon flushing the surface with fresh buffer.

It is interesting to note that this experimental set-up allows the creation of a non-equilibrium situation within the QCM cell through the continuous flushing with buffer for several minutes and therefore of favourable conditions for measuring the dissociation of high affinity binders such as ThT [256].
A subsequent incubation with 50 μM CR solution also shows binding, similar to that shown in Figure 6.1 a). Surprisingly, however, when the ThT solution is injected again into the liquid cell, a large drop in resonant frequency is observed. Even more remarkably, renewed contact with the CR solution leads to an apparent loss in mass that is approximately equal to the original mass associated with the addition of ThT. These observations, that have been confirmed in multiple repeats of these experiments, lead to the conclusion that the binding of the two dyes to the amyloid fibrils is not independent, but rather the presence of CR has a strong effect on the binding of ThT. This conclusion may be drawn even under the assumption that only part of the frequency shift directly stems from rigidly attached inertial mass of dye molecules; under the assumption of independent binding sites, the frequency shifts induced by the binding of the dyes should be additive regardless of whether or not a change in rigidly attached mass or hydrodynamic mass gives rise to the change in frequency.
In order to obtain independent experimental insight into the potential interaction between the two dyes revealed by the QCM experiments, dynamic light scattering experiments were performed, shown in Figure 6.2 a), with solutions of the individual dyes and with a mixture of the two molecules (see Methods section for details). The DLS measurements indicate that in the latter situation structures are formed that are of considerably larger size than the monomers or small oligomers observed in the corresponding pure dye solutions. Such an intermolecular interaction can be attributed at least in part to the ionic nature of the two dyes: CR is negatively charged at physiological pH, because of its sulphonic acid groups and the reduced basicity of its amines due to the partial delocalization of the nitrogen lone pairs, whereas ThT, being a quaternary ammonium cation, is positively charged (Figure 6.2 c). The large frequency shift during the QCM experiment described above is consistent with the formation of such CR-ThT clusters on the surface of Aβ (1-42) amyloid fibrils. Indeed, the binding of CR is likely to increase the negative surface charge density of the Aβ (1-42) fibrils (the net charge per peptide monomer at pH 7.4 is -3) as every dye molecule carries a net negative charge, therefore facilitating the binding of the positively charged ThT molecules.

To explore further the significance of this result, ThT fluorescence experiments with Aβ (1-42) amyloid fibrils in the presence or absence of CR (Figure 6.2 b) were performed. The fluorescence was first measured in the absence of CR, then CR was added and the fluorescence was immediately measured again. The fluorescence spectra obtained in these experiments indicate that the presence of CR leads in this case to a substantial suppression of ThT fluorescence. Similar phenomena have been observed previously [240; 273; 275] and were interpreted either as fluorescence quenching or as displacement of the ThT from the fibrils. However, this potential interference with ThT fluorescence does not seem to be widely known or taken into account when inhibition data is analyzed. It is interesting to note, that this effect

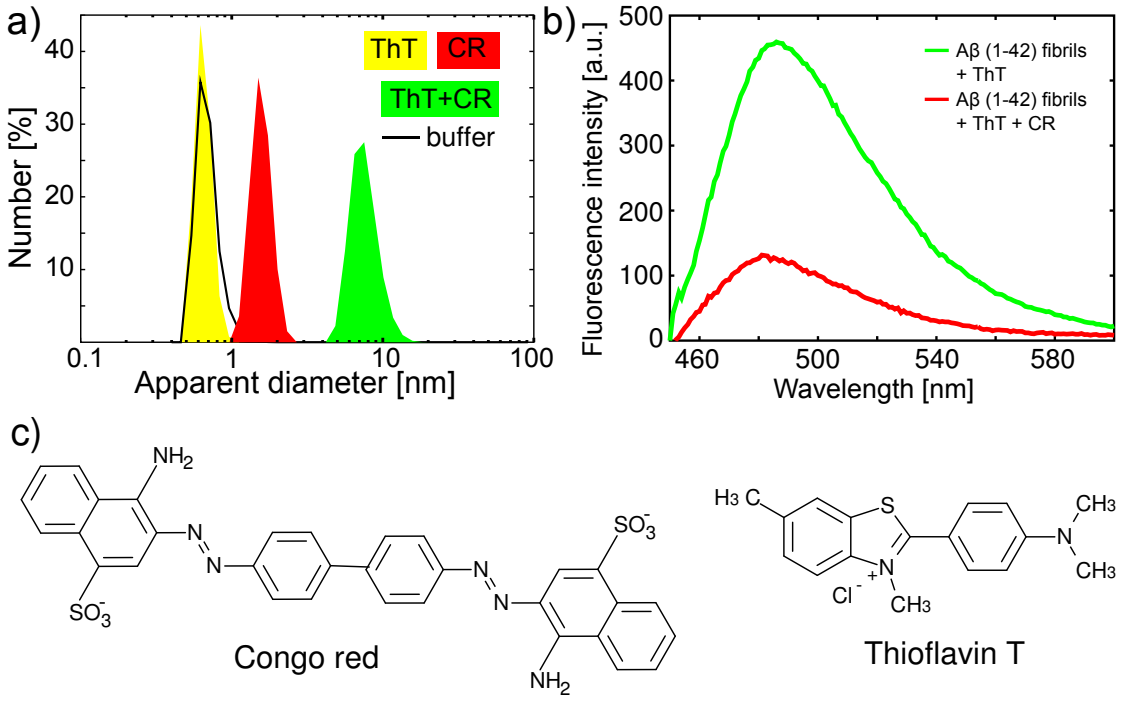

Figure 6.2: a) DLS measurements probing the interactions of CR and ThT. The results of four independent particle size distribution measurements are shown: 100 mM PB pH 7.4, (dark line), 30μM ThT solution in PB, 50μM CR solution and a 1:1 (by volume) mixture of the ThT and CR solutions. The data for the ThT solution are indistinguishable from buffer, indicating that the scattering intensity from monomeric/oligomeric ThT is too weak at this concentration to be detected. A mixture of CR and ThT shows the presence of structures of considerably larger size than both components separately. In b) the fluorescence of a solution of $\sim$ 2 μM Aβ (1-42) and 1.2 μM ThT was measured (excitation wavelength: 440 nm, ThT background signal subtracted). Then, CR was added to the sample to obtain a concentration of $\sim$ 1.2 μM and the fluorescence was again immediately measured. As a result the observed fluorescence drastically decreases, an effect attributable to the quenching of ThT fluorescence or the displacement of ThT by CR (see text). c) The chemical formulas of Congo red and Thioflavin T are shown. The molecules carry opposite charges at pH 7.4, therefore making an interaction between them plausible.

already occurs at concentrations of both ThT and CR that are below the respective critical concentrations for the formation of supra-molecular aggregates.
Because the experimental system used here is not reliant on optical detection, it is possible to study the effects of the presence of CR on the rate of elongation of the Aβ (1-42) fibrils (Figure 6.3) without the interference of CR on the signal used to evaluate the kinetics. The fibrils were first exposed to the soluble Aβ (1-42) peptide in the absence of CR, then the fibrils were brought into contact with a solution of

CR and finally with a mixture of peptide and CR.

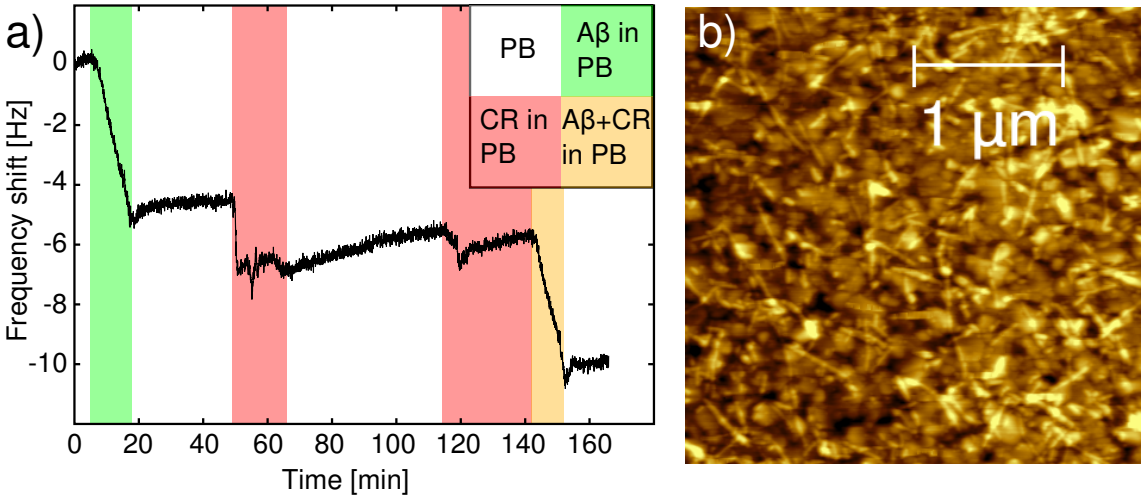

Figure 6.3: a) Probing the influence of CR on the elongation of Aβ (1-42) amyloid fibrils. The surface-bound fibrils were exposed to a 2 μM solution of peptide, and then to a 50 μM solution of CR. Subsequently, they were brought into contact with a solution containing both CR and Aβ (1-42) and the slopes of the resulting frequency shifts, proportional to the elongation rates, were compared. Within experimental error, the fibrils grow with the same rate in the presence or absence of CR. b) AFM image of the QCM crystal after the experiment, showing the absence of non-fibrillar aggregates, confirming that the fibrils grow in the presence of CR.

It can be seen in Figure 6.3 that the elongation rate in the presence (0.46 Hz/min) or absence (0.49 Hz/min) of CR was identical within error and therefore it can be concluded that the presence of CR does not interfere with the process of elongation of the fibrils. Recent work of Lendel et al. shows that soluble Aβ (1-42) peptide can interact with CR micelles [80]. It appears, however, that these interactions are not strong enough to prevent the peptide from incorporating into the fibrils; fibril formation therefore competes successfully with the weaker interactions between peptide and dye; an observation in agreement with the data in [80].
In order to determine, whether the findings described above also apply for proteins other than Aβ (1-42), similar QCM experiments were carried out with bovine insulin. As in the case of the Aβ (1-42) experiments, first surface-bound seed fibrils (Figure 6.4 a) were allowed to elongate further, in order to maximize the total amount of fibrillar material on the surface. This aim was for example achieved by using the QCM-sensors that had served for a study of the influence of ionic strength on the elongation rate of insulin fibrils (see Chapter 5) for subsequent dye binding experiments. During the fibril elongation experiments that the sensors had undergone, on average more than 100 Hz frequency shift was induced, corresponding to a dense coverage of the sensor surface with insulin fibrils, as can be seen in Figure 6.4 a). Prior to use in the dye binding experiments, the fibrils were stored for several hours in HCl at pH 2.0, and the liquid cell of the QCM was flushed with HCl periodically,

in order to ensure that residual ions from the previous experiments were washed out of the fibril layer. The poor solubility of CR in HCl at pH 2.0 did not allow, however, to carry out the dye binding experiments under the solution conditions, where insulin amyloid fibril elongation most readily occurs. It was therefore investigated if the surface-bound insulin fibrils were stable under conditions more favourable for the dissolution of CR. A QCM sensor covered with insulin amyloid was incubated with 100 mM phosphate buffer (PB) at pH 7.4, and after the experiments described further below had been carried out, the liquid cell of the QCM was again filled with 0.01 M HCl. At the end of the experiment, the surface was dried and imaged by AFM (6.4 b)). The image demonstrates that the fibrils have not been dissolved due to the change in solution conditions and indeed, no clear change in morphology is observed. Therefore, the change in solution conditions to probe the binding of CR and the potential inhibition of fibril elongation caused by this binding can be safely carried out and provides a valid way to circumvent the problem of limited solubility of CR at acidic pH values.

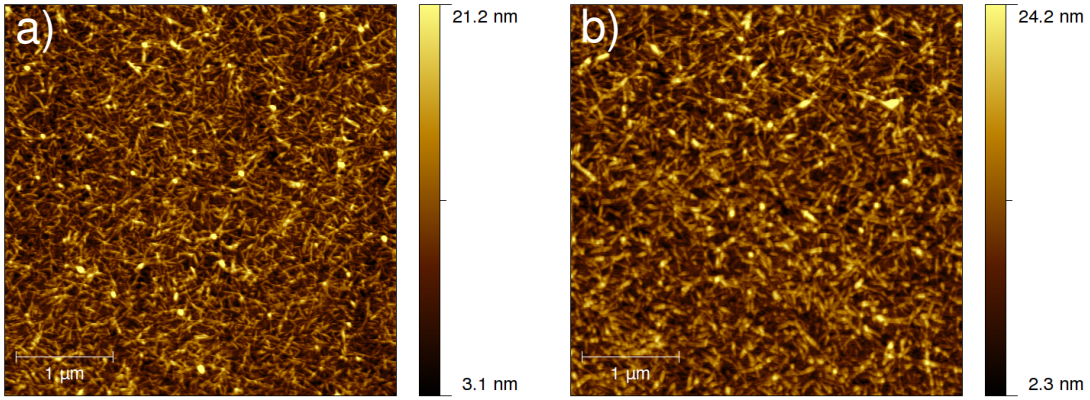

Figure 6.4: a) QCM sensor surface covered with insulin amyloid fibrils at the end of an experiment probing the influence of a change in ionic strength on the amyloid elongation rate (see chapter 5). These fibrils were only in contact with solutions of pH 2. b) QCM sensor with a similar history to the one in a), but it had been subsequently brought into contact with 100 mM phosphate buffer at pH 7.4, and then CR binding and inhibition experiments similar to the ones shown in Figure 6.5 have been carried out. At the end, the sensor has been incubated again with 0.01 M HCl, dried and imaged.

When surface-bound insulin fibrils were brought into contact with 100 mM phosphate buffer at pH 7.4, a strong drop in resonant frequency occurred, that ranged from the order of 30 Hz to more than 150 Hz, (compare Figure 6.5 a and b), with higher surface densities of fibrils showing larger drops in frequency. This strong decrease in resonant frequency, indicating a structural rearrangement of the protein fibrils or a change in coupling to the solution due to a change in the charge of the fibrils, was generally followed by a slower increase in frequency that indicated the

loss of some surface-bound material. This increase in resonant frequency did not scale with the magnitude of the previous drop, but was in all cases of the order of 10 Hz, suggesting that it corresponds to the detachment of a small amount of non-specifically absorbed protein, rather than dissociation of the surface-bound fibrils.
The upper panel of Figure 6.5 demonstrates that the overall interaction pattern between the two amyloidophilic dyes CR and ThT and insulin amyloid fibrils is very similar to what had been observed for Aβ (1-42) and is described above. The binding of CR can be detected and, even more pronounced than in the case of Aβ, enhances the binding of ThT. Indeed, in the absence of any bound CR, no binding of ThT can be detected at all. This finding could be rationalized as follows. A calculation assuming independent pK_a values indicates that insulin and Aβ (1-42) have a very similar net charge of $\sim$ -2 at pH 7.4, suggesting that charge cannot explain a very different binding behaviour of ThT to the fibrils. However, the fibrils have undergone different treatments; the Aβ fibrils have formed at this neutral pH, whereas the insulin fibrils have formed at pH 2.0 and have subsequently been brought to pH 7.4. As this big change in solution conditions does not dissociate the insulin fibrils it is possible that not all the acidic protons on or in the fibrils will be taken up by the buffer. It is likely that some of the charges are not solvent exposed and therefore less easily removed by the buffer; this effect can potentially be increased due to the surface attachment of the fibrils. In this case, the net charge of surface-bound insulin amyloid fibrils could be positive, even at neutral pH, leading to the binding of the Thioflavin T cation to the amyloid fibrils to be less favourable than in the case of Aβ.

Similar as in the case of Aβ (1-42), a subsequent incubation of the fibrils with CR, after the fibrils had been in contact with ThT leads to an increase in frequency, indicating that the interaction between the two dyes is strong enough to remove the ThT from the fibrils. At this point, as a general control and in order to ensure that the observed phenomena do not arise from interactions of the two dyes within the flow system of the QCM and therefore are independent of the presence of fibrils, the experiment illustrated in Figure 6.5 c) was performed. Here, a QCM sensor that had no fibrils attached to it, but was only passivated by a SAM of methoxy-PEG thiol was repeatedly incubated with solutions of the dyes in PB. It can be seen that the contact of the passivated surface with a solution of ThT leads to a very small amount of non-specific absorption. Subsequent contact with CR seems to remove the adsorbed ThT, confirming once more that a strong interaction exists between the dyes. In this experiment, the contact of the surface with CR does not influence the later behaviour in contact with ThT, contrarily to the situation where fibrils are attached; this finding unambiguously confirms that the presence of fibrils is indeed necessary to yield a significant amount of CR binding.
Having thus confirmed the similarities in the interaction behaviour, the effect of bound CR on the rate of insulin elongation (Figure 6.5 d) was tested, in analogy to the experiment in Figure 6.3. Due to the necessity to destabilize the native state of insulin sufficiently to enable fibril formation at a low temperature, the solution in contact with the fibrils had to be changed back to 0.01 M HCl. Very interestingly, upon bringing the fibrils back to pH 2, the initial change in resonant frequency when

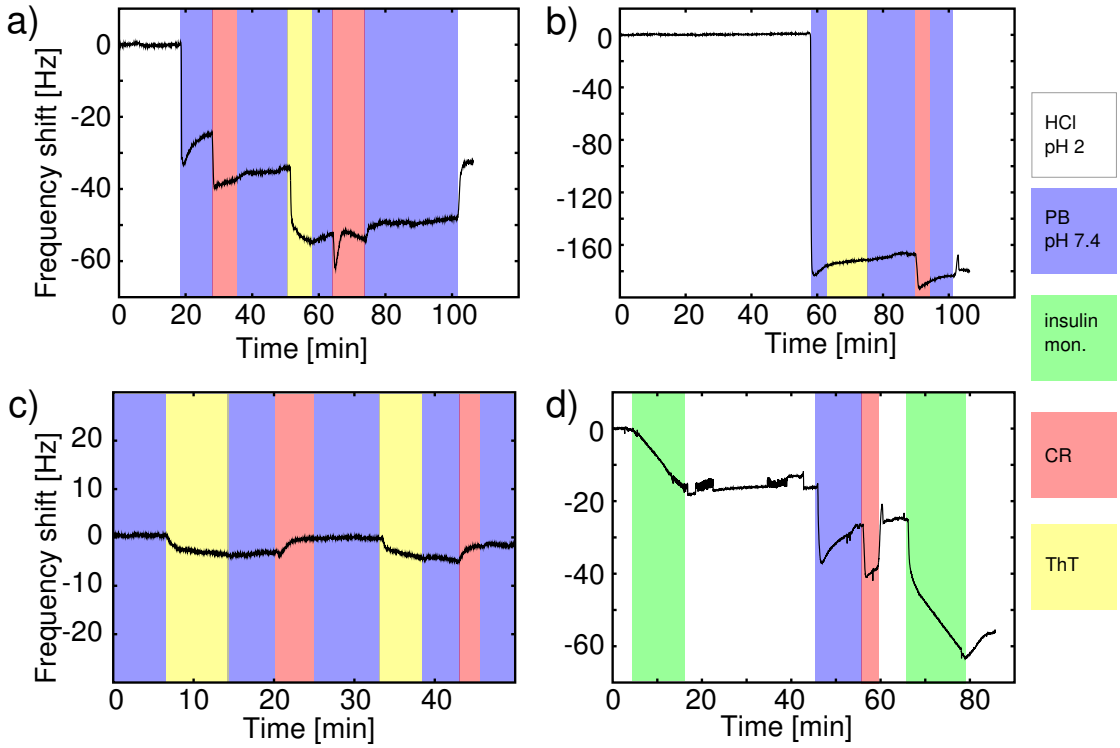

Figure 6.5: a) A QCM sensor covered with insulin amyloid fibrils is incubated with solutions of CR (50 μM) and ThT (100 μM) in PB at pH 7.4 after the solution in contact with the fibrils had been changed from 0.01 M HCl to PB pH 7.4. The resulting frequency changes demonstrate that similar to what has been observed for Aβ (1-42) described earlier, the CR and ThT interact such that CR can remove bound ThT. b) Contact of a ThT solution with a QCM sensor that is covered with a very high density of insulin fibrils (as judged from the previous elongation rates and total frequency shifts in the experiments where the sensor had been used) shows that the presence of bound CR is necessary to observe any ThT binding. c) Control experiment, demonstrating that a passivated QCM sensor that has no insulin fibrils attached only shows a very small degree of non-specific ThT adsorption, that can be removed through contact with a CR solution. The enhancement of ThT binding through previous CR binding clearly requires the presence of fibrils. d) Experiment designed to probe the inhibitive effect of CR binding on insulin amyloid fibril elongation. The presence of bound CR does not influence the steady state elongation rate; however, it induces some non-specific protein absorption upon the first contact with insulin monomer.

the pH had been increased from 2 to 7.4 was only fully reversible in cases where the fibrils had not been in contact with CR. If CR was bound, the reversibility was in some cases entirely eliminated; however, a small increase in frequency of the order of 10 Hz was observed in all cases. This frequency increase can be attributed to the differences in density and viscosity between HCl at pH 2.0 and 100 mM PB at pH

7.4 (Figure 6.5 b), as suggested by the observation that a passivated empty control sensor showed the same change in frequency upon exchange of buffers (not shown). Obviously, it is not possible to deduce if during this change of buffer some or all of the CR is washed off based on the observed frequency shift alone. However, the subsequent incubation with monomer lead to a different signature in frequency change if the fibrils had been in contact with CR (see Figure 6.5 d) compared to an equivalent experiment where the fibrils had been brought to pH 7.4 and back to pH 2.0 without intermediate contact with CR (not shown). The second period of contact with insulin monomer in Figure 6.5 d) is characterized by a high initial rate of frequency change that is followed by the usual linear steady state behaviour. In the steady state phase, a rate of frequency change is measured that is very similar to the one observed before the first contact with PB, indicating that neither the change in solution condition, nor the presence of bound CR has any inhibitory effect on insulin fibril elongation. The first few minutes of contact with monomer reproducibly show a different rate of change of frequency. The most likely explanation is that the fibril-bound CR facilitates lateral association of insulin monomer onto the fibrils via a partial neutralization or screening of the charges on the fibrils.
Taken together, therefore, these results show that the use of Thioflavin T to detect amyloid growth requires careful controls if it is to be used in quantitative studies. In particular, care has to be taken to exclude interactions with ThT that can interfere with its potential to reflect accurately the quantity of amyloid present at a given time point. Monitoring a quantity more directly related to the incorporation of soluble peptide into fibrils, the shift of resonant frequency of a biosensor in a quartz crystal microbalance, is therefore a powerful and independent method for the study of amyloid growth. In addition, the same procedure can be used to probe the interaction between small molecules and amyloid fibrils. This biosensor approach therefore enables a detailed study of the mechanism of small molecule/amyloid interactions and has the potential to contribute significantly to an effective search for inhibitors of amyloid formation.

Chapter 7

Conclusions

Several conclusions can be drawn from the work presented in this PhD thesis.
It was demonstrated that label-free surface-bound measurements of amyloid elongation kinetics provide a convenient and highly accurate way to measure the effects that changes of external conditions have on the kinetics. Small changes in elongation rate of less than 50% can be easily resolved, allowing very subtle modifications of a protein's free energy landscape to be quantitatively investigated. It was shown that the methods are applicable to a wide range of solution conditions and peptide sequences, therefore allowing to explore almost the entire variety of amyloidogenic sequence-space.
Application of these methods allowed the free energy barriers that separate the soluble states of a range of polypeptides from their ordered aggregated state to be determined. In addition, the unique features of the surface-bound techniques in conjunction with an analytical kinetic theory describing amyloid fibril elongation as a diffusive process, allowed the free energy barriers to be decomposed into their respective enthalpic and entropic contributions. A correlation of these energetic contributions with structural and sequence parameters of the respective polypeptides enabled an understanding of the origin of large parts of the overall free energy barrier. The residual structure and the hydrophobicity of the soluble form of the protein are the single most important factors.
On the background of these contributions to the free energy barriers, electrostatic interactions can modify the elongation kinetics by more than an order of magnitude. The presence of ions in the solution has a twofold effect, even in the simplest situation studied in this work. In addition to a classical Debye-Hückel type screening mechanism, where the Coulomb repulsion between equally charged reaction partners is screened by a diffuse ionic cloud of counter-ions, chemically non-specific ion association of salt ions with the protein macro-ions can change their net charge relevant for the aggregation reaction.
In addition to being able to extract such fundamental knowledge about protein-protein interactions and their modulation by external and sequence parameters, the methods and results presented in this thesis have important consequences for more applied aspects of the field of protein aggregation. In the last chapter, it was shown how the quartz crystal microbalance with surface-bound amyloid can be used to

probe the interaction between amyloid and small molecules. These experiments can be combined with studies of the inhibitory effect of the small molecule binding on amyloid fibril elongation. This highly systematic approach is an important contribution to the overwhelmingly large field of study of small molecule drug candidates for protein misfolding diseases, that is full of apparently contradictory reports on the effects of many candidate molecules.

Chapter 8

Future directions

The work presented in this thesis opens up manifold avenues that are worthwhile to pursue. It was clearly demonstrated, that highly accurate measurements of the influence of external factors on the kinetics of amyloid fibril elongation can provide fundamental insight into the free energy surface. Factors other than temperature and ionic strength that have important effects on the dynamics of protein folding and misfolding are the solvent composition and the presence of small molecules known to shift the relative stabilities between folded and unfolded states, such as osmolytes and denaturants. If the influence of these factors on the kinetics is systematically studied, it will be possible to characterize structural and energetic features of the transition state ensembles to even higher detail than achieved in this work. In addition, a systematic variation of the amino acid sequence of a polypeptide along the lines of Φ-value analysis of protein folding [276] should be able to provide detail on the exact reaction mechanism on a single residue detail.

However, in order to approach the final aim of a full characterization of the protein's free energy landscape, including the regions that correspond to ordered aggregation, and to further unify the concepts of folding and misfolding, the energetics of the final fibrillar state have to be characterized in as much detail as the barriers in this work. The free energy differences between soluble polypeptides and their aggregated counterparts have only recently been measured for a large variety of amyloidogenic systems [34]. However, in this work, the free energy values have not been decomposed into their respective enthalpic and entropic contributions. If this decomposition could be achieved, it would be possible to follow the evolution of the relative energetic contributions along the reactive trajectories from soluble to aggregated state. This analysis would provide an even more thorough understanding of the driving forces for protein aggregation and of the fine balance between folding and misfolding.
Several experimental routes exist towards this goal; the temperature dependence of the equilibrium between soluble and aggregated states can be measured, according to:

$$\frac{\partial \ln(K)}{\partial T} = \frac{\Delta H^0}{RT^2} \tag{8.1}$$

where K is the equilibrium constant and ΔH^0 is the difference in enthalpy between the two states. Therefore, a measurement of the change in relative concentrations of soluble and aggregated states with temperature will provide the required quantity. Alternatively, the enthalpy release upon addition of a monomer onto a fibril end can be directly measured by highly sensitive calorimetric methods.

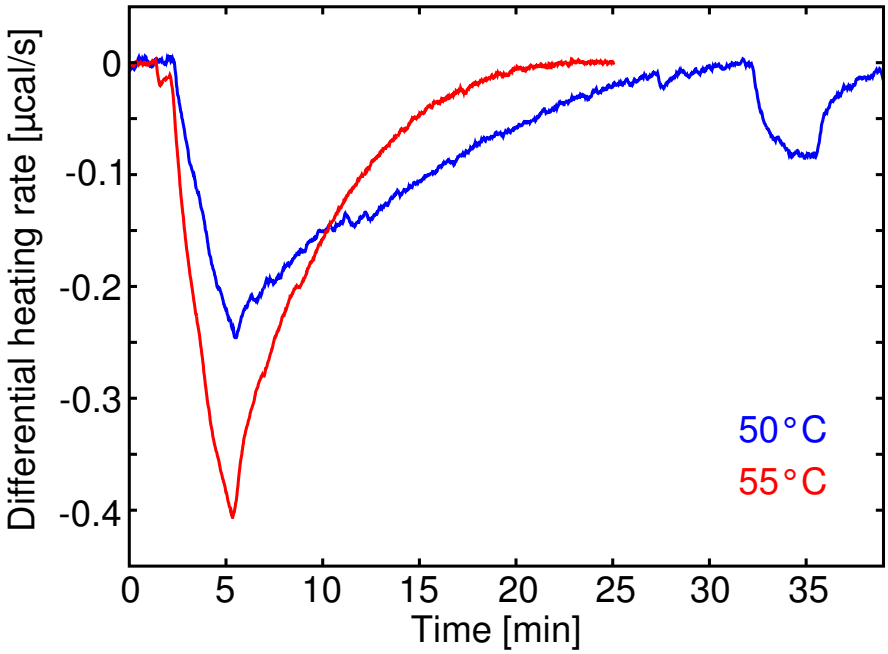

Figure 8.1: The enthalpy that is released when soluble insulin incorporates into an insulin seed fibril is measured, using isothermal titration calorimetry (ITC, see Experimental Chapter for details). Seed fibrils are titrated into the ITC sample cell that was filled with soluble insulin, at two different temperatures. The integral of the curves yields the released enthalpy. The smaller signal around 35 min corresponds to a second injection of seeds to probe if all the monomer in the cell has been consumed. The heat release presumably stems from the heat of dilution of the seed fibrils. The experiment suggests that ΔH^0 is of the order of 10 kJ/mol.

This has been reported before for individual polypeptides [116; 119; 120]. Preliminary experiments were carried out in the framework of this thesis, that are presented in Figure 8.1, and it was therefore demonstrated that this method can be extended to other proteins. Being able to measure the same quantity with two very different experimental methods will allow to assess the validity of the results. The result of the experiment in Figure 8.1 suggests, that insulin fibrils are enthalpically only marginally stable (of the order of 10 kJ/mol) compared to soluble protein. In the light of the high enthalpy of activation measured (100 kJ/mol, see Chapter 4), this indicates that the stabilizing interactions that form when the soluble protein incorporates into the fibril are very similar in magnitude to the sum of the interactions in the reactants. This finding could indicate that both the transition state

and the final fibril are stabilized by an increase in entropy. These highly interesting, but still quite speculative findings deserve further investigation.
For the more applied aspects of protein aggregation, it should be worthwhile to re-assess many of the small molecule inhibitors that have been reported in the literature to bind to amyloid and to inhibit fibril elongation. The systematic label-free nature of the techniques presented here will most certainly reveal that Congo red is not the only small molecule the inhibitory effect of which has been misinterpreted in the past. Small molecules that selectively bind to amyloid, either to report on its presence (diagnostics) or to inhibit its progression (cure) form a huge part of the pharmaceutical industry's efforts to fight neurodegenerative diseases. Therefore, the need for such systematic approaches cannot be stressed enough.

List of publications

Journal articles

1) Alexander K. Buell, Gian Gaetano Tartaglia, Neil R. Birkett, Christopher A. Waudby, Michele Vendruscolo, Xavier Salvatella, Mark E. Welland, Christopher M. Dobson and Tuomas P.J. Knowles, **Position dependent electrostatic protection against protein aggregation**, *ChemBioChem*, 2009, 10(8), pp 1309-12

2) Duncan A. White, Alexander K. Buell, Christopher M. Dobson, Mark E. Welland and Tuomas P.J. Knowles, **Biosensor-based label-free assays of amyloid growth**, *FEBS Lett.*, 2009, 583 (16), pp 2587-2592

3) Tuomas P. J. Knowles, Tomas W. Oppenheim, Alexander K. Buell, Dimitri Y. Chirgadze and Mark E. Welland, **Nanostructured films from hierarchical self-assembly of amyloidogenic proteins**, *Nature Nanotechnology*, 2010, 5, pp 204-207

4) Duncan A. White, Alexander K. Buell, Tuomas P.J. Knowles, Mark E. Welland and Christopher M. Dobson, **Protein aggregation in crowded environments**, *J. Am. Chem. Soc.*, 2010, 132 (14), pp 5170-5175

5) Alexander K. Buell, Jamie R. Blundell, Christopher M. Dobson, Mark E. Welland, Eugene M. Terentjev and Tuomas P. J. Knowles, **Frequency factors in a landscape model of filamentous protein aggregation**, *Phys. Rev. Lett.*, 2010, 104, 228101

6) Alexander K. Buell, Duncan A. White, Christoph Meier, Mark E. Welland, Tuomas P.J. Knowles and Christopher M. Dobson, **Surface attachment of protein fibrils via covalent modification strategies**, *J. Phys. Chem. B*, 2010, 114, pp 10925-10938

7) Alexander K. Buell, Christopher M. Dobson, Tuomas P.J. Knowles and Mark E. Welland, **Interactions between amyloidophilic dyes and their relevance to studies of amyloid inhibitors**, *Biophys. J.*, 2010, 99(10), pp 3492-3497

8) Yi-Qian Wang, Alexander K. Buell, Xin-Yu Wang, Mark E. Welland, Christo-

pher M. Dobson, Tuomas P.J Knowles, Sarah Perrett, **Relationship Between Prion Propensity and the Rates of Individual Molecular Steps of Fibril Assembly**, *J. Biol. Chem.*, 2011, 286, pp 12101-12107

9) Alexander K. Buell, Anne Dhulesia (joint first authors), Nunilo Cremades, Janet R. Kumita, Maria F. Mossuto, Mireille Dumoulin, Mark E. Welland, Tuomas P. J. Knowles, Xavier Salvatella, Christopher M. Dobson, **Population of non-native states of lysozyme mutants drives amyloid fibril formation**, *J. Am. Chem. Soc.*, 2011, 133, pp 7737-7743

10) Sarah Shammas, Christopher A. Waudby, Shuyu Wang, Alexander K. Buell, Heath Ecroyd, John A. Carver, Christopher M. Dobson, Sarah Meehan, **Binding of αB-crystallin to Aβ amyloid fibrils inhibits fibril elongation**, *Biophys. J.*, accepted for publication

11) Li-Qiong Xu, Alexander K. Buell, Samuel I.A. Cohen, Sarah A. Cusack, Hong Zhang, Laura S. Itzhaki, Tuomas P.J. Knowles, Christopher M. Dobson, Mark E. Welland, Gary W. Jones and Sarah Perrett, **Influence of specific Hsp70 domains on fibril formation of the yeast prion protein Ure2**, under review

12) Alexander K. Buell, Peter Hung, Xavier Salvatella, Mark E. Welland, Christopher M. Dobson and Tuomas P.J. Knowles, **Non-specific electrostatic effects in protein aggregation**, in preparation

13) Alexander K. Buell, Anne Dhulesia, Duncan A. White, Tuomas P.J. Knowles, Christopher M. Dobson and Mark E. Welland **The energy barriers for amyloid growth**, in preparation

14) Alexander K. Buell, Elin Esbjorner-Winters, Patrick J. Riss, Duncan White, Franklin I. Aigbirhio, Gergely Toth, Mark E. Welland, Christopher M. Dobson and Tuomas P.J. Knowles, **Probing the mechanisms of amyloid binding by small molecules**, invited review from *Phys. Chem. Chem. Phys.*, in preparation

15) Tim Guilliams, Alexander K. Buell, Nunilo Cremades, Duncan A. White, Farah El-Turk, Liz O-day, Francesco Aprile, Elin Esbjorner-Winters, Els Pardon, Tuomas P.J. Knowles, Lode Wyns, Christopher Dobson and Erwin De Genst, **Influences of Nanobodies on the elongation of α-synuclein**, in preparation

Book chapters

Alexander K. Buell, Christopher M. Dobson, Mark E. Welland, **Measuring the kinetics of amyloid fibril elongation using Quartz Crystal Microbalances (QCM)** in METHODS IN MOLECULAR BIOLOGY Amyloid Proteins Methods and Protocols (2011), Humana Press, NY, USA

References

[1] George D Rose, Patrick J Fleming, Jayanth R Banavar, and Amos Maritan. A backbone-based theory of protein folding. *Proc Natl Acad Sci U S A*, 103(45):16623–16633, Nov 2006. 1, 3

[2] Christopher M Dobson. Protein folding and misfolding. *Nature*, 426(6968):884–890, Dec 2003. 1, 2, 5

[3] C. Levinthal. *Moessbauer Spectroscopy in Biological Sytems*. Univ of Illinois Press, Urbana, 1969. 1

[4] Jan Kubelka, James Hofrichter, and William A Eaton. The protein folding 'speed limit'. *Curr Opin Struct Biol*, 14(1):76–88, Feb 2004. 1

[5] P. E. Leopold, M. Montal, and J. N. Onuchic. Protein folding funnels: a kinetic approach to the sequence-structure relationship. *Proc Natl Acad Sci U S A*, 89(18):8721–8725, Sep 1992. 1

[6] J. D. Bryngelson, J. N. Onuchic, N. D. Socci, and P. G. Wolynes. Funnels, pathways, and the energy landscape of protein folding: a synthesis. *Proteins*, 21(3):167–195, Mar 1995. 1, 58

[7] K. A. Dill and H. S. Chan. From Levinthal to pathways to funnels. *Nat Struct Biol*, 4(1):10–19, Jan 1997. 3

[8] J. D. Bryngelson and P. G. Wolynes. Spin glasses and the statistical mechanics of protein folding. *Proc Natl Acad Sci U S A*, 84(21):7524–7528, Nov 1987. 2

[9] Robert L Baldwin. Energetics of protein folding. *J Mol Biol*, 371(2):283–301, Aug 2007. 2, 3, 68, 76

[10] Kingshuk Ghosh and Ken A Dill. Computing protein stabilities from their chain lengths. *Proc Natl Acad Sci U S A*, 106(26):10649–10654, Jun 2009. 2

[11] David De Sancho, Urmi Doshi, and Victor Muñoz. Protein folding rates and stability: how much is there beyond size? *J Am Chem Soc*, 131(6):2074–2075, Feb 2009. 2, 77

[12] H. Jane Dyson, Peter E Wright, and Harold A Scheraga. The role of hydrophobic interactions in initiation and propagation of protein folding. *Proc Natl Acad Sci U S A*, 103(35):13057–13061, Aug 2006. 2

[13] M. Sunde, L. C. Serpell, M. Bartlam, P. E. Fraser, M. B. Pepys, and C. C. Blake. Common core structure of amyloid fibrils by synchrotron X-ray diffraction. *J Mol Biol*, 273(3):729–739, Oct 1997. 3, 5

[14] J. D. Sipe and A. S. Cohen. Review: history of the amyloid fibril. *J Struct Biol*, 130(2-3):88–98, Jun 2000. 3

[15] A. S. Cohen and E. Calkins. Electron microscopic observations on a fibrous component in amyloid of diverse origins. *Nature*, 183(4669):1202–1203, Apr 1959. 3

[16] David F. Waugh. The linkage of corpuscular protein molecules. I. A fibrous modification of insulin. *J. Am. Chem. Soc.*, 66 (4):663, 1944. 3

[17] Massimo Stefani. Protein misfolding and aggregation: new examples in medicine and biology of the dark side of the protein world. *Biochim Biophys Acta*, 1739(1):5–25, Dec 2004. 3, 4

[18] Neal D Hammer, Xuan Wang, Bryan A McGuffie, and Matthew R Chapman. Amyloids: friend or foe? *J Alzheimers Dis*, 13(4):407–419, May 2008. 4

[19] J. I. Guijarro, M. Sunde, J. A. Jones, I. D. Campbell, and C. M. Dobson. Amyloid fibril formation by an SH3 domain. *Proc Natl Acad Sci U S A*, 95(8):4224–4228, Apr 1998. 4, 12, 14

[20] Tuomas P.J. Knowles, Anthony W. Fitzpatrick, Sarah Meehan, Helen R. Mott, Michele Vendruscolo, Christopher M. Dobson, and Mark E. Welland. Role of intermolecular forces in defining material properties of protein nanofibrils. *Science*, 318(5858):1900–1903, Dec 2007. 4, 5, 46

[21] T. Shirahama and A. S. Cohen. Structure of amyloid fibrils after negative staining and high-resolution electron microscopy. *Nature*, 206(985):737–738, May 1965. 5

[22] Tuomas P J Knowles, Jeffrey F Smith, Aidan Craig, Christopher M Dobson, and Mark E Welland. Spatial persistence of angular correlations in amyloid fibrils. *Phys Rev Lett*, 96(23):238301, Jun 2006. 5, 67

[23] O. Sumner Makin and Louise C Serpell. Structures for amyloid fibrils. *FEBS J*, 272(23):5950–5961, Dec 2005. 5, 58

[24] M. J. Burke and M. A. Rougvie. Cross-beta protein structures. I. Insulin fibrils. *Biochemistry*, 11(13):2435–2439, Jun 1972. 5

[25] Patrizia Polverino de Laureto, Niccolo Taddei, Erica Frare, Cristina Capanni, Silvia Costantini, Jesus Zurdo, Fabrizio Chiti, Christopher M Dobson, and Angelo Fontana. Protein aggregation and amyloid fibril formation by an SH3 domain probed by limited proteolysis. *J Mol Biol*, 334(1):129–141, Nov 2003. 5, 80

[26] Natalia Carulla, Gemma L Caddy, Damien R Hall, Jesus Zurdo, Margarida Gairi, Miguel Feliz, Ernest Giralt, Carol V Robinson, and Christopher M Dobson. Molecular recycling within amyloid fibrils. *Nature*, 436(7050):554–558, Jul 2005. 5

[27] Anders Olofsson, A. Elisabeth Sauer-Eriksson, and Anders Ohman. The solvent protection of Alzheimer amyloid-beta-(1-42) fibrils as determined by solution NMR spectroscopy. *J Biol Chem*, 281(1):477–483, Jan 2006. 5, 80

[28] J. L. Jimenez, J. I. Guijarro, E. Orlova, J. Zurdo, C. M. Dobson, M. Sunde, and H. R. Saibil. Cryo-electron microscopy structure of an SH3 amyloid fibril and model of the molecular packing. *EMBO J*, 18(4):815–821, Feb 1999. 5, 58

[29] Rui Zhang, Xiaoyan Hu, Htet Khant, Steven J Ludtke, Wah Chiu, Michael F Schmid, Carl Frieden, and Jin-Moo Lee. Interprotofilament interactions between Alzheimer's abeta (1-42) peptides in amyloid fibrils revealed by cryo-EM. *Proc Natl Acad Sci U S A*, 106(12):4653–4658, Mar 2009. 5, 6

[30] Christian Wasmer, Adam Lange, Helene Van Melckebeke, Ansgar B Siemer, Roland Riek, and Beat H Meier. Amyloid fibrils of the HET-s (218-289) prion form a beta solenoid with a triangular hydrophobic core. *Science*, 319(5869):1523–1526, Mar 2008. 5

[31] Rebecca Nelson, Michael R Sawaya, Melinda Balbirnie, Anders O Madsen, Christian Riekel, Robert Grothe, and David Eisenberg. Structure of the cross-beta spine of amyloid-like fibrils. *Nature*, 435(7043):773–778, Jun 2005. 5

[32] Brandon H Toyama and Jonathan S Weissman. Amyloid structure: Conformational diversity and consequences. *Annu Rev Biochem*, Jun 2010. 6

[33] Thorsten Luhrs, Christiane Ritter, Marc Adrian, Dominique Riek-Loher, Bernd Bohrmann, Heinz Dobeli, David Schubert, and Roland Riek. 3D structure of Alzheimer's amyloid-beta (1-42) fibrils. *Proc Natl Acad Sci U S A*, 102(48):17342–17347, Nov 2005. 6

[34] Andrew James Baldwin, Tuomas Pertti Jonathan Knowles, Gian Tartaglia, Anthony Fitzpatrick, Glyn Devlin, Sarah Shammas, Christopher Andrew Waudby, Maria Francesca Mossuto, Sally Louise Gras, John Christodoulou, Spencer J Anthony-Cahill, Paul D Barker, Michele Vendruscolo, and Christopher M Dobson. Metastability of native proteins and the phenomenon of amyloid formation. *J Am Chem Soc*, Jun 2011. 5, 17, 58, 65, 113

[35] Douglas M Fowler, Atanas V Koulov, Christelle Alory-Jost, Michael S Marks, William E Balch, and Jeffery W Kelly. Functional amyloid formation within mammalian tissue. *PLoS Biol*, 4(1):e6, Jan 2006. 5

[36] A. H Y Kwan, R. D. Winefield, M. Sunde, J. M. Matthews, R. G. Haverkamp, M. D. Templeton, and J. P. Mackay. Structural basis for rodlet assembly in

fungal hydrophobins. *Proc Natl Acad Sci U S A*, 103(10):3621–3626, Mar 2006. 5

[37] Peter Chien, Jonathan S Weissman, and Angela H DePace. Emerging principles of conformation-based prion inheritance. *Annu Rev Biochem*, 73:617–656, 2004. 5

[38] D. E. Otzen, O. Kristensen, and M. Oliveberg. Designed protein tetramer zipped together with a hydrophobic Alzheimer homology: a structural clue to amyloid assembly. *Proc Natl Acad Sci U S A*, 97(18):9907–9912, Aug 2000. 5

[39] Fabrizio Chiti, Massimo Stefani, Niccolo Taddei, Giampietro Ramponi, and Christopher M Dobson. Rationalization of the effects of mutations on peptide and protein aggregation rates. *Nature*, 424(6950):805–808, Aug 2003. 5, 74, 77

[40] Fabrizio Chiti and Christopher M Dobson. Protein misfolding, functional amyloid, and human disease. *Annu Rev Biochem*, 75:333–366, 2006. 5, 33, 36, 101

[41] C. Zhang and C. DeLisi. Estimating the number of protein folds. *J Mol Biol*, 284(5):1301–1305, Dec 1998. 5

[42] Keith J Laidler. Chemical kinetics and the origins of physical chemistry. *Archive for History of Exact Sciences*, 32(1):43–75, 1985. 7

[43] C.F. Wenzel. *Lehre von der Verwandtschaft der Koerper*. 1777. 7

[44] Ludwig F Wilhelmy. Über das Gesetz nach welchem die Einwirkungen der Saeuren auf den Rohrzucker stattfindet. *Poggendorf's Annalen der Physik und Chemie*, 81:413–433, 1850. 7

[45] C.M. Guldberg and P. Waage. *Forhandlinger Videnskabs-Selskabet i Christiania*, pages 35–40 92–94 111–120, 1864. 7

[46] A.G.V. Harcourt and W. Esson. *Proc. Roy. Soc.*, 14:470–474, 1865. 7

[47] Jacobus Henricus van't Hoff. *Etudes de dynamique chimique*. 1884. 7

[48] Svante Arrhenius. Über die Reaktionsgeschwindigkeit bei der Inversion von Rohrzucker durch Säuren. *Zeitschrift für Physikalische Chemie*, 4:226–248, 1889. 8

[49] Albert Einstein. Über die von der molekularkinetischen Theorie der Wärme geforderte Bewegung von in ruhenden Flüssigkeiten suspendierten Teilchen. *Annalen der Physik*, 17:549–560, 1905. 8

[50] Marian von Smoluchowski. Zur kinetischen Theorie der Brown'schen Molekularbewegung und der Suspensionen. *Bullet Int Crac*, pages 756–780, 1906. 8

[51] Marian von Smoluchowski. Versuch einer mathematischen Theorie der Koagulationskinetik kolloider Lösungen. *Zeitschrift für Physikalische Chemie*, 92:129, 1917. 8

[52] Robert A. Alberty and Gordon G. Hammes. Application of the theory of diffusion-controlled reactions to enzyme kinetics. *J Phys Chem*, 62:154–159, 1958. 8

[53] Henry Eyring and Michael Polanyi. Über einfache Gasreaktionen. *Zeitschrift für Physikalische Chemie B*, 12:279, 1931. 9

[54] Henry Eyring. The activated complex in chemical reactions. *J. Chem. Phys.*, 3:107–115, 1935. 9

[55] Jean Perrin. Radiation and chemistry. *Trans. Faraday. Soc.*, 17:546, 1922. 9

[56] H A Kramers. Brownian motion in a field of force and the diffusion model of chemical reactions. *Physica*, 7:284–304, 1940. 9, 10, 62

[57] J. Skinner and Peter G. Wolynes. Relaxation processes and chemical kinetics. *J. Chem. Phys. 69:2143.*, 69:2143–2150, 1978. 10

[58] S. Pedersen, J. L. Herek, and A. H. Zewail. The validity of the "diradical" hypothesis: direct femtoscond studies of the transition-state structures. *Science*, 266(5189):1359–1364, Nov 1994. 10

[59] K. Yutani, A. Yutani, A. Imanishi, and T. Isemura. The mechanism of refolding of the reduced random coil form of lysozyme. *J Biochem*, 64(4):449–455, Oct 1968. 10

[60] A. N. Schechter, R. F. Chen, and C. B. Anfinsen. Kinetics of folding of staphylococcal nuclease. *Science*, 167(3919):886–887, Feb 1970. 10

[61] Hoi Sung Chung, John M Louis, and William A Eaton. Experimental determination of upper bound for transition path times in protein folding from single-molecule photon-by-photon trajectories. *Proc Natl Acad Sci U S A*, 106(29):11837–11844, Jul 2009. 10

[62] Fumio Oosawa, Sho Asakura, Ken Hotta, Nobuhisa Imai, and Tatsuo Ooi. G-f transformation of actin as a fibrous condensation. *Journal of Polymer Science*, 37:323–336, 1959. 10

[63] J. Hofrichter, P. D. Ross, and W. A. Eaton. Kinetics and mechanism of deoxyhemoglobin s gelation: a new approach to understanding sickle cell disease. *Proc Natl Acad Sci U S A*, 71(12):4864–4868, Dec 1974. 10

[64] P. S. Vassar and C. F. Culling. Fluorescent stains, with special reference to amyloid and connective tissues. *Arch Pathol*, 68:487–498, Nov 1959. 10

[65] H. Naiki, K. Higuchi, M. Hosokawa, and T. Takeda. Fluorometric determination of amyloid fibrils in vitro using the fluorescent dye, thioflavin T. *Anal Biochem*, 177(2):244–249, Mar 1989. 11

[66] H. Naiki, K. Higuchi, K. Nakakuki, and T. Takeda. Kinetic analysis of amyloid fibril polymerization in vitro. *Lab Invest*, 65(1):104–110, Jul 1991. 11, 82

[67] H. LeVine. Thioflavine T interaction with synthetic Alzheimer's disease beta-amyloid peptides: detection of amyloid aggregation in solution. *Protein Sci*, 2(3):404–410, Mar 1993. 11, 16, 101

[68] W. Colon and J. W. Kelly. Partial denaturation of transthyretin is sufficient for amyloid fibril formation in vitro. *Biochemistry*, 31(36):8654–8660, Sep 1992. 11

[69] G. J. Miroy, Z. Lai, H. A. Lashuel, S. A. Peterson, C. Strang, and J. W. Kelly. Inhibiting transthyretin amyloid fibril formation via protein stabilization. *Proc Natl Acad Sci U S A*, 93(26):15051–15056, Dec 1996. 11

[70] A. Lomakin, D. S. Chung, G. B. Benedek, D. A. Kirschner, and D. B. Teplow. On the nucleation and growth of amyloid beta-protein fibrils: detection of nuclei and quantitation of rate constants. *Proc Natl Acad Sci U S A*, 93(3):1125–1129, Feb 1996. 11, 54, 62

[71] Y. Kusumoto, A. Lomakin, D. B. Teplow, and G. B. Benedek. Temperature dependence of amyloid beta-protein fibrillization. *Proc Natl Acad Sci U S A*, 95(21):12277–12282, Oct 1998. 11, 54, 67, 70

[72] W. P. Esler, E. R. Stimson, J. R. Ghilardi, A. M. Felix, Y. A. Lu, H. V. Vinters, P. W. Mantyh, and J. E. Maggio. A beta deposition inhibitor screen using synthetic amyloid. *Nat Biotechnol*, 15(3):258–263, Mar 1997. 11

[73] Tadato Ban, Daizo Hamada, Kazuhiro Hasegawa, Hironobu Naiki, and Yuji Goto. Direct observation of amyloid fibril growth monitored by thioflavin T fluorescence. *J Biol Chem*, 278(19):16462–16465, May 2003. 11

[74] C. Goldsbury, J. Kistler, U. Aebi, T. Arvinte, and G. J. Cooper. Watching amyloid fibrils grow by time-lapse atomic force microscopy. *J Mol Biol*, 285(1):33–39, Jan 1999. 11

[75] Kazuhiro Hasegawa, Kenjiro Ono, Masahito Yamada, and Hironobu Naiki. Kinetic modeling and determination of reaction constants of Alzheimer's beta-amyloid fibril extension and dissociation using surface plasmon resonance. *Biochemistry*, 41(46):13489–13498, Nov 2002. 11, 20, 67, 70

[76] Tuomas P J Knowles, Wenmiao Shu, Glyn L Devlin, Sarah Meehan, Stefan Auer, Christopher M Dobson, and Mark E Welland. Kinetics and thermodynamics of amyloid formation from direct measurements of fluctuations in fibril

mass. *Proc Natl Acad Sci U S A*, 104(24):10016–10021, Jun 2007. 11, 14, 22, 34, 35, 48, 50, 62, 67, 70, 80

[77] Mads Bruun Hovgaard, Mingdong Dong, Daniel Erik Otzen, and Flemming Besenbacher. Quartz crystal microbalance studies of multilayer glucagon fibrillation at the solid-liquid interface. *Biophys J*, 93(6):2162–2169, Sep 2007. 11, 22

[78] Wolfgang Hoyer, Thomas Antony, Dmitry Cherny, Gudrun Heim, Thomas M Jovin, and Vinod Subramaniam. Dependence of alpha-synuclein aggregate morphology on solution conditions. *J Mol Biol*, 322(2):383–393, Sep 2002. 12

[79] Gunnar T Dolphin, Myriam Ouberai, Pascal Dumy, and Julian Garcia. Designed amyloid beta peptide fibril - a tool for high-throughput screening of fibril inhibitors. *ChemMedChem*, 2(11):1613–1623, Nov 2007. 12

[80] Christofer Lendel, Benedetta Bolognesi, Anna Wahlström, Christopher M Dobson, and Astrid Gräslund. Detergent-like interaction of Congo red with the amyloid beta peptide. *Biochemistry*, 49(7):1358–1360, Feb 2010. 12, 101, 106

[81] Anthony L Fink. The aggregation and fibrillation of alpha-synuclein. *Acc Chem Res*, 39(9):628–634, Sep 2006. 14

[82] Glyn L Devlin, Tuomas P J Knowles, Adam Squires, Margaret G McCammon, Sally L Gras, Melanie R Nilsson, Carol V Robinson, Christopher M Dobson, and Cait E MacPhee. The component polypeptide chains of bovine insulin nucleate or inhibit aggregation of the parent protein in a conformation-dependent manner. *J Mol Biol*, 360(2):497–509, Jul 2006. 14

[83] Mark R. H. Krebs, Deborah K. Wilkins, Evonne W. Chung, Maureen C. Pitkeathly, Aaron K. Chamberlain, Jesus Zurdo, Carol V. Robinson, and Christopher M. Dobson. Formation and seeding of amyloid fibrils from wild-type hen lysozyme and a peptide fragment from the beta-domain. *J Mol Biol*, 300(3):541–549, 7 2000. 14

[84] Erica Frare, Maria F Mossuto, Patrizia Polverino de Laureto, Mireille Dumoulin, Christopher M Dobson, and Angelo Fontana. Identification of the core structure of lysozyme amyloid fibrils by proteolysis. *J Mol Biol*, 361(3):551–561, Aug 2006. 14, 80

[85] Walraj S Gosal, Allan H Clark, and Simon B Ross-Murphy. Fibrillar beta-lactoglobulin gels: Part 1. Fibril formation and structure. *Biomacromolecules*, 5(6):2408–2419, 2004. 14

[86] John Goers, Sergei E Permyakov, Eugene A Permyakov, Vladimir N Uversky, and Anthony L Fink. Conformational prerequisites for alpha-lactalbumin fibrillation. *Biochemistry*, 41(41):12546–12551, Oct 2002. 14

[87] Francoise Immel, Yi Jiang, Yi-Qian Wang, Christelle Marchal, Laurent Maillet, Sarah Perrett, and Christophe Cullin. In vitro analysis of Sp Ure2p, a prion-related protein, exemplifies the relationship between amyloid and prion. *J Biol Chem*, 282(11):7912–7920, Mar 2007. 14

[88] J.L. Fauchere and V Pliska. Hydrophobic parameters-pi of amino acid side-chains from the partitioning of n-acetyl-amino-acid amides. *Eur J Med Chem*, 18 (4):369–375, 1983. 15, 73, 76, 77

[89] D. Eisenberg and A. D. McLachlan. Solvation energy in protein folding and binding. *Nature*, 319(6050):199–203, 1986. 15

[90] A. Kim and F. C. Szoka. Amino acid side-chain contributions to free energy of transfer of tripeptides from water to octanol. *Pharm Res*, 9(4):504–514, Apr 1992. 15

[91] S. Fukuchi and K. Nishikawa. Protein surface amino acid compositions distinctively differ between thermophilic and mesophilic bacteria. *J Mol Biol*, 309(4):835–843, Jun 2001. 15

[92] Yi-Qian Wang, Alexander K Buell, Xin-Yu Wang, Mark E Welland, Christopher M Dobson, Tuomas P J Knowles, and Sarah Perrett. Relationship between prion propensity and the rates of individual molecular steps of fibril assembly. *J Biol Chem*, 286(14):12101–12107, Apr 2011. 17

[93] Bo Liedberg, Claes Nylander, and Ingemar Lunström. Surface plasmon resonance for gas detection and biosensing. *Sensors and Actuators*, 4:299–304, 1983. 19

[94] L. G. Fägerstam, A. Frostell, R. Karlsson, M. Kullman, A. Larsson, M. Malmqvist, and H. Butt. Detection of antigen-antibody interactions by surface plasmon resonance. Application to epitope mapping. *J Mol Recognit*, 3(5-6):208–214, 1990. 19

[95] P.A. van der Merwe. *Surface plasmon resonance, Protein-Ligand Interactions: A Practical Approach*. Oxford University Press, 2000. 19

[96] Michelle J Cannon, Angela D Williams, Ronald Wetzel, and David G Myszka. Kinetic analysis of beta-amyloid fibril elongation. *Anal Biochem*, 328(1):67–75, May 2004. 20, 31, 39, 42, 85

[97] Wen-Pin Hu, Guan-Liang Chang, Shean-Jen Chen, and Yu-Min Kuo. Kinetic analysis of beta-amyloid peptide aggregation induced by metal ions based on surface plasmon resonance biosensing. *J Neurosci Methods*, 154(1-2):190–197, Jun 2006. 20, 31, 39, 42, 102

[98] Jungki Ryu, Hyou-Arm Joung, Min-Gon Kim, and Chan Beum Park. Surface plasmon resonance analysis of Alzheimer's beta-amyloid aggregation on a solid

surface: from monomers to fully-grown fibrils. *Anal Chem*, 80(7):2400–2407, Apr 2008. 20, 85

[99] Günther Sauerbrey. Verwendung von Schwingquarzen zur Wägung duenner Schichten und zur Mikrowaegung. *Zeitschrift f. Physik A: Hadrons and Nuclei*, 155 (2):206–222, 1959. 21, 49

[100] K. Keiji Kanazawa and Joseph G. Gordon II. The oscillation frequency of a quartz resonator in contact with liquid. *Anal Chim Acta*, 175:99–105, 1985. 21

[101] M.V. Voinova, M. Rodahl, M.Johnson, and B. Kasemo. Viscoelastic acoustic response of layered polymer films at fluid-solid interfaces: Continuum mechanics approach. *Pysica Scripta*, 59:391–396, 1999. 21, 53

[102] Stephen J. Martin, Victoria Edwards Granstaff, and Gregory C. Frye. Characterization of a quartz crystal microbalance with simultaneous mass and liquid loading. *Anal. Chem.*, 63:2272–2281, 1991. 21

[103] M. V. Voinova, M. Jonson, and B. Kasemo. Missing mass effect in biosensor's QCM applications. *Biosens Bioelectron*, 17(10):835–841, Oct 2002. 21

[104] Lubica Macakova, Eva Blomberg, and Per M. Claesson. Effect of adsorbed layer surface roughness on the QCM-D response: Focus on trapped water. *Langmuir*, 23:12436–12444, 2007. 22, 53

[105] G. McHale and M. I. Newton. Surface roughness and interfacial slip boundary condition for quartz crystal microbalances. *J Appl Phys*, 95:373–380, 2004. 22, 102, 103

[106] Hiroaki Okuno, Kanae Mori, Tomoko Okada, Yuusaku Yokoyama, and Hideharu Suzuki. Development of aggregation inhibitors for amyloid-beta peptides and their evaluation by quartz-crystal microbalance. *Chem Biol Drug Des*, 69(5):356–361, May 2007. 22

[107] Joseph A Kotarek, Kathryn C Johnson, and Melissa A Moss. Quartz crystal microbalance analysis of growth kinetics for aggregation intermediates of the amyloid-beta protein. *Anal Biochem*, 378(1):15–24, Jul 2008. 22, 31

[108] Ana M Saraiva, M. Carmo Pereira, and Gerald Brezesinski. Is the viscoelasticity of Alzheimer's abeta42 peptide oligomers a general property of protein oligomers related to their toxicity? *Langmuir*, Jun 2010. 22

[109] Daijiro Yanagisawa, Hiroyasu Taguchi, Akitsugu Yamamoto, Nobuaki Shirai, Koichi Hirao, and Ikuo Tooyama. Curcuminoid binds to amyloid-1-42 oligomer and fibril. *J Alzheimers Dis*, Feb 2011. 22

[110] D. Johannsmann. Viscoelastic analysis of organic thin films on quartz resonators. *Macromol. Chem. Phys.*, 200:501–541, 1999. 23

[111] J. Christopher Love, Lara A Estroff, Jennah K Kriebel, Ralph G Nuzzo, and George M Whitesides. Self-assembled monolayers of thiolates on metals as a form of nanotechnology. *Chem Rev*, 105(4):1103–1169, Apr 2005. 24

[112] Bruce J. Berne and Robert Pecora. *Dynamic Light Scattering: With Applications to Chemistry, Biology, and Physics*. Dover Publication, 2000. 25, 54, 56, 83

[113] P. Debye and E. Hückel. The theory of electrolytes. I. Lowering of freezing point and related phenomena. *Phys Zeitschr*, 24:185–206, 1923. 26, 81, 85

[114] D C Henry. The cataphoresis of suspended particles. Part I. The equation of cataphoresis. *Proc R Soc Lond A*, 133:106–129, 1931. 26

[115] Jason C.W. Corbett and Robert O. Jack. Measuring protein mobility using modern microelectrophoresis. *Colloids and Surfaces A: Physicochemical and Engineering Aspects*, 376:31–41, 2010. 28

[116] Martin D Jeppesen, Peter Westh, and Daniel E Otzen. The role of protonation in protein fibrillation. *FEBS Lett*, 584(4):780–784, Feb 2010. 28, 29, 87, 114

[117] Peter Wagner, Martin Hegner, Hans-Joachim Guntherodt, and Giorgio Semenza. Formation and in situ modification of monolayers chemisorbed on ultraflat template-stripped gold surfaces. *Langmuir*, 11:3867–3875, 1995. 29, 46

[118] Matthew W Freyer and Edwin A Lewis. Isothermal titration calorimetry: experimental design, data analysis, and probing macromolecule/ligand binding and kinetic interactions. *Methods Cell Biol*, 84:79–113, 2008. 29

[119] Jozsef Kardos, Kaori Yamamoto, Kazuhiro Hasegawa, Hironobu Naiki, and Yuji Goto. Direct measurement of the thermodynamic parameters of amyloid formation by isothermal titration calorimetry. *J Biol Chem*, 279(53):55308–55314, Dec 2004. 29, 114

[120] Ming-Shen Lin, Hsiu-Mei Chiu, Fu-Jung Fan, Hui-Ting Tsai, Steven S-S Wang, Yung Chang, and Wen-Yih Chen. Kinetics and enthalpy measurements of interaction between beta-amyloid and liposomes by surface plasmon resonance and isothermal titration microcalorimetry. *Colloids Surf B Biointerfaces*, 58(2):231–236, Aug 2007. 29, 114

[121] Alexander K Buell, Duncan A White, Christoph Meier, Mark E Welland, Tuomas P J Knowles, and Christopher M Dobson. Surface attachment of protein fibrils via covalent modification strategies. *J Phys Chem B*, 114(34):10925–10938, Sep 2010. 31

[122] C.D. Bain, E.B Troughton, Y.-T. Tao, J. Evall, G.M. Whitesides, and R.G. Nuzzo. Formation of monolayer films by the spontaneous assembly of organic thiols from solution onto gold. *J. Am. Chem. Soc.*, 111:321–335, 1989. 31

[123] I. Yamaguchi, K. Hasegawa, N. Takahashi, F. Gejyo, and H. Naiki. Apolipoprotein E inhibits the depolymerization of beta 2-microglobulin-related amyloid fibrils at a neutral pH. *Biochemistry*, 40(29):8499–8507, Jul 2001. 33

[124] P. Fenter, A. Eberhardt, and P. Eisenberger. Self-assembly of n-alkyl thiols as disulfides on Au(111). *Science*, 266(5188):1216–1218, Nov 1994. 34

[125] Hans A. Biebuyck, Colin D. Bain, and George M. Whitesides. Comparison of organic monolayers on polycrystalline gold spontaneously assembled from solutions containing dialkyl disulfides or alkanethiols. *Langmuir*, 10:1825–1831, 1994. 34

[126] R. Jue, J. M. Lambert, L. R. Pierce, and R. R. Traut. Addition of sulfhydryl groups to escherichia coli ribosomes by protein modification with 2-iminothiolane (methyl 4-mercaptobutyrimidate). *Biochemistry*, 17(25):5399–5406, Dec 1978. 34, 39

[127] Tai-Horng Young, Jui-Nan Lu, Dar-Jong Lin, Chi-Lin Chang, Hsu-Hsien Chang, and Liao-Ping Cheng. Immobilization of l-lysine on dense and porous poly(vinylidene fluoride) surfaces for neuron culture. *Desalination*, 234:134–143, 2008. 35

[128] Chanki Ha, Jungki Ryu, and Chan Beum Park. Metal ions differentially influence the aggregation and deposition of Alzheimer's beta-amyloid on a solid template. *Biochemistry*, 46(20):6118–6125, May 2007. 39, 42

[129] R. R. Traut, A. Bollen, T. T. Sun, J. W. Hershey, J. Sundberg, and L. R. Pierce. Methyl 4-mercaptobutyrimidate as a cleavable cross-linking reagent and its application to the escherichia coli 30s ribosome. *Biochemistry*, 12(17):3266–3273, Aug 1973. 39

[130] R. Singh, L. Kats, W. A. Blaettler, and J. M. Lambert. Formation of n-substituted 2-iminothiolanes when amino groups in proteins and peptides are modified by 2-iminothiolane. *Anal Biochem*, 236(1):114–125, Apr 1996. 39

[131] D.J. Lavrich, S.M. Wetterer, S.L. Bernasek, and G. Scoles. Physisorption and chemisorption of alkanethiols and alkyl sulfides on Au(111). *Journal of Physical Chemistry B*, 102 (18):3456–3465, 1998. 39

[132] Hirotomo Miake, Hidehiro Mizusawa, Takeshi Iwatsubo, and Masato Hasegawa. Biochemical characterization of the core structure of alpha-synuclein filaments. *J Biol Chem*, 277(21):19213–19219, May 2002. 40, 80

[133] Cynthia Akkermans, Paul Venema, Atze Jan van der Goot, Harry Gruppen, Edwin J Bakx, Remko M Boom, and Erik van der Linden. Peptides are building blocks of heat-induced fibrillar protein aggregates of beta-lactoglobulin formed at pH 2. *Biomacromolecules*, 9(5):1474–1479, May 2008. 40, 80

[134] A. C. Alagon and T. P. King. Activation of polysaccharides with 2-iminothiolane and its uses. *Biochemistry*, 19(18):4341–4345, Sep 1980. 41, 45

[135] G. Mukhopadhyay. On the interaction of a planar metal surface with a charge and with a molecule. *Physica Scripta*, 36:676–688, 1987. 46

[136] K. Rechendorff, M. B. Hovgaard, M. Foss, V. P. Zhdanov, and F. Besenbacher. Enhancement of protein adsorption induced by surface roughness. *Langmuir*, 22(26):10885–10888, Dec 2006. 46

[137] Paul Roach, David Farrar, and Carole C Perry. Surface tailoring for controlled protein adsorption: effect of topography at the nanometer scale and chemistry. *J Am Chem Soc*, 128(12):3939–3945, Mar 2006. 46

[138] Wilhelm R Glomm, Oyvind Halskau, Ann-Mari D Hanneseth, and Sondre Volden. Adsorption behavior of acidic and basic proteins onto citrate-coated Au surfaces correlated to their native fold, stability, and pI. *J Phys Chem B*, 111(51):14329–14345, Dec 2007. 46

[139] Hui Li, Andrew D Robertson, and Jan H Jensen. Very fast empirical prediction and rationalization of protein pka values. *Proteins*, 61(4):704–721, Dec 2005. 47

[140] Miklos S Z Kellermayer, Arpad Karsai, Margit Benke, Katalin Soos, and Botond Penke. Stepwise dynamics of epitaxially growing single amyloid fibrils. *Proc Natl Acad Sci U S A*, 105(1):141–144, Jan 2008. 49

[141] Jesper Ferkinghoff-Borg, Jesper Fonslet, Christian Beyschau Andersen, Sandeep Krishna, Simone Pigolotti, Hisashi Yagi, Yuji Goto, Daniel Otzen, and Mogens H. Jensen. Stop-and-go kinetics in amyloid fibrillation. *Phys Rev E*, 82 (1):010901, 2010. 49

[142] Wolfgang Hoyer, Dmitry Cherny, Vinod Subramaniam, and Thomas M Jovin. Rapid self-assembly of alpha-synuclein observed by in situ atomic force microscopy. *J Mol Biol*, 340(1):127–139, Jun 2004. 49

[143] A. V. Filippov, A. V. Suleimanova, G. Grobner, and O. N. Antsutkin. Effect of freezing on amyloid peptide aggregation and self-diffusion in an aqueous solution. *Colloid Journal*, 70(4):501–506, 2008. 52

[144] Hong Yang, Shan-Yu Fung, Mark Pritzker, and P. Chen. Surface-assisted assembly of an ionic-complementary peptide: controllable growth of nanofibers. *J Am Chem Soc*, 129(40):12200–12210, Oct 2007. 54

[145] Christian Beyschau Andersen, Hisashi Yagi, Mauro Manno, Vincenzo Martorana, Tadato Ban, Gunna Christiansen, Daniel Erik Otzen, Yuji Goto, and Christian Rischel. Branching in amyloid fibril growth. *Biophys J*, 96(4):1529–1536, Feb 2009. 54

[146] Karunakar Kar, Murali Jayaraman, Bankanidhi Sahoo, Ravindra Kodali, and Ronald Wetzel. Critical nucleus size for disease-related polyglutamine aggregation is repeat-length dependent. *Nat Struct Mol Biol*, 18(3):328–336, Mar 2011. 54

[147] J. G. Garcia de la Torre and V. A. Bloomfield. Hydrodynamic properties of complex, rigid, biological macromolecules: theory and applications. *Q Rev Biophys*, 14(1):81–139, Feb 1981. 55, 56, 57, 83

[148] Robert Pecora. Spectral distribution of light scattered by monodisperse rigid rods. *J Chem Phys*, 48,:4126–4128, 1968. 56

[149] Y. Y. Huang, T. P. J. Knowles, and E. M. Terentjev. Strength of nanotubes, filaments, and nanowires from sonication-induced scission. *Advanced materials*, 21 (38-39):39453948, 2009. 57, 83

[150] Giulia Calloni, Christofer Lendel, Silvia Campioni, Silva Giannini, Alessandra Gliozzi, Annalisa Relini, Michele Vendruscolo, Christopher M. Dobson, Xavier Salvatella, and Fabrizio Chiti. Structure and dynamics of a partially folded protein are decoupled from its mechanism of aggregation. *J. Am. Chem. Soc.*, 130(39):13040–13050, 10 2008. 58

[151] Jeffrey F Smith, Tuomas P J Knowles, Christopher M Dobson, Cait E Macphee, and Mark E Welland. Characterization of the nanoscale properties of individual amyloid fibrils. *Proc Natl Acad Sci U S A*, 103(43):15806–15811, Oct 2006. 58

[152] P. G. Wolynes, J. N. Onuchic, and D. Thirumalai. Navigating the folding routes. *Science*, 267(5204):1619–1620, Mar 1995. 58

[153] T. Lazaridis and M. Karplus. "New view" of protein folding reconciled with the old through multiple unfolding simulations. *Science*, 278(5345):1928–1931, Dec 1997. 58

[154] Alexander K Buell, Jamie R Blundell, Christopher M Dobson, Mark E Welland, Eugene M Terentjev, and Tuomas P J Knowles. Frequency factors in a landscape model of filamentous protein aggregation. *Phys Rev Lett*, 104(22):228101, Jun 2010. 59, 62

[155] M. Doi and S. F. Edwards. *The Theory of Polymer Dynamics*. Oxford University Press, 1988. 60

[156] Robert M Mazo. *Brownian Motion*. Oxford University Press, 2002. 61

[157] S Chandrasekhar. Stochastic problems in physics and astronomy. *Rev. Mod. Phys*, 15:1, 1943. 62

[158] A Polson. On the diffusion constants of the amino-acids. *Biochem. J.*, 31:1903, 1937. 62

[159] Thomas Scheibel, Jesse Bloom, and Susan L Lindquist. The elongation of yeast prion fibers involves separable steps of association and conversion. *Proc Natl Acad Sci U S A*, 101(8):2287–2292, Feb 2004. 62

[160] Sean R Collins, Adam Douglass, Ronald D Vale, and Jonathan S Weissman. Mechanism of prion propagation: amyloid growth occurs by monomer addition. *PLoS Biol*, 2(10):e321, Oct 2004. 62

[161] Kristin R Domike and Athene M Donald. Thermal dependence of thermally induced protein spherulite formation and growth: kinetics of beta-lactoglobulin and insulin. *Biomacromolecules*, 8(12):3930–3937, Dec 2007. 62, 67, 70

[162] M. Oliveberg, Y. J. Tan, and A. R. Fersht. Negative activation enthalpies in the kinetics of protein folding. *Proc Natl Acad Sci U S A*, 92(19):8926–8929, Sep 1995. 64

[163] M. Jacob and F. X. Schmid. Protein folding as a diffusional process. *Biochemistry*, 38(42):13773–13779, Oct 1999. 65, 71

[164] V. N. Uversky, J. Li, and A. L. Fink. Evidence for a partially folded intermediate in alpha-synuclein fibril formation. *J Biol Chem*, 276(14):10737–10744, Apr 2001. 67, 70

[165] Yong-Sung Kim, Theodore W Randolph, Fred J Stevens, and John F Carpenter. Kinetics and energetics of assembly, nucleation, and growth of aggregates and fibrils for an amyloidogenic protein. Insights into transition states from pressure, temperature, and co-solute studies. *J Biol Chem*, 277(30):27240–27246, Jul 2002. 67, 70, 80

[166] Rita Carrotta, Mauro Manno, Donatella Bulone, Vincenzo Martorana, and Pier Luigi San Biagio. Protofibril formation of amyloid beta-protein at low pH via a non-cooperative elongation mechanism. *J Biol Chem*, 280(34):30001–30008, Aug 2005. 67, 70

[167] Nasrollah Rezaei-Ghaleh, Azadeh Ebrahim-Habibi, Ali Akbar Moosavi-Movahedi, and Mohsen Nemat-Gorgani. Role of electrostatic interactions in 2,2,2-trifluoroethanol-induced structural changes and aggregation of alpha-chymotrypsin. *Arch Biochem Biophys*, 457(2):160–169, Jan 2007. 67, 70, 80

[168] Katja Skerget, Andrej Vilfan, Marusa Pompe-Novak, Vito Turk, Jonathan P Waltho, Dusan Turk, and Eva Zerovnik. The mechanism of amyloid-fibril formation by stefin B: temperature and protein concentration dependence of the rates. *Proteins*, 74(2):425–436, Feb 2009. 67, 70, 80

[169] Wei-Feng Xue, Steve W Homans, and Sheena E Radford. Amyloid fibril length distribution quantified by atomic force microscopy single-particle image analysis. *Protein Eng Des Sel*, 22(8):489–496, Aug 2009. 67

[170] Karolin Klement, Karin Wieligmann, Jessica Meinhardt, Peter Hortschansky, Walter Richter, and Marcus Fändrich. Effect of different salt ions on the propensity of aggregation and on the structure of Alzheimer's abeta(1-40) amyloid fibrils. *J Mol Biol*, 373(5):1321–1333, Nov 2007. 67, 82

[171] Josue Juarez, Sonia Goy Lopez, Adriana Cambon, Pablo Taboada, and Victor Mosquera. Influence of electrostatic interactions on the fibrillation process of human serum albumin. *J Phys Chem B*, 113(30):10521–10529, Jul 2009. 67, 82

[172] R. Sabate, V. Castillo, A. Espargaro, Sven J Saupe, and S. Ventura. Energy barriers for HET-s prion forming domain amyloid formation. *FEBS J*, 276(18):5053–5064, Sep 2009. 68, 70, 74, 80

[173] Benjamin Schuler, Everett A Lipman, and William A Eaton. Probing the free-energy surface for protein folding with single-molecule fluorescence spectroscopy. *Nature*, 419(6908):743–747, Oct 2002. 70, 71, 72

[174] N. D. Socci, J. N. Onuchic, and P.G. Wolynes. Diffusive dynamics of the reaction coordinate for protein folding funnels. *J. Chem. Phys.*, 104 (15):5860–5868, 1996. 68

[175] Christopher M. Dobson, Andrej Sali, and Martin Karplus. Protein folding: a perspective from theory and experiment. *Angew. Chem. Intern. Ed.*, 37:868–893, 1998. 68

[176] Justin L MacCallum, Maria Sabaye Moghaddam, Hue Sun Chan, and D. Peter Tieleman. Hydrophobic association of alpha-helices, steric dewetting, and enthalpic barriers to protein folding. *Proc Natl Acad Sci U S A*, 104(15):6206–6210, Apr 2007. 69

[177] Yoshihisa Inoue, Tadao Hakushi, Yu Liu, Lin-Hui Tong, Bao-Jian Shen, and Dao-Sen Jin. Thermodynamics of molecular recognition by cyclodextrins. 1. Calorimetric titration of inclusion complexation of naphthalenesulfonates with alpha-, beta-, and gamma-cyclodextrins: Enthalpy-entropy compensation. *J. Am. Chem. Soc.*, 115:475–481, 1993. 69

[178] Arya Akmal and Victor Muoz. The nature of the free energy barriers to two-state folding. *Proteins*, 57(1):142–152, Oct 2004. 71, 72

[179] Thomas R Jahn, O. Sumner Makin, Kyle L Morris, Karen E Marshall, Pei Tian, Pawel Sikorski, and Louise C Serpell. The common architecture of cross-beta amyloid. *J Mol Biol*, 395(4):717–727, Jan 2010. 71

[180] Joan Torrent, Stephane Marchal, Marc Ribo, Maria Vilanova, Cedric Georges, Yves Dupont, and Reinhard Lange. Distinct unfolding and refolding pathways of ribonuclease a revealed by heating and cooling temperature jumps. *Biophys J*, 94(10):4056–4065, May 2008. 72

[181] Anatoly I Dragan, Sergey A Potekhin, Andrei Sivolob, Min Lu, and Peter L Privalov. Kinetics and thermodynamics of the unfolding and refolding of the three-stranded alpha-helical coiled coil, Lpp-56. *Biochemistry*, 43(47):14891–14900, Nov 2004. 72

[182] B. Ibarra-Molero, G. I. Makhatadze, and C. R. Matthews. Mapping the energy surface for the folding reaction of the coiled-coil peptide GCN4-p1. *Biochemistry*, 40(3):719–731, Jan 2001. 72

[183] Hannah J Wong, Peter B Stathopulos, Julia M Bonner, Marc Sawyer, and Elizabeth M Meiering. Non-linear effects of temperature and urea on the thermodynamics and kinetics of folding and unfolding of hisactophilin. *J Mol Biol*, 344(4):1089–1107, Dec 2004. 72

[184] M. L. Scalley and D. Baker. Protein folding kinetics exhibit an Arrhenius temperature dependence when corrected for the temperature dependence of protein stability. *Proc Natl Acad Sci U S A*, 94(20):10636–10640, Sep 1997. 72

[185] B. Kuhlman, J. A. Boice, R. Fairman, and D. P. Raleigh. Structure and stability of the N-terminal domain of the ribosomal protein L9: evidence for rapid two-state folding. *Biochemistry*, 37(4):1025–1032, Jan 1998. 72

[186] Anne Dhulesia, Nunilo Cremades, Janet R Kumita, Shang-Te Danny Hsu, Maria F Mossuto, Mireille Dumoulin, Daniel Nietlispach, Mikael Akke, Xavier Salvatella, and Christopher M Dobson. Local cooperativity in an amyloidogenic state of human lysozyme observed at atomic resolution. *J Am Chem Soc*, 132(44):15580–15588, Nov 2010. 74

[187] Alexander K Buell, Anne Dhulesia, Maria F Mossuto, Nunilo Cremades, Janet R Kumita, Mireille Dumoulin, Mark E Welland, Tuomas P J Knowles, Xavier Salvatella, and Christopher M Dobson. Population of nonnative states of lysozyme variants drives amyloid fibril formation. *J Am Chem Soc*, 133(20):7737–7743, May 2011. 74

[188] Alexander K Buell, Gian Gaetano Tartaglia, Neil R Birkett, Christopher A Waudby, Michele Vendruscolo, Xavier Salvatella, Mark E Welland, Christopher M Dobson, and Tuomas P J Knowles. Position-dependent electrostatic protection against protein aggregation. *Chembiochem*, 10(8):1309–1312, May 2009. 74, 88

[189] R. B. Wickner, K. L. Taylor, H. K. Edskes, M. L. Maddelein, H. Moriyama, and B. T. Roberts. Prions of yeast as heritable amyloidoses. *J Struct Biol*, 130(2-3):310–322, Jun 2000. 74

[190] Simon Alberti, Randal Halfmann, Oliver King, Atul Kapila, and Susan Lindquist. A systematic survey identifies prions and illuminates sequence features of prionogenic proteins. *Cell*, 137(1):146–158, Apr 2009. 74

[191] Mathai Mammen, Eugene I. Shakhnovich, John M. Deutch, and George M. Whitesides. Estimating the entropic cost of self-assembly of multiparticle hydrogen-bonded aggregates based on the cyanuric acidmelamine lattice. *J. Org. Chem.*, 63:3821–3830, 1998. 75

[192] Ka Lum, David Chandler, and John D. Weeks. Hydrophobicity at small and large length scales. *J. Phys. Chem. B*, 103:4570–4577, 1999. 76

[193] Yung Sam Kim, Liu Liu, Paul H Axelsen, and Robin M Hochstrasser. 2D IR provides evidence for mobile water molecules in beta-amyloid fibrils. *Proc Natl Acad Sci U S A*, 106(42):17751–17756, Oct 2009. 76

[194] Amol P Pawar, Kateri F Dubay, Jesus Zurdo, Fabrizio Chiti, Michele Vendruscolo, and Christopher M Dobson. Prediction of "aggregation-prone" and "aggregation-susceptible" regions in proteins associated with neurodegenerative diseases. *J Mol Biol*, 350(2):379–392, Jul 2005. 77

[195] J. Zurdo, J. I. Guijarro, J. L. Jimenez, H. R. Saibil, and C. M. Dobson. Dependence on solution conditions of aggregation and amyloid formation by an SH3 domain. *J Mol Biol*, 311(2):325–340, Aug 2001. 79, 82

[196] P. H. Weinreb, W. Zhen, A. W. Poon, K. A. Conway, and P. T. Lansbury. NACP, a protein implicated in Alzheimer's disease and learning, is natively unfolded. *Biochemistry*, 35(43):13709–13715, Oct 1996. 79

[197] Nikolaos G Sgourakis, Yilin Yan, Scott A McCallum, Chunyu Wang, and Angel E Garcia. The Alzheimer's peptides abeta 40 and 42 adopt distinct conformations in water: a combined MD/NMR study. *J Mol Biol*, 368(5):1448–1457, May 2007. 79

[198] D. Hamada and Y. Goto. The equilibrium intermediate of beta-lactoglobulin with non-native alpha-helical structure. *J Mol Biol*, 269(4):479–487, Jun 1997. 79

[199] T. L. Blundell, J. F. Cutfield, S. M. Cutfield, E. J. Dodson, G. G. Dodson, D. C. Hodgkin, D. A. Mercola, and M. Vijayan. Atomic positions in rhombohedral 2-zinc insulin crystals. *Nature*, 231(5304):506–511, Jun 1971. 79

[200] J. J. Ewbank and T. E. Creighton. The molten globule protein conformation probed by disulphide bonds. *Nature*, 350(6318):518–520, Apr 1991. 79

[201] B. Hawkins, K. Cross, and D. Craik. Solution structure of the B-chain of insulin as determined by 1H NMR spectroscopy. comparison with the crystal structure of the insulin hexamer and with the solution structure of the insulin monomer. *Int J Pept Protein Res*, 46(5):424–433, Nov 1995. 79

[202] Eric D Ross, Allen Minton, and Reed B Wickner. Prion domains: sequences, structures and interactions. *Nat Cell Biol*, 7(11):1039–1044, Nov 2005. 79

[203] C. Boesch, A. Bundi, M. Oppliger, and K. Wüthrich. 1H nuclear-magnetic-resonance studies of the molecular conformation of monomeric glucagon in aqueous solution. *Eur J Biochem*, 91(1):209–214, Nov 1978. 79

[204] Geoffrey W Platt, Victoria J McParland, Arnout P Kalverda, Steve W Homans, and Sheena E Radford. Dynamics in the unfolded state of beta2-microglobulin studied by NMR. *J Mol Biol*, 346(1):279–294, Feb 2005. 79

[205] Axelle Balguerie, Suzana Dos Reis, Christiane Ritter, Stephane Chaignepain, Benedicte Coulary-Salin, Vincent Forge, Katell Bathany, Ioan Lascu, Jean-Marie Schmitter, Roland Riek, and Sven J Saupe. Domain organization and structure-function relationship of the HET-s prion protein of podospora anserina. *EMBO J*, 22(9):2071–2081, May 2003. 79

[206] D. B. Huang, C. H. Chang, C. Ainsworth, G. Johnson, A. Solomon, F. J. Stevens, and M. Schiffer. Variable domain structure of kappa IV human light chain len: high homology to the murine light chain McPC603. *Mol Immunol*, 34(18):1291–1301, Dec 1997. 79

[207] Sasa Jenko Kokalj, Gregor Guncar, Igor Stern, Gareth Morgan, Sabina Rabzelj, Manca Kenig, Rosemary A Staniforth, Jonathan P Waltho, Eva Zerovnik, and Dusan Turk. Essential role of proline isomerization in stefin B tetramer formation. *J Mol Biol*, 366(5):1569–1579, Mar 2007. 79

[208] H. T. Wright. Comparison of the crystal structures of chymotrypsinogen-A and alpha-chymotrypsin. *J Mol Biol*, 79(1):1–11, Sep 1973. 79

[209] Jens Brange, Jean Whittingham, David Edwards, Zhang You-Shang, Axel Wollmer, Dietrich Brandenburg, Guy Dodson, and John Finch. Insulin structure and diabetes treatment. *Current Science*, 72 (7):470–476, 1997. 80

[210] Patrizia Polverino de Laureto, Erica Frare, Francesca Battaglia, Maria F Mossuto, Vladimir N Uversky, and Angelo Fontana. Protein dissection enhances the amyloidogenic properties of alpha-lactalbumin. *FEBS J*, 272(9):2176–2188, May 2005. 80

[211] Ulrich Baxa, Kimberly L Taylor, Joseph S Wall, Martha N Simon, Naiqian Cheng, Reed B Wickner, and Alasdair C Steven. Architecture of Ure2p prion filaments: the N-terminal domains form a central core fiber. *J Biol Chem*, 278(44):43717–43727, Oct 2003. 80

[212] M. Monti, A. Amoresano, S. Giorgetti, V. Bellotti, and P. Pucci. Limited proteolysis in the investigation of beta2-microglobulin amyloidogenic and fibrillar states. *Biochim Biophys Acta*, 1753(1):44–50, Nov 2005. 80

[213] B Derjaguin and L Landau. Theory of the stability of strongly charged lyophobic sols and of the adhesion of strongly charged particles in solutions of electrolytes. *Acta Physico Chemica URSS*, 14:633, 1941. 81, 96

[214] EJW Verwey and JTG Overbeek. *Theory of the stability of lyophobic colloids.* Elsevier, Amsterdam, 1948. 81, 96

[215] Barry W. Ninham and Pierandrea Lo Nostro. *Molecular Forces and Self Assembly: In Colloid, Nano Sciences and Biology.* Cambridge University Press, 2010. 81, 82

[216] M. Boström, D. R. Williams, and B. W. Ninham. Specific ion effects: why DLVO theory fails for biology and colloid systems. *Phys Rev Lett*, 87(16):168103, Oct 2001. 82

[217] A. Yu. Grosberg, T. T. Nguyen, and B. I. Shklovskii. Colloquium: The physics of charge inversion in chemical and biological systems. *Reviews of modern Physics*, 74:329–345, 2002. 82

[218] F. Zhang, M. W A Skoda, R. M J Jacobs, S. Zorn, R. A. Martin, C. M. Martin, G. F. Clark, S. Weggler, A. Hildebrandt, O. Kohlbacher, and F. Schreiber. Reentrant condensation of proteins in solution induced by multivalent counterions. *Phys Rev Lett*, 101(14):148101, Oct 2008. 82

[219] Larissa A Munishkina, Jeremy Henriques, Vladimir N Uversky, and Anthony L Fink. Role of protein-water interactions and electrostatics in alpha-synuclein fibril formation. *Biochemistry*, 43(11):3289–3300, Mar 2004. 82

[220] Bakthisaran Raman, Eri Chatani, Miho Kihara, Tadato Ban, Miyo Sakai, Kazuhiro Hasegawa, Hironobu Naiki, Ch Mohan Rao, and Yuji Goto. Critical balance of electrostatic and hydrophobic interactions is required for beta 2-microglobulin amyloid fibril growth and stability. *Biochemistry*, 44(4):1288–1299, Feb 2005. 82, 93

[221] Jesper Søndergaard Pedersen, James M Flink, Dantcho Dikov, and Daniel Erik Otzen. Sulfates dramatically stabilize a salt-dependent type of glucagon fibrils. *Biophys J*, 90(11):4181–4194, Jun 2006. 82, 93

[222] Kristin R Domike and Athene M Donald. Kinetics of spherulite formation and growth: salt and protein concentration dependence on proteins beta-lactoglobulin and insulin. *Int J Biol Macromol*, 44(4):301–310, May 2009. 82

[223] L. Nielsen, R. Khurana, A. Coats, S. Frokjaer, J. Brange, S. Vyas, V. N. Uversky, and A. L. Fink. Effect of environmental factors on the kinetics of insulin fibril formation: elucidation of the molecular mechanism. *Biochemistry*, 40(20):6036–6046, May 2001. 82

[224] Victor Yeh, James M Broering, Andrey Romanyuk, Buxin Chen, Yury O Chernoff, and Andreas S Bommarius. The Hofmeister effect on amyloid formation using yeast prion protein. *Protein Sci*, 19(1):47–56, Jan 2010. 82

[225] Shweta Jain and Jayant B Udgaonkar. Salt-induced modulation of the pathway of amyloid fibril formation by the mouse prion protein. *Biochemistry*, 49(35):7615–7624, Sep 2010. 82

[226] Motomasa Tanaka, Peter Chien, Nariman Naber, Roger Cooke, and Jonathan S Weissman. Conformational variations in an infectious protein determine prion strain differences. *Nature*, 428(6980):323–328, Mar 2004. 82

[227] Aneta T Petkova, Richard D Leapman, Zhihong Guo, Wai-Ming Yau, Mark P Mattson, and Robert Tycko. Self-propagating, molecular-level polymorphism in Alzheimer's beta-amyloid fibrils. *Science*, 307(5707):262–265, Jan 2005. 82

[228] Jacob Israelachvili. *Intermolecular and surface forces*. Academic Press, 1992. 83

[229] Satoshi Kawatake, Yuki Nishimura, Suehiro Sakaguchi, Toru Iwaki, and Katsumi Doh-ura. Surface plasmon resonance analysis for the screening of antiprion compounds. *Biol Pharm Bull*, 29(5):927–932, May 2006. 85, 100, 101

[230] Walter J. Moore. *Physical Chemistry*. Prentice-Hall, 1972. 86

[231] Myung-Suk Chun and Intaek Lee. Rigorous estimation of effective protein charge from experimental electrophoretic mobilities for proteomics analysis using microchip electrophoresis. *Colloids and Surfaces A: Physicochem. Eng. Aspects*, 318:191198, 2008. 87

[232] D. John Mitchell and Barry W. Ninham. Range of the screened Coulomb interaction in electrolytes and double layer problems. *Chem Phys Lett*, 53(2):397–399, 1978. 88

[233] George Scatchard, I. Herbert Scheinberg, and S. Howard Armstrong Jr. Physical chemistry of protein solutions. IV. The combination of human serum albumin with chloride ion. *J Am Chem Soc*, 72(1):535540, 1950. 88, 94, 95

[234] Charles Tanford. The interpretation of hydrogen ion titration curves of proteins. *Advances in Protein Chemistry*, 17:69–165, 1963. 88

[235] Christopher L. Ford and Donald J. Winzor. Measurement of the net charge (valence) of a protein. *Biochim et Biophys Acta*, 703:109–112, 1982. 94

[236] J. Gao, F. A. Gomez, R. Härter, and G. M. Whitesides. Determination of the effective charge of a protein in solution by capillary electrophoresis. *Proc Natl Acad Sci U S A*, 91(25):12027–12030, Dec 1994. 95

[237] Hubert H. Girault. *Analytical and Physical Electrochemistry*. EPFL Press, 2004. 96

[238] Alexander K Buell, Christopher M Dobson, Tuomas P J Knowles, and Mark E Welland. Interactions between amyloidophilic dyes and their relevance to studies of amyloid inhibitors. *Biophys J*, 99(10):3492–3497, Nov 2010. 99

[239] Brian Y Feng, Brandon H Toyama, Holger Wille, David W Colby, Sean R Collins, Barnaby C H May, Stanley B Prusiner, Jonathan Weissman, and Brian K Shoichet. Small-molecule aggregates inhibit amyloid polymerization. *Nat Chem Biol*, 4(3):197–199, Mar 2008. 99, 101

[240] Christofer Lendel, Carlos W Bertoncini, Nunilo Cremades, Christopher A Waudby, Michele Vendruscolo, Christopher M Dobson, Dale Schenk, John Christodoulou, and Gergely Toth. On the mechanism of nonspecific inhibitors of protein aggregation: dissecting the interactions of alpha-synuclein with Congo red and lacmoid. *Biochemistry*, 48(35):8322–8334, Sep 2009. 99, 101, 104

[241] William E Klunk, Henry Engler, Agneta Nordberg, Yanming Wang, Gunnar Blomqvist, Daniel P Holt, Mats Bergström, Irina Savitcheva, Guo feng Huang, Sergio Estrada, Birgitta Ausen, Manik L Debnath, Julien Barletta, Julie C Price, Johan Sandell, Brian J Lopresti, Anders Wall, Pernilla Koivisto, Gunnar Antoni, Chester A Mathis, and Bengt Långström. Imaging brain amyloid in Alzheimer's disease with Pittsburgh Compound-B. *Ann Neurol*, 55(3):306–319, Mar 2004. 100

[242] Z. P. Zhuang, M. P. Kung, C. Hou, D. M. Skovronsky, T. L. Gur, K. Plössl, J. Q. Trojanowski, V. M. Lee, and H. F. Kung. Radioiodinated styrylbenzenes and thioflavins as probes for amyloid aggregates. *J Med Chem*, 44(12):1905–1914, Jun 2001. 100, 102

[243] W. E. Klunk, M. L. Debnath, and J. W. Pettegrew. Development of small molecule probes for the beta-amyloid protein of Alzheimer's disease. *Neurobiol Aging*, 15(6):691–698, 1994. 100

[244] P. Kuner, B. Bohrmann, L. O. Tjernberg, J. Näslund, G. Huber, S. Celenk, F. Grüninger-Leitch, J. G. Richards, R. Jakob-Roetne, J. A. Kemp, and C. Nordstedt. Controlling polymerization of beta-amyloid and prion-derived peptides with synthetic small molecule ligands. *J Biol Chem*, 275(3):1673–1678, Jan 2000. 100

[245] Nicolette S Honson, Ronald L Johnson, Wenwei Huang, James Inglese, Christopher P Austin, and Jeff Kuret. Differentiating Alzheimer disease-associated aggregates with small molecules. *Neurobiol Dis*, 28(3):251–260, Dec 2007. 100

[246] Yair Porat, Yariv Mazor, Shimon Efrat, and Ehud Gazit. Inhibition of islet amyloid polypeptide fibril formation: a potential role for heteroaromatic interactions. *Biochemistry*, 43(45):14454–14462, Nov 2004. 100

[247] Ben N G Giepmans, Stephen R Adams, Mark H Ellisman, and Roger Y Tsien. The fluorescent toolbox for assessing protein location and function. *Science*, 312(5771):217–224, Apr 2006. 100

[248] Y. Engelborghs. The analysis of time resolved protein fluorescence in multitryptophan proteins. *Spectrochim Acta A Mol Biomol Spectrosc*, 57(11):2255–2270, Sep 2001. 100

[249] Chirlmin Joo, Hamza Balci, Yuji Ishitsuka, Chittanon Buranachai, and Taekjip Ha. Advances in single-molecule fluorescence methods for molecular biology. *Annu Rev Biochem*, 77:51–76, 2008. 100

[250] Andrea Hawe, Marc Sutter, and Wim Jiskoot. Extrinsic fluorescent dyes as tools for protein characterization. *Pharm Res*, 25(7):1487–1499, Jul 2008. 100

[251] Ritu Khurana, Chris Coleman, Cristian Ionescu-Zanetti, Sue A Carter, Vinay Krishna, Rajesh K Grover, Raja Roy, and Shashi Singh. Mechanism of thioflavin T binding to amyloid fibrils. *J Struct Biol*, 151(3):229–238, Sep 2005. 101, 103

[252] Raimon Sabate, Ioan Lascu, and Sven J Saupe. On the binding of Thioflavin-T to HET-s amyloid fibrils assembled at pH 2. *J Struct Biol*, 162(3):387–396, Jun 2008. 101, 103

[253] Catherine C Kitts and David A Vanden Bout. Near-field scanning optical microscopy measurements of fluorescent molecular probes binding to insulin amyloid fibrils. *J Phys Chem B*, 113(35):12090–12095, Sep 2009. 101

[254] Matthew Biancalana and Shohei Koide. Molecular mechanism of thioflavin-t binding to amyloid fibrils. *Biochim Biophys Acta*, 1804(7):1405–1412, Jul 2010. 101

[255] Chun Wu, Zhixiang Wang, Hongxing Lei, Wei Zhang, and Yong Duan. Dual binding modes of Congo red to amyloid protofibril surface observed in molecular dynamics simulations. *J Am Chem Soc*, 129(5):1225–1232, Feb 2007. 101

[256] Chun Wu, Zhixiang Wang, Hongxing Lei, Yong Duan, Michael T. Bowers, and Joan-Emma Shea. The binding of Thioflavin-T and its neutral analog BTA-1 to protofibrils of the Alzheimer abeta 16-22 peptide probed by molecular dynamics simulations. *J Mol Biol*, 384 (3):718729, 2008. 101, 104

[257] Cristina Rodriguez-Rodriguez, Albert Rimola, Luis Rodriguez-Santiago, Piero Ugliengo, Angel Alvarez-Larena, Hugo Gutierrez de Teran, Mariona Sodupe, and Pilar Gonzalez-Duarte. Crystal structure of thioflavin-T and its binding to amyloid fibrils: insights at the molecular level. *ChemComm*, 46:11561158, 2010. 101

[258] Minna Groenning. Binding mode of Thioflavin T and other molecular probes in the context of amyloid fibrils-current status. *J Chem Biol*, 3 (1):1–18, Aug 2009. 101

[259] Vitali I Stsiapura, Alexander A Maskevich, Valery A Kuzmitsky, Vladimir N Uversky, Irina M Kuznetsova, and Konstantin K Turoverov. Thioflavin t as a molecular rotor: Fluorescent properties of thioflavin t in solvents with different viscosity. *J Phys Chem B*, Nov 2008. 101

[260] Anna I Sulatskaya, Alexander A Maskevich, Irina M Kuznetsova, Vladimir N Uversky, and Konstantin K Turoverov. Fluorescence quantum yield of thioflavin t in rigid isotropic solution and incorporated into the amyloid fibrils. *PLoS One*, 5(10):e15385, 2010. 101

[261] Leslie S Wolfe, Matthew F Calabrese, Abhinav Nath, Dorottya V Blaho, Andrew D Miranker, and Yong Xiong. Protein-induced photophysical changes to the amyloid indicator dye thioflavin t. *Proc Natl Acad Sci U S A*, 107(39):16863–16868, Sep 2010. 101

[262] Anvita Srivastava, Prabhat K Singh, Manoj Kumbhakar, Tulsi Mukherjee, Subrata Chattopadyay, Haridas Pal, and Sukhendu Nath. Identifying the bond responsible for the fluorescence modulation in an amyloid fibril sensor. *Chemistry*, 16(30):9257–9263, Aug 2010. 101

[263] Petrea Frid, Sergey V Anisimov, and Natalija Popovic. Congo red and protein aggregation in neurodegenerative diseases. *Brain Res Rev*, 53(1):135–160, Jan 2007. 101

[264] Jacqueline F Aitken, Kerry M Loomes, Barbara Konarkowska, and Garth J S Cooper. Suppression by polycyclic compounds of the conversion of human amylin into insoluble amyloid. *Biochem J*, 374(Pt 3):779–784, Sep 2003. 101

[265] Manuela Bartolini, Carlo Bertucci, Maria Laura Bolognesi, Andrea Cavalli, Carlo Melchiorre, and Vincenza Andrisano. Insight into the kinetic of amyloid beta (1-42) peptide self-aggregation: elucidation of inhibitors' mechanism of action. *Chembiochem*, 8(17):2152–2161, Nov 2007. 101

[266] A. Lorenzo and B. A. Yankner. Beta-amyloid neurotoxicity requires fibril formation and is inhibited by Congo red. *Proc Natl Acad Sci U S A*, 91(25):12243–12247, Dec 1994. 101

[267] Mihaela Necula, Rakez Kayed, Saskia Milton, and Charles G Glabe. Small molecule inhibitors of aggregation indicate that amyloid beta oligomerization and fibrillization pathways are independent and distinct. *J Biol Chem*, 282(14):10311–10324, Apr 2007. 101

[268] Sean A Hudson, Heath Ecroyd, Tak W Kee, and John A Carver. The thioflavin T fluorescence assay for amyloid fibril detection can be biased by the presence of exogenous compounds. *FEBS J*, 276(20):5960–5972, Oct 2009. 101

[269] Izumi Maezawa, Hyun-Seok Hong, Ruiwu Liu, Chun-Yi Wu, R. Holland Cheng, Mei-Ping Kung, Hank F Kung, Kit S Lam, Salvatore Oddo, Frank M

Laferla, and Lee-Way Jin. Congo red and thioflavin-T analogs detect abeta oligomers. *J Neurochem*, 104(2):457–468, Jan 2008. 101

[270] Matthew Biancalana, Koki Makabe, Akiko Koide, and Shohei Koide. Molecular mechanism of thioflavin-T binding to the surface of beta-rich peptide self-assemblies. *J Mol Biol*, 385(4):1052–1063, Jan 2009. 101

[271] M. R H Krebs, E. H C Bromley, and A. M. Donald. The binding of thioflavin-T to amyloid fibrils: localisation and implications. *J Struct Biol*, 149(1):30–37, Jan 2005. 101

[272] H. LeVine. Stopped-flow kinetics reveal multiple phases of thioflavin T binding to Alzheimer beta (1-40) amyloid fibrils. *Arch Biochem Biophys*, 342(2):306–316, Jun 1997. 101

[273] Harry LeVine. Mechanism of abeta (1-40) fibril-induced fluorescence of (trans,trans)-1-bromo-2,5-bis(4-hydroxystyryl)benzene (K114). *Biochemistry*, 44(48):15937–15943, Dec 2005. 102, 104

[274] Tatsuya Yasunaga and Sadakatsu Nishikawa. Kinetic studies of association and dissociation reactions of Congo red by the temperature-jump method. *Bull Chem Soc Jap*, 45 (4):1262–1263, 1972. 103

[275] Fanling Meng, Peter Marek, Kathryn J Potter, C. Bruce Verchere, and Daniel P Raleigh. Rifampicin does not prevent amyloid fibril formation by human islet amyloid polypeptide but does inhibit fibril thioflavin-T interactions: implications for mechanistic studies of beta-cell death. *Biochemistry*, 47(22):6016–6024, Jun 2008. 104

[276] A. R. Fersht, A. Matouschek, and L. Serrano. The folding of an enzyme. I. Theory of protein engineering analysis of stability and pathway of protein folding. *J Mol Biol*, 224(3):771–782, Apr 1992. 113